Signals of non-minimal higgs sectors at future colliders

Andrew Gerard Akeroyd

Signals of Non–minimal Higgs Sectors at Future Colliders

Andrew Gerard Akeroyd
Centre for Particle Theory
University of Durham

A thesis submitted to the University of Durham
for the Degree of Doctor of Philosophy
August 1996

Abstract

This thesis concerns the study of extended Higgs sectors at future colliders. Such studies are well motivated since enlarged Higgs models are a necessity in many extensions of the Standard Model (SM), although these structures may be considered purely in the context of the SM, to be called the 'non–minimal SM'. The continuous theme of the thesis is the task of distinguishing between the (many) theoretically sound non–minimal Higgs sectors at forthcoming colliders. If a Higgs boson is found it is imperative to know from which model it originates. In particular, the possible differences between the Higgs sectors of the Minimal Supersymmetric Standard Model (MSSM) and the non–minimal SM are highlighted.

Considered first are the detection prospects of light charged Higgs scalars ($H^{\pm}$) at e^+e^- colliders. The discovery of a $H^{\pm}$ would provide unambiguous evidence for a non–minimal Higgs sector. We show that in certain (but not all) non–minimal models a light $H^{\pm}$ may exist i.e. be within the mass range accessible at LEP2 ($M_{H^{\pm}} \leq M_W$). In particular the MSSM requires $M_{H^{\pm}} \geq M_W$, and thus detection of a $H^{\pm}$ at LEP2 is strong evidence against the MSSM. We discuss ways of distinguishing between the models which may contain a light $H^{\pm}$ by exploiting differences in the decay channels. Attention is then given to the neutral Higgs bosons of the non–minimal SM. It is possible that these particles may possess a greatly different phenomenology to that of the minimal SM and MSSM, and we explore the feasibility of observing these differences at LEP2 and the LHC. It is found that distinct, sometimes spectacular signatures are possible. The thesis next considers a more exotic Higgs representation, namely that of Higgs triplets, and compares its phenomenology at LEP2 with that of the non–minimal models covered thus far. The phenomenon of Higgs bosons decoupling from the fermions (fermiophobia) arises naturally in the above triplet model, and this concept is studied in more depth in the final chapter. It is emphasized that such particles are not possible in the MSSM.

Acknowledgements

First and foremost I must give credit to James Stirling for his supervision. He has approved my ideas, and kept me from being over–ambitious. Thanks to his advice and guidance my PhD has gone more smoothly than I could ever have imagined.

For me to do a PhD without funding would have been impossible. Therefore I wish to thank PPARC for providing me with the necessary financial support, and for their contributions to my attendance at overseas conferences.

During the course of three years in a small city like Durham one speaks to many people, although it is usually only a relatively small number who may be called 'good friends' – with whom correspondence will continue for several years or more. However, all social contacts add to a general feeling of fondness for a place. I wish to single out a few names, those who added most to my enjoyment in Durham: Glenn, Julia, Charlie and Monica, who left at the end of either my first or second year – I missed their company in the subsequent years; Kirsten, David and Claire, who have ensured a thoroughly enjoyable departmental atmosphere; Dave and the rest of 'The Fisher house crowd' who have provided a welcome respite after a day of work. In addition I wish to thank the members of the Graduate Society Cricket Club who made captaining a very enjoyable experience. We probably had more laughs than runs (which is a lot of laughs, but not many runs!), and I will certainly miss this sport when I move to Spain – the game has not caught on over there yet..... I also participated in the University 'B' chess team and was satisfied to play a part in the promotion we obtained.

I leave Durham for a postdoctoral appointment in Valencia, the next step on the academic ladder. I will certainly miss the 'small town feel' of my previous two universities, but the time for another country and another language has come.

To Mum and Dad

Declaration

I declare that no material in this thesis has previously been submitted at this or any other university.

Essentially all of the research in Chapters 5 to 8 may be summarized by the following papers. Chapter 5 was carried out in collaboration with W.J. Stirling.

- *'Light charged Higgs scalars at high–energy e^+e^- colliders'*
  A.G. Akeroyd and W.J. Stirling, **Nucl. Phys. B447** (1995) 3.
- *'Higgs triplets at LEP2'*
  A.G. Akeroyd, **Phys. Lett. B353** (1995) 519.
- *'Fermiophobic Higgs bosons at the Fermilab Tevatron'*
  A.G. Akeroyd, **Phys. Lett. B368** (1996) 89.
- *'Non–minimal neutral Higgs bosons at LEP2'*
  A.G. Akeroyd, **Phys. Lett. B377** (1996) 95.
- *'Non–minimal neutral Higgs bosons at the LHC'*
  A.G. Akeroyd, Durham preprint, DTP 96/46.

Contents

Chapter 1

Introduction

Particle physics is the study of matter at the smallest scale. Chemistry concerns itself with molecules and conventional physics deals with the atom, but particle physics delves deeper. The subject studies the interactions of the fundamental particles and is therefore the building blocks of applied science. The current best theory in particle physics is named 'The Standard Model'; it postulates the physical world as being formed from 'quarks' and 'leptons', which interact by the emission and absorption of mediating particles. There are three generations of quarks and three generations of leptons, each with their own anti–particles (see Tables 1.1 and 1.2). The mediating particles (or force carriers) are displayed in Table 1.3.

The Standard Model is in excellent agreement with current experimental measurements, although there are many aesthetic theoretical deficiencies associated with it. All of its particles have been found with the exception of the Higgs boson. This latter particle

Particle	Symbol	Charge(e)
Electron	e^-	-1
e–Neutrino	ν_e	0
Muon	μ^-	-1
μ–Neutrino	ν_μ	0
Tau	τ^-	-1
τ–Neutrino	ν_τ	0

Table 1.1: The three generations of leptons with associated neutrinos.

Particle	Symbol	Charge(e)
Down	d	$-\frac{1}{3}$
Up	u	$\frac{2}{3}$
Strange	s	$-\frac{1}{3}$
Charm	c	$\frac{2}{3}$
Bottom	b	$-\frac{1}{3}$
Top	t	$\frac{2}{3}$

Table 1.2: The six flavours of quarks.

Particle	Symbol	Spin	Charge(e)
Photon	γ	1	0
Neutral weak boson	Z	1	0
Charged weak boson	W	1	± 1
Gluons	g_i	1	0
Higgs boson	ϕ^0	0	0

Table 1.3: The mediating particles of the Standard Model.

is required theoretically to provide mass for the particles and to correct inconsistences in the theory. The theoretical motivation for its existence is compelling, although it has so far evaded searches at present particle accelerators. The Higgs boson was predicted in 1964 and much work has been done on it in the ensuing 32 years. However it is only more recently that models with more than one Higgs boson have been studied vehemently, the studies being motivated by the fact that favourable extensions of the Standard Model often require more than one Higgs boson. This thesis considers a group of non–minimal Higgs models and explores their phenomenology at future colliders. Since there are many possible Higgs representations, it is prudent and necessary to find ways of distinguishing among the various models. If a Higgs boson is detected at a future collider it is imperative to know from which model it originates. This is the central theme to the thesis.

Chapter 2

The Standard Model

2.1 Introduction

In this chapter the mathematical foundations of the Standard Model are introduced (2.1) and the deficiencies of the unbroken theory are shown. The Higgs mechanism, which provides an attractive solution to these problems, is described in (2.2). The interaction of the Higgs field with the fermions (2.3) concludes the chapter. We shall not be presenting a review of Quantum Chromodynamics (QCD) which concerns the interactions of quarks and gluons; QCD is however an integral part of the SM.

2.2 The Standard Model

The Standard Model (SM) [1] has proved remarkably successful to date in describing the interactions of nature. It is a 'gauge theory' which ensures that it is renormalizable. The successes are numerous with many precision measurements at LEP [2] agreeing with the SM within experimental error (see Table 2.1).

There remains one part of the SM which is as yet untested – the Higgs sector – on which this thesis focuses. In this section we shall describe the 'unbroken' SM, i.e. the theory without a Higgs sector, and show that such a theory is unsatisfactory for a variety of reasons. There are many good reviews of the SM in the literature; see e.g. Ref. [3].

Parameter	Measurement	SM fit	Pull
M_Z (GeV)	91.1863 ± 0.0020	91.1861	0.1
Γ_Z (GeV)	2.4946 ± 0.0027	2.4960	-0.5
σ^0_{had} (nb)	41.506 ± 0.056	41.465	0.8
R_l	20.778 ± 0.029	20.757	0.7
$A^{l,0}_{\rm FB}$	0.0174 ± 0.0010	0.0159	1.4
$\mathcal{A}_\tau$	0.1401 ± 0.0067	0.1458	-0.9
$\mathcal{A}_e$	0.1382 ± 0.0076	0.1455	-1.0
R_b	0.2179 ± 0.0012	0.2158	1.8
R_c	0.1715 ± 0.0056	0.1723	-0.1
$A^{b,0}_{\rm FB}$	0.0979 ± 0.0023	0.1026	-1.8
$A^{c,0}_{\rm FB}$	0.0733 ± 0.0049	0.0730	0.1
$\sin^2\theta^{Lep}_{eff}$	0.2320 ± 0.0010	0.23167	0.3

Table 2.1: LEP measurements of SM parameters (from Ref. [2]).

In the SM the fermions (i.e. the quarks and leptons) appear in the Lagrangian as Dirac spinors, ψ. Left–handed and right–handed fields are defined by

$$\psi_L = \frac{1}{2}(1-\gamma_5)\psi, \quad \psi_R = \frac{1}{2}(1+\gamma_5)\psi\,. \tag{2.1}$$

In the case of massless particles, left–handed particles correspond to helicity states of $-1/2$ (the spin vector being in the opposite direction to the momentum vector) and right–handed particles correspond to helicity $+1/2$. At high energy colliders the fermion masses are usually negligible (with the exception of the t quark) and so all particles can be considered as being in definite states of helicity.

In the SM Lagrangian left–handed fermions are represented as isospin doublets ψ_L while right–handed fermions are represented as isospin singlets, ψ_R. For example u_L, d_L, e and ν_e would appear in the Lagrangian as

$$\begin{pmatrix} u \\ d \end{pmatrix}_L \quad \text{and} \quad \begin{pmatrix} \nu_e \\ e \end{pmatrix}_L . \tag{2.2}$$

Right–handed fermions would appear as u_R, d_R and e_R. In experiment the neutrino appears only in a left–handed state (–ve helicity), or right–handed anti–particle state, and so there is no term ν_R in the Lagrangian. Left–handed doublets are required to transform in the following way:

$$\psi_L \rightarrow \psi'_L = exp[ig\alpha_i(x)T_i + ig'\beta(x)Y]\psi_L\,. \tag{2.3}$$

The right–handed singlets transform as

$$\psi_R \rightarrow \psi'_R = exp[ig'\beta(x)Y]\psi_R \,. \tag{2.4}$$

The operators T and Y are the generators of the $SU(2)_L$ and $U(1)_Y$ groups, and g and g' are the respective couplings; $T_i = \tau_i/2$ where τ_i is a Pauli matrix. Of course, the Lagrangian must remain invariant under such transformations. Eqs. (2.3) and (2.4) ensure that only left–handed particles couple to $W^{\pm}$, which is observed experimentally. The various quantum numbers of the particles are displayed in Tables 2.2 and 2.3, with Q signifying electric charge. The quantum numbers are related by the formula

Lepton	T	T_3	$\frac{1}{2}Y$	Q
ν_e	$\frac{1}{2}$	$\frac{1}{2}$	$-\frac{1}{2}$	0
e_L^-	$\frac{1}{2}$	$-\frac{1}{2}$	$-\frac{1}{2}$	-1
e_R^-	0	0	-1	-1

Table 2.2: The quantum numbers of the leptons.

Quark	T	T_3	$\frac{1}{2}Y$	Q
u_L	$\frac{1}{2}$	$\frac{1}{2}$	$\frac{1}{6}$	$2/3$
d_L	$\frac{1}{2}$	$-\frac{1}{2}$	$\frac{1}{6}$	$-1/3$
u_R	0	0	$2/3$	$2/3$
d_R	0	0	$-1/3$	$-1/3$

Table 2.3: The quantum numbers of the quarks.

$$Q = T_3 + \frac{Y}{2} \,. \tag{2.5}$$

Mass terms for fermions must be of the form

$$m\overline{f}f = m(\overline{f}_L f_R + \overline{f}_R f_L) \,, \tag{2.6}$$

although this term is not invariant under the gauge transformations since f_L and f_R transform differently. Hence such a term is not allowed by gauge invariance, leaving us with massless fermions. Similarly, all the gauge bosons are massless in this theory, again in direct conflict with experimental results which show that $W^{\pm}$ and Z both possess

mass. In addition, when the amplitude for the scattering process $W^+W^- \rightarrow W^+W^-$ is evaluated, one finds

$$-i\mathcal{M}(W^+W^- \rightarrow W^+W^-) \sim s/M_W^2 \tag{2.7}$$

as $s \rightarrow \infty$. Thus at large enough collider energy this process is predicted to violate unitarity. The Lagrangian for the unbroken theory is:

$$-\frac{1}{4}\mathbf{W}_{\mu\nu}.\mathbf{W}^{\mu\nu} - \frac{1}{4}B_{\mu\nu}B^{\mu\nu} + \overline{L}\gamma^{\mu}\left(i\partial_{\mu} - g\frac{1}{2}\tau.\mathbf{W}_{\mu} - g'\frac{Y}{2}B_{\mu}\right)L$$
$$+\overline{R}\gamma^{\mu}\left(i\partial_{\mu} - g'\frac{Y}{2}B_{\mu}\right)R. \tag{2.8}$$

Here τ_i denotes a Pauli matrix. The first two terms are the $W^{\pm}$, Z, γ kinetic energies and self–interactions. The last two terms are the lepton and quark kinetic energies and their interactions with $W^{\pm}$, Z, γ. As mentioned above there are no particle mass terms, and thus this cannot be the complete Lagrangian. Our aim is to find a gauge invariant way of providing mass and this is made possible by 'the Higgs mechanism'.

2.3 The Higgs Mechanism

The Higgs mechanism [4] was first proposed in 1964 and solves the problems caused by the unbroken SM. To the SM Lagrangian one adds the term $\mathcal{L}_{Higgs}$ defined by

$$\mathcal{L}_{Higgs} = \mathcal{L}_{Pot} + \mathcal{L}_{Yuk} + \mathcal{L}_{Kin}\ . \tag{2.9}$$

Here $\mathcal{L}_{Yuk}$ is the Yukawa coupling of the Higgs boson to the fermions which will be discussed later; $\mathcal{L}_{Kin}$ is the kinetic energy term of the Higgs bosons, $(D_{\mu}\Phi)^{\dagger}(D^{\mu}\Phi)$, and $\mathcal{L}_{Pot}$ is the Higgs potential. The scalar doublet field is defined by

$$\Phi = \begin{pmatrix} \phi^+ \\ \phi^0 \end{pmatrix}, \tag{2.10}$$

where ϕ^+ and ϕ^0 are complex fields with quantum numbers displayed in Table 2.4.

The potential is defined by:

$$V(\Phi) = \mu^2\Phi^{\dagger}\Phi + \lambda(\Phi^{\dagger}\Phi)^2\ . \tag{2.11}$$

	T	T_3	$\frac{1}{2}Y$	Q
ϕ^+	$\frac{1}{2}$	$\frac{1}{2}$	$\frac{1}{2}$	1
ϕ^0	$\frac{1}{2}$	$-\frac{1}{2}$	$\frac{1}{2}$	0

Table 2.4: The quantum numbers of ϕ^+ and ϕ^0.

If $\mu^2 \geq 0$ and $\lambda \geq 0$ then the minimum of $V(\Phi)$ is at $\Phi^\dagger\Phi = 0$. However, if we choose $\mu^2 \leq 0$ the minimum now lies at $\Phi^\dagger\Phi = -\frac{1}{2}\mu^2/\lambda$. This can be interpreted as Φ possessing a non–vanishing vacuum expectation value (VEV). The VEV is denoted by v and defined as

$$\frac{v}{\sqrt{2}} = (-\mu^2/2\lambda)^{\frac{1}{2}} . \tag{2.12}$$

The presence of a non–zero VEV enables the problems of the unbroken model to be solved. We can choose a particular vacuum to be

$$\Phi_0 = \frac{1}{\sqrt{2}} \begin{pmatrix} 0 \\ v \end{pmatrix} , \tag{2.13}$$

which is a very special choice. It is chosen so that the vacuum does not break the $U(1)_Q$ symmetry. We stress that the above choice can always be obtained under global SU(2) transformations. The real Higgs field can be expanded around the vacuum, while the other three degrees of freedom can be removed by a gauge transformation (Eq. (2.14)), thus ensuring that no Goldstone bosons remain in the Lagrangian. This is due to the equality:

$$\Phi = \exp\left(\frac{i\xi(x).\tau}{2v}\right) \begin{pmatrix} 0 \\ v + h(x) \end{pmatrix} . \tag{2.14}$$

Therefore it is sufficient to substitute the scalar doublet

$$\Phi = \frac{1}{\sqrt{2}} \begin{pmatrix} 0 \\ v + h(x) \end{pmatrix} \tag{2.15}$$

into the Lagrangian, and this will generate the masses for the vector bosons from the Higgs kinetic energy term:

$$(D_\mu\phi)^\dagger(D^\mu\phi) = \left|(igT.W_\mu + ig'\frac{Y}{2}B_\mu)\frac{1}{\sqrt{2}} \begin{pmatrix} 0 \\ v + h(x) \end{pmatrix}\right|^2 \tag{2.16}$$

$$= \frac{g^2v^2}{8}(W_\mu^1 W_1^\mu + W_\mu^2 W_2^\mu) + \frac{v^2(g^2 + g'^2)}{8}\left|\frac{W_\mu^3 g - g'B_\mu}{\sqrt{g^2 + g'^2}}\right|^2 \tag{2.17}$$

$$\begin{aligned} &+\text{interaction term} \\ \equiv \frac{1}{2}M_W^2 W_\mu^+ W_-^\mu + \frac{1}{2}M_Z^2 Z^\mu Z_\mu + \frac{1}{2}M_A^2 A^\mu A_\mu \\ &+\text{interaction term}. \end{aligned} \tag{2.18}$$

with the fields defined by

$$W_\mu^+ = \frac{1}{\sqrt{2}}(W_\mu^1 - iW_\mu^2)\,, \tag{2.19}$$

$$W_\mu^- = \frac{1}{\sqrt{2}}(W_\mu^1 + iW_\mu^2)\,, \tag{2.20}$$

$$Z_\mu = \frac{W_\mu^3 g - g' B_\mu}{\sqrt{(g^2+g'^2)}} = W_\mu^3 \cos\theta_w - B_\mu \sin\theta_w\,, \tag{2.21}$$

$$A_\mu = \frac{W_\mu^3 g' + g B_\mu}{\sqrt{(g^2+g'^2)}} = W_\mu^3 \sin\theta_w + B_\mu \cos\theta_w\,. \tag{2.22}$$

The following masses are generated:

$$M_W = \frac{gv}{2}\,, \tag{2.23}$$

$$M_Z = \frac{v}{2}\sqrt{g^2+g'^2}\,, \tag{2.24}$$

$$M_A = 0\,. \tag{2.25}$$

The result that $M_A = 0$ (i.e. the photon remains massless) is due to the fact that the $U(1)_Q$ symmetry is intact after SSB and any gauge symmetry must have an associated massless gauge boson, in this case the field A^μ. One finds that

$$e = g\sin\theta_w = g'\cos\theta_w\,. \tag{2.26}$$

and the Weinberg angle θ_w is defined as

$$\tan\theta_w = \frac{g'}{g}\,. \tag{2.27}$$

The three basic parameters of the SM are g, g' and v, although it is more favourable to use M_Z, $G_F = \sqrt{2}g^2/8M_W^2$ and $\alpha_{\text{em}} = e^2/4\pi$ since the latter can be measured with considerable accuracy. The interaction terms are

$$\begin{aligned} &gM_W h W_\mu^+ W_-^\mu + (g^2+g'^2)\frac{M_Z}{2}hZ_\mu Z^\mu + \frac{g^2}{4}h^2 W_\mu^+ W_-^\mu \\ &+\frac{\sqrt{(g^2+g'^2)}}{8}h^2 Z_\mu Z^\mu\,. \end{aligned} \tag{2.28}$$

which are interpreted as the triple and quartic vertices for h interacting with the massive gauge bosons.

2.4 Masses of the Fermions

So far we have obtained mass terms for the massive gauge bosons. The other massive particles in the SM are, of course, the fermions. The mass term for fermions must be of the form $m\overline{\Phi}\Phi$; this term is forbidden by gauge invariance since it can be written as $m(\overline{\Phi}_L\Phi_R+\overline{\Phi}_R\Phi_L)$, and the left and right components transform differently under the gauge groups. The Higgs boson can provide masses for the fermions by introducing couplings of the form:

$$\mathcal{L}_Y = g_d\left[(\overline{u},\ \overline{d})_L\begin{pmatrix}\phi^+\\ \phi^0\end{pmatrix}d_R + \overline{d}_R(\phi^-,\ \overline{\phi^0})\begin{pmatrix}u\\ d\end{pmatrix}_L\right]. \tag{2.29}$$

Here g_d is the down-type fermion Yukawa coupling, and $u(d)$ represents the up-type (down-type) fermion. The Higgs boson has the correct quantum numbers to allow this term to be gauge invariant. When the Higgs doublet is replaced by its VEV one finds:

$$\mathcal{L}_Y = -\frac{g_d}{\sqrt{2}}v(\overline{d}_Ld_R + \overline{d}_Rd_L) - \frac{g_d}{\sqrt{2}}(\overline{d}_Ld_R + \overline{d}_Rd_L)h\,. \tag{2.30}$$

The first term is a Dirac mass term, in which g_d can be chosen to satisfy

$$m_d = \frac{g_dv}{\sqrt{2}}\,, \tag{2.31}$$

and so generates the required mass for the down-type fermions (i.e. leptons and down-type quarks):

$$-\,m_d\overline{d}d - \frac{m_d}{v}\overline{d}dh\,. \tag{2.32}$$

Since g_d is arbitrary the mass of the fermions is not actually predicted, although mass has been accommodated in a gauge invariant way. The second term in Eq. (2.32) is an interaction term between the Higgs field h and the fermions. Note that the coupling for this interaction is proportional to the mass of the fermion, and for all but the heaviest fermions this coupling (m_d/v) is very small.

The masses for the up–type quarks are generated in a similar way. The only difference is that we must form a new Higgs doublet (ϕ_c) from ϕ:

$$\phi_c = -i\tau_2\phi^* = \begin{pmatrix} -\overline{\phi}^0 \\ \phi^- \end{pmatrix} . \tag{2.33}$$

The neutral component ϕ^0 is now the upper member of the doublet, and due to the special properties of $SU(2)$, ϕ_c transforms identically to ϕ. To give mass to the up–type quarks the gauge invariant contribution to the Lagrangian is

$$g_u \left[(\overline{u},\ \overline{d})_L \begin{pmatrix} -\overline{\phi}^0 \\ \phi^- \end{pmatrix} u_R + h.c \right] . \tag{2.34}$$

which provides the mass and interaction terms

$$- m_u \overline{u} u - \frac{m_u}{v} \overline{u} u h \ . \tag{2.35}$$

This mechanism can be extended to give masses to the three generations of quarks and leptons. One finds that the couplings would take the form

$$g_d^{ij} \left[(\overline{u}_i,\ \overline{d}_i')_L \begin{pmatrix} \phi^+ \\ \phi^0 \end{pmatrix} d_{jR} \right] + g_u^{ij} \left[(\overline{u}_i,\ \overline{d}_i')_L \begin{pmatrix} -\overline{\phi}^0 \\ \phi^- \end{pmatrix} u_{jR} \right] + h.c \ , \tag{2.36}$$

where the $\overline{d}_i'$ refers to a weak eigenstate composed of a linear combination of mass eigenstates from the three generations.

This leads to the following Lagrangian:

$$- m_d^i \overline{d}_i d_i \left(1 + \frac{h}{v} \right) - m_u^i \overline{u}_i u_i \left(1 + \frac{h}{v} \right) . \tag{2.37}$$

The Higgs–fermion interaction conserves flavour, and thus is in agreement with the requirement that flavour changing neutral currents must be suppressed. Theoretically this can be explained due to the results:

$$m_{ij}^d = g_{ij}^u \frac{v}{\sqrt{2}} , \quad m_{ij}^d = g_{ij}^d \frac{v}{\sqrt{2}} . \tag{2.38}$$

Hence the diagonalization of the mass matrix causes the Yukawa couplings to be automatically diagonalized, and hence there are no tree–level flavour changing neutral currents.

Chapter 3

Properties of the Higgs boson

3.1 Introduction

In this section we shall describe the properties of the minimal SM Higgs boson. Our convention now is to label the particle as ϕ^0, since this nomenclature is frequently used in the literature. In Chapter 2 ϕ^0 was taken as a neutral complex field in the column vector Φ, and h represented the physical Higgs field.

As mentioned several times already M_{ϕ^0} is not predicted by the theory although various loose upper bounds (3.2) on its value can be obtained from considering internal consistency conditions in perturbation theory. Section (3.3) displays the most useful Feynman rules of the Higgs boson, from which the partial decay widths and thus the branching ratos (BRs) of ϕ^0 can be evaluated (3.4). Next the phenomenology at LEP2 (3.5 and 3.6) and at the Large Hadron Collider (LHC) are studied (3.7 and 3.8). The predicted event numbers will be displayed in later chapters when the question of distinguishing between ϕ^0 and Higgs bosons of non–minimal models becomes an important issue.

3.2 Mass bounds

Three ways to indirectly constrain M_{ϕ^0} are reviewed. The first is obtained from requiring that unitarity is preserved in vector boson scattering processes; the second demands that

the Higgs self–coupling constant (λ) remains perturbative up to a certain scale where new physics then enters. Both these methods produce upper bounds on M_{ϕ^0}. The third analysis enables a lower bound on M_{ϕ^0} to be obtained by requiring that the Higgs vacuum remains stable.

We shall start with the unitarity considerations [5], [6]. Let us consider WW elastic scattering.

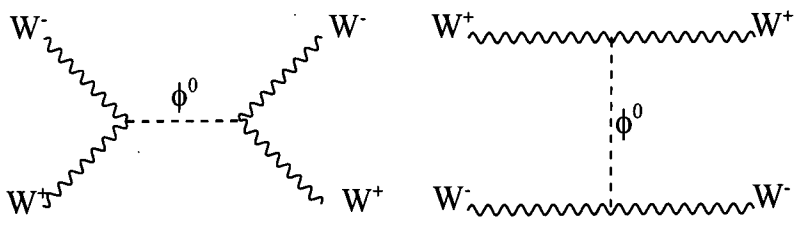

Figure 3.1: The contribution of ϕ^0 to W^+W^- scattering.

Using the SM Feynman rules for the tree–level diagrams, but omitting any diagrams involving the Higgs boson, it can be shown that the amplitude grows linearly in s (Eq. (2.7)), thus violating unitarity. The inclusion of ϕ^0 cures this problem (see Figure 3.1), although since ϕ^0 can be removed from the spectrum by taking $M_{\phi^0} \to \infty$ it follows that tree–level unitarity must break down for some large value of M_{ϕ^0}. It can be shown that the scattering of the longitudinally polarized Ws (W_L) gives the most serious bad high energy behaviour (this is because the polarization vector of W_L in the large energy limit is approximated by $\epsilon_L^\mu(p) \approx p^\mu/M_W$). The amplitude for $W_L^+W_L^- \to W_L^+W_L^-$ in the limit where s, $M_{\phi^0}^2 \gg M_W^2$, M_Z^2 is

$$\mathcal{A}(W_L^+W_L^- \to W_L^+W_L^-) = -\sqrt{2}G_F M_{\phi^0}^2 \left[\frac{s}{s - M_{\phi^0}^2} + \frac{t}{t - M_{\phi^0}^2}\right]. \tag{3.1}$$

As mentioned earlier the amplitude grows linearly in s if we take $M_{\phi^0} \to \infty$. The presence of a finite M_{ϕ^0} cause the amplitude to tend to a constant value as $s \to \infty$. However, even at finite M_{ϕ^0} this amplitude may violate unitarity. To show this explicitly we can show that the contribution to the $J = 0$ partial wave from Eq. (3.1) is given by

$$a_0 = \frac{1}{16\pi s}\int_{-s}^{0} \mathcal{A}(W_L^+W_L^- \to W_L^+W_L^-)dt = \frac{-G_F M_{\phi^0}^2}{4\pi\sqrt{2}}, \tag{3.2}$$

in the limit of $s \gg M_{\phi^0}^2$. Partial wave unitarity requires

$$|\text{Re } a_J| \leq \frac{1}{2} . \tag{3.3}$$

Applying Eq. (3.3) to Eq. (3.2) produces the bound $M_{\phi^0} \leq 850$ GeV. Further analysis which includes other scattering channels ($Z_L Z_L$, $Z_L \phi^0$ and $\phi^0 \phi^0$) obtains the stronger bound $M_{\phi^0} \leq 700$ GeV. How should this bound be interpreted? We have shown that the *tree–level* amplitude violates unitarity at sufficiently large energy if ϕ^0 violates the mass bound $M_{\phi^0} \leq 700$ GeV. If higher order self–interactions among the scalars were included then maybe this bound would be weakened, allowing larger values of M_{ϕ^0}. However, this is not possible in practice since for larger M_{ϕ^0} the Higgs self–coupling would also be large and so perturbation theory would not be valid. Hence we should interpret the bound $M_{\phi^0} \leq 700$ GeV as being the largest Higgs mass for which perturbation theory is reliable for all s.

It is useful from a conceptual point of view to consider the unitarity constraints in a different limit where M_W^2, $M_Z^2 \ll s \ll M_{\phi^0}^2$. If we denote by s_c the maximum s allowed by tree–level unitarity in the limit of $M_{\phi^0} \to \infty$, then s_c is the scale at which new physics must enter. It can be shown that

$$s \leq s_c = (1.2 \text{ TeV})^2 , \tag{3.4}$$

and so new physics must enter around the 1 TeV scale. The result has important consequences since this scale that will be probed by the LHC. This ends our discussion of unitarity constraints on M_{ϕ^0}.

The second method of indirectly constraining M_{ϕ^0} can be obtained from considering the energy evolution of λ. This parameter 'runs' with the energy scale Q. The expression for the one–loop corrected coupling $\lambda(t)$ (with $t = \ln(Q^2/\mu^2)$, μ is the renormalization scale, and g_t is the top quark Yukawa coupling) can be written as [7]:

$$\frac{d\lambda}{dt} = \frac{1}{16\pi^2}\left\{12\lambda^2 + 6\lambda g_t^2 - 3g_t^4 - \frac{3}{2}\lambda(3g^2 + g'^2) + \frac{3}{16}\left[2g^4 + (g^2 + g'^2)^2\right]\right\} . \tag{3.5}$$

This expression is obtained from evaluating all one –loop diagrams in the process $\phi^0\phi^0 \to \phi^0\phi^0$, with the internal particles being respectively ϕ^0, t, W and Z; lighter

fermions also contribute although their Yukawa couplings are suppressed by the factor m_f/v, and are hence negligible compared to the heavier particles mentioned above. The above equation can be solved in the large λ limit by only keeping the term in λ^2 on the r.h.s. One finds in this approximation:

$$\lambda(Q) = \frac{\lambda(v)}{1 - \frac{3\lambda(v)}{4\pi^2} \ln\left(\frac{Q^2}{v^2}\right)}. \tag{3.6}$$

Therefore it is apparent that regardless of how small $\lambda(v)$ is, $\lambda(Q)$ will eventually develop a pole (the Landau pole) at large Q, *if* the one–loop beta function remains an adequate description of the theory at large λ. We must be aware that when $\lambda(Q)$ becomes too large the one–loop beta function is no longer a reliable description of the theory. Above a certain point it would be necessary to include higher order corrections or non–perturbative techniques.

As Q increases it becomes increasingly likely that the SM is embedded in a more complete theory, which takes effect at scales $Q = \Lambda$. Therefore Λ acts as a cut off for the SM, and so presumably $\Lambda < m_{pl} \approx 10^{19}$ GeV. Possible values for Λ may be set by some grand unification scale or supersymmetry breaking scale.

For sufficiently small $\lambda(v)$, which corresponds to a small M_{ϕ^0} since $M_{\phi^0}^2 = 2v^2\lambda$, it is possible to keep $\lambda(\Lambda)$ in the perturbative regime, thus allowing the one–loop β function to remain an accurate description of the theory. We can label the scale at which the one–loop beta function breaks down as Λ_{NP}, and thus our assumption is that $\Lambda < \Lambda_{NP}$. This means that there is no energy region where it it is necessary to use non–perturbative techniques. Of course it is possible that $\Lambda > \Lambda_{NP}$, in which case one would have to use non–perturbative techniques between the energies Λ_{NP} and Λ. We shall not be considering this possibility. First let us see what the maximum allowed M_{ϕ^0} is for $\Lambda = m_{pl}$, assuming that the one–loop β function is exact throughout this range. We impose $\lambda(\Lambda) = \infty$ as a condition, although in practice this leads to almost the same numerical results as imposing $\lambda(\Lambda) = 1$. The maximum value for the Higgs mass is given by

$$(M_{\phi^0}^{\max})^2 = \frac{8\pi^2 v^2}{3\ln(\Lambda^2/v^2)}. \tag{3.7}$$

For $\Lambda = m_{pl}$ we find $M_{\phi^0}^{\max} = 140$ GeV. Eq. (3.7) is plotted in Figure 3.2 and we can see that $M_{\phi^0}^{\max}$ quickly asymptotes to fairly low values. The lower the scale of new physics, the

larger the allowed mass of M_{ϕ^0}. Is there a lowest Λ that we should allow? If we allowed $\Lambda = v$ then the phenomenology and detection of the Higgs boson would be influenced and possibly preceded by the new physics itself. This new physics may not possess a fundamental scalar as the source of the electroweak symmetry breaking, and so the value of the Higgs boson mass may not be meaningful. Alternatively one could demand that the Higgs boson mass is less than the energy scale of new physics, which means that one can safely evolve the coupling up to the scale Λ, and the phenomenology of the Higgs boson would not be influenced by the new physics. Thus imposing $M_{\phi^0}^{max} \leq \Lambda$ one can see from the graph that $M_{\phi^0}^{max} \leq 800$ GeV.

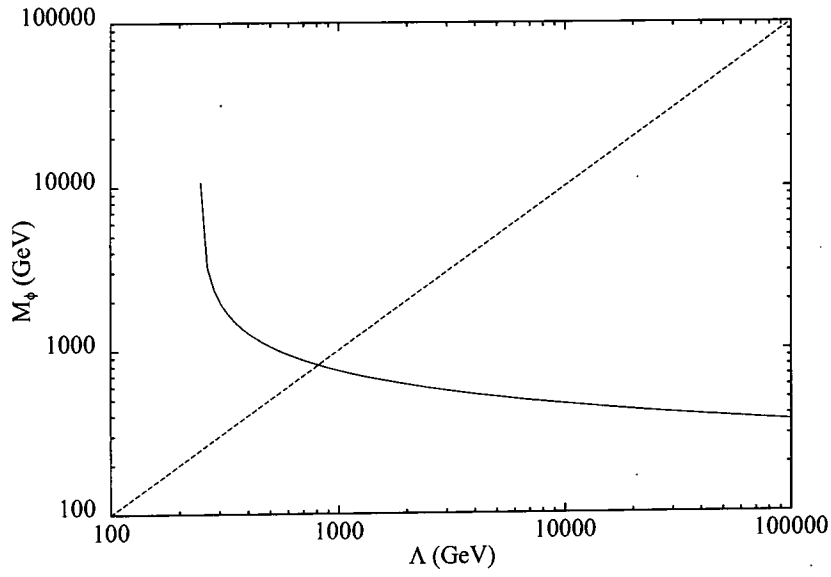

Figure 3.2: Maximum value of M_{ϕ^0} as a function of Λ, for which we may apply the pure Φ^4 renormalization group equations, and assuming $\lambda(\Lambda) = \infty$.

We have so far discussed two ways of obtaining an upper bound on M_{ϕ^0}. A lower bound on M_{ϕ^0} can be obtained from considerations of the one–loop potential. It is desirable to have $\lambda(Q) > 0$, otherwise the Higgs vacuum becomes unstable and the potential becomes unbounded from below [8]. The one–loop potential can be obtained by replacing the bare coupling λ in the tree–level potential with the running coupling $\lambda(Q)$. One can see that for a large enough value of m_t, the rate of change of λ with energy $(\frac{d\lambda}{dt})$ is negative, and

so $\lambda(Q)$ will eventually be driven negative, thus destabilizing the vacuum. Demanding $\lambda(Q) > 0$ up to a certain scale Λ, with $\lambda(\Lambda) = 0$ as a boundary condition, imposes a relationship between m_t and M_{ϕ^0}. This can be seen from the fact that including the g_t terms in Eq. (3.5) one would find

$$\lambda(Q) = f(\lambda(v),\ m_t,\ Q) \tag{3.8}$$

and after imposing $\lambda(\Lambda) = 0$ it has been shown that [9]

$$M_{\phi^0} > 130.5\,\text{GeV} + 2.1(m_t - 174\,\text{GeV})\,, \tag{3.9}$$

with $\Lambda = m_{pl}$. For $\Lambda = 1$ TeV one finds

$$M_{\phi^0} > 71\,\text{GeV} + 0.9(m_t - 174\,\text{GeV})\,. \tag{3.10}$$

It can be shown that the discovery of ϕ^0 at LEP2, i.e. $M_{\phi^0} \leq 100$ GeV would imply that new physics occurs below a scale of around 5 TeV. A precise measurement of m_t and M_{ϕ^0} enables information to be obtained on Λ.

This ends our discussion on indirect methods of constraining the Higgs mass. Although all make various assumptions the general conclusion is that we would expect a Higgs boson to have a mass of less than $O(1$ TeV).

3.3 Feynman rules of the Higgs boson (ϕ^0)

Having obtained various upper and lower bounds on M_{ϕ^0} we now wish to consider the couplings of ϕ^0 to fermions and gauge bosons, in order to investigate its phenomenology. In Figures 3.3 to 3.5 we list the principle Feynman rules for ϕ^0 which are used to evaluate the production cross-sections and BRs of ϕ^0. We shall be using these throughout the thesis, even when considering extended Higgs models.

The corresponding Feynman rule for each diagram is given in the caption. As we shall see in later chapters the Feynman rules for non-minimal neutral Higgs bosons will be related to these rules, differing only by a scaling parameter particular to that model. Therefore studying the phenomenology of ϕ^0 provides an important benchmark for the

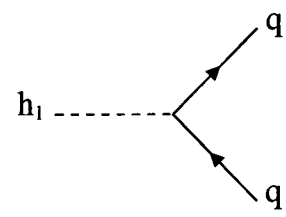

Figure 3.3: $-igm_f/2M_W$.

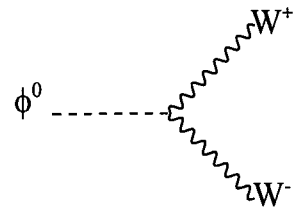

Figure 3.4: $igM_W g^{\mu\nu}$.

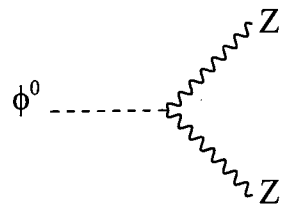

Figure 3.5: $igM_Z g^{\mu\nu}/2\cos\theta_w$.

analogous phenomenology of a non–minimal Higgs model. In the next few sections we will describe the decays and production processes of ϕ^0 at LEP2 and at the LHC, two approved colliders. This review follows the work of the LEP2 workshop [10] and the most recent ATLAS reports [11]→[14], and the results given will be built upon later in the thesis when non–minimal Higgs models are considered.

3.4 Decays of the Higgs boson (ϕ^0)

To search for ϕ^0 one must have accurate predictions for its decays i.e. its BRs. The main decay modes for Higgs masses relevant at LEP2 are:

$$\text{quark decays} : \phi^0 \to b\bar{b}\,, c\bar{c}\,. \tag{3.11}$$

$$\text{lepton decays} : \phi^0 \to \tau^+\tau^-\,, \tag{3.12}$$

$$\text{gluon decays} : \phi^0 \to gg\,. \tag{3.13}$$

$$\text{vector boson decay} : \phi^0 \to WW^*\,. \tag{3.14}$$

All the BRs are predicted once M_{ϕ^0} is known; deviations from these values would suggest a Higgs boson of a non–minimal nature. The partial width for $\phi^0 \to \tau^+\tau^-$ is given by [15]:

$$\Gamma(\phi^0 \to \tau^+\tau^-) = \frac{G_F m_\tau^2}{4\sqrt{2}\pi} M_{\phi^0} \tag{3.15}$$

and electroweak corrections are small. For the decays to $b\bar{b}$ and $c\bar{c}$ quarks the QCD corrections must be included [16]. The corrected width is given by (in the $\overline{\text{MS}}$ scheme):

$$\Gamma(\phi^0 \to q\bar{q}) = \frac{3G_F}{4\sqrt{2}\pi} m_q^2(M_{\phi^0}) M_{\phi^0} \left[1 + \frac{5.67\alpha_s}{\pi} + (35.94 - 1.36N_F + \delta_t + \delta_t')\frac{\alpha_s^2}{\pi^2}\right]. \tag{3.16}$$

Here δ_t accounts for the top quark triangle coupled in second order by 2–gluon s channel exchange [17], with value $\delta_t = 1.57 - \frac{2}{3}\log(M_{\phi^0}^2/m_t^2) + \frac{1}{9}\log^2(m_q^2(M_{\phi^0})/M_{\phi^0}^2)$, while δ_t' accounts for the Higgs decay to two gluons with one gluon splitting into a $q\bar{q}$ pair [18]. The strong coupling is to be evaluated at the scale M_{ϕ^0}, and $N_F = 5$ is the number of active flavours.

The gluon–gluon decays are primarily mediated by top quark loops and the partial width is:

$$\Gamma(\phi^0 \to gg(g),\, q\bar{q}g) = \frac{G_F \alpha_s^2}{36\sqrt{2}\pi^3} M_{\phi^0}^3 \left[1 + \left(\frac{95}{4} - \frac{7}{6} N_F\right) \frac{\alpha_s}{\pi}\right] . \tag{3.17}$$

The QCD corrections are sizeable, nearly doubling the tree-level result. Figures 3.6 and 3.7 show the BRs as a function of M_{ϕ^0}, for $M_{\phi^0} \leq 200$ GeV. We can see that $b\bar{b}$ decays are the strongest up to $M_{\phi^0} = 150$ GeV, being an order of magnitude greater than the rest. Decays to vector bosons become strong for the mass range outside the range of LEP2 (see Figure 3.8), and these channels will be exploited at the LHC. All the figures are taken from Ref. [19] with $m_t = 175$ GeV

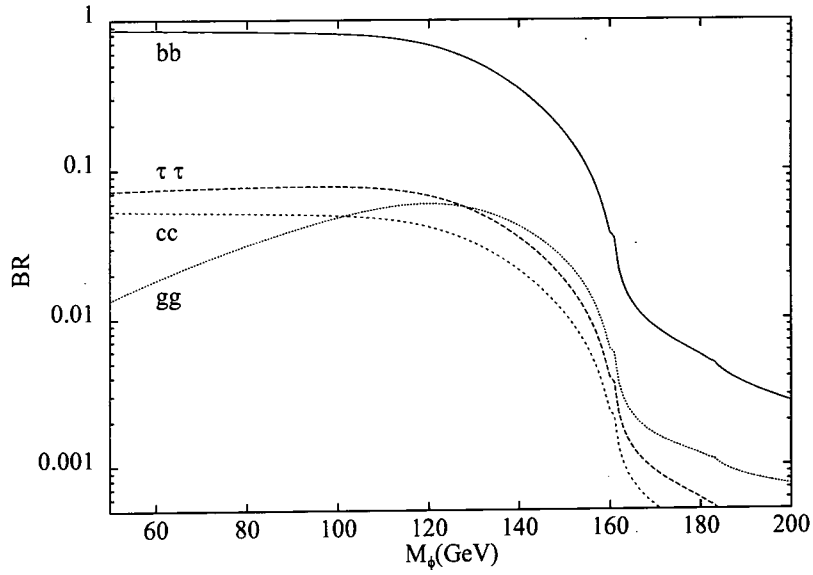

Figure 3.6: BRs of ϕ^0 (from Ref. [19]).

3.5 Production Processes at LEP2

LEP2 is an e^+e^- collider at CERN, Geneva, and is expected to attain a centre of mass energy of $\sqrt{s} = 192$ GeV in 1998. An integrated luminosity of $\mathcal{L} = 500$ pb^{-1} is anticipated.

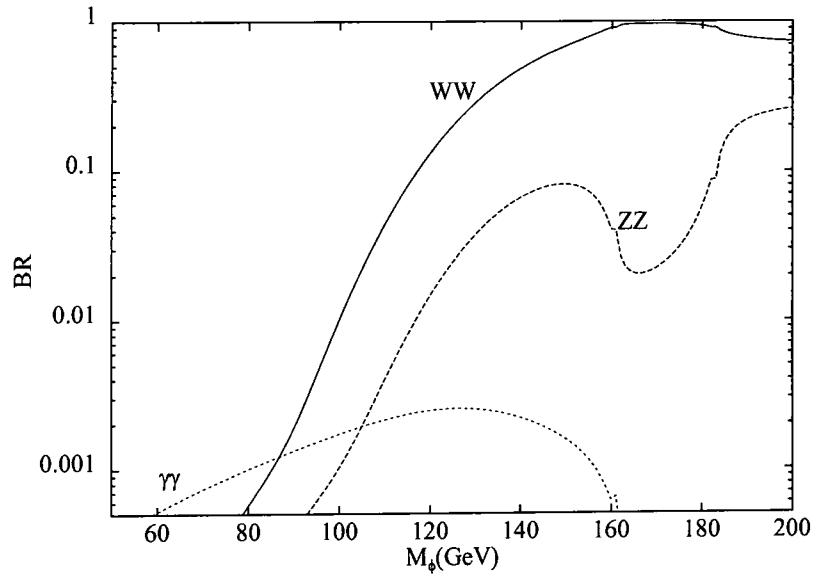

Figure 3.7: BRs of ϕ^0 (from Ref. [19]).

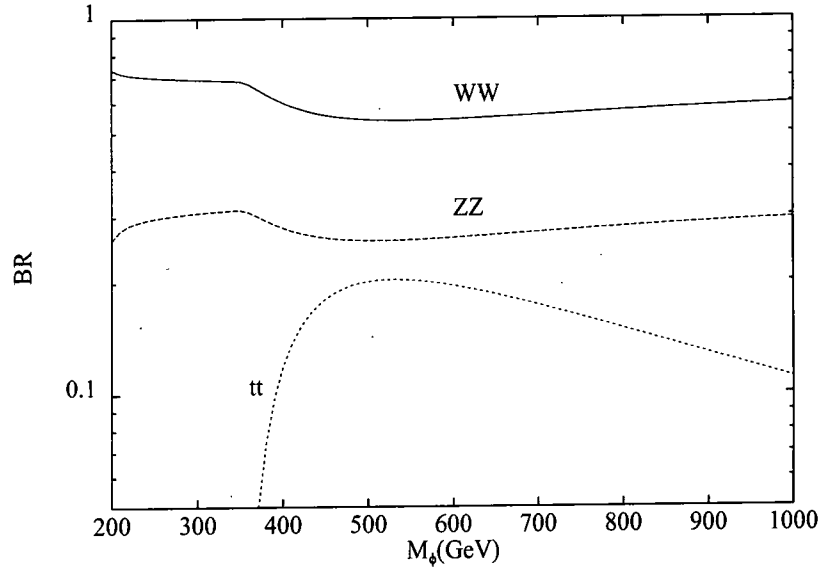

Figure 3.8: BRs of ϕ^0 (from Ref. [19]).

gg

The collider is an upgraded version of LEP which has been taking data since 1987. In this section we shall consider the various production channels for ϕ^0 at LEP2.

The main mechanism for the production of ϕ^0 at LEP2 will be the Higgs–strahlung process [20]

$$e^+e^- \to Z^* \to Z\phi^0 . \tag{3.18}$$

The WW fusion process [21],

$$e^+e^- \to \nu_e\overline{\nu}_e\phi^0 , \tag{3.19}$$

has a much smaller cross–section at LEP2 energies, mainly due to the extra suppression of an additional power of the electroweak coupling.

The cross–section for the Higgs–strahlung process can be written as

$$\sigma(e^+e^- \to Z\phi^0) = \frac{G_F^2 M_Z^4}{96\pi s}(v_e^2 + a_e^2)\lambda^{\frac{1}{2}}\frac{\lambda + 12M_Z^2/s}{(1 - M_Z^2/s)^2} , \tag{3.20}$$

where $\sqrt{s}$ is the centre of mass energy, and $a_e = -1$, $v_e = -1 + 4s_w^2$ are the Z couplings to the electron; $\lambda = (1 - M_{\phi^0}^2/s - M_Z^2/s)^2 - 4M_{\phi^0}^2 M_Z^2/s^2$ is the usual two–particle phase space function. The genuine electroweak corrections [22] are small at the LEP2 energy, being less than 1.5%. Photon radiation [23] affects the cross–section more. The variation of the cross–section with M_{ϕ^0} is shown in Figure 3.9 for two values of the collider energy [10].

3.6 Experimental Search at LEP2

Experimental simulations have been carried out for four channels, which together account for more than 90% of the possible final states for ϕ^0 in the range of LEP2.

(i) The 'missing mass' or leptonic channel: $Z \to e^+e^-$; $\mu^+\mu^-$, $\phi^0 \to$ anything.

(ii) The $\tau^+\tau^- q\overline{q}$ channel: $Z \to \tau^+\tau^-$, $\phi^0 \to$ hadrons and vice versa.

(iii) The missing energy channel: $Z \to \nu\overline{\nu}$, $\phi^0 \to$ hadrons.

(iv) The four–jet channel: $Z \to$ hadrons, $\phi^0 \to b\overline{b}$.

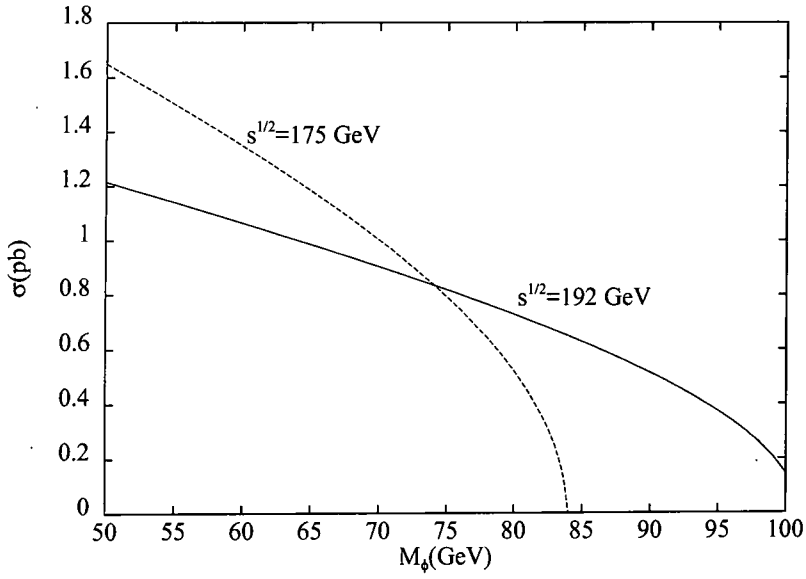

Figure 3.9: Production cross–section of the process $e^+e^- \to Z^* \to Z\phi^0$ (from Ref. [19]).

All important backgrounds have been considered in the analysis, and whose magnitudes before cuts are displayed in Table 3.1 [10].

	$\sqrt{s} = 175$ GeV	$\sqrt{s} = 192$ GeV	$\sqrt{s} = 205$ GeV
$e^+e^- \to ff$	173.4	135.5	116.5
$e^+e^- \to WW$	14.63	17.74	18.07
$e^+e^- \to ZZ$	0.45	1.20	1.43
$e^+e^- \to Ze^+e^-$	2.75	2.93	3.05
$e^+e^- \to We\nu$	0.68	0.90	1.10
$e^+e^- \to Z\nu\overline{\nu}$	0.011	0.015	0.020
$\gamma\gamma \to ff$	22.3	24.9	26.3

Table 3.1: Principal backgrounds (in pb) for ϕ^0 searches at LEP2 (from Ref. [10].

We shall now consider in turn the aforementioned channels for which simulations have been carried out. The event numbers in the specific channels will be given in later chapters, when the signals for non–minimal Higgs bosons will be compared with the signal for ϕ^0.

(a) The four jet topology arises when the Z decays into quarks (70% of the time) and ϕ^0 decays into quarks (90% of the time). This is the most common final state for the Higgs–strahlung process, occurring 65% of the time. Unfortunately the 4–jet signal is plagued by backgrounds from multijet events originating from $e^+e^- \rightarrow q\overline{q}$, WW and ZZ production e.g. see Table 3.1.

Only events with an invariant mass of one pair of jets consistent with M_Z are kept. Events consistent with $e^+e^- \rightarrow W^+W^-$ are rejected, i.e. two pairs of jets consistent with the W mass. These requirements are not sufficient to bring the background to a manageable level. It is necessary to exploit the $b\overline{b}$ decays of ϕ^0 with b–tagging methods in order to substantially reduce this background. This is possible by using a microvertex detector which enables secondary vertices and large impact parameters to be resolved. By requiring identified b jets in the final state the background can be reduced below the signal, resulting in good detection chances for this channel.

(b) The missing energy channel occurs in 18% of the cases, the topology being an acoplanar pair of b jets with invariant mass M_{ϕ^0}, accompanied by large missing energy and missing mass, close to the M_Z. These requirements strongly suppress any 4–jet backgrounds from $e^+e^- \rightarrow q\overline{q}$, WW or ZZ (no missing p_T), backgrounds from $q\overline{q}(\gamma)$, $WW \rightarrow l\nu +$ 2 jets, Ze^+e^- (no missing mass and isolated particles) etc. The main background comes from the processes $ZZ \rightarrow b\overline{b}\nu\overline{\nu}$ and $Z\nu\overline{\nu}$ with subsequent decay $Z \rightarrow b\overline{b}$. With b–tagging requirements a reasonable signal to background ratio can be obtained.

(c) The leptonic channel occurs in only 6.7% of the cases, although the backgrounds (both reducible and irreducible are smaller than in the above cases). The event selection criteria are a high mass pair of energetic, isolated and thus well identifiable leptons (e or μ), in conjunction with a high multiplicity hadron system. There are two irreducible backgrounds: $e^+e^- \rightarrow ZZ$, with $ZZ \rightarrow llq\overline{q}$, and $e^+e^- \rightarrow Ze^+e^-$. If $M_{\phi^0} \approx M_Z$ then a mild b–tagging requirement can be imposed to improve the signal to background ratio. The Higgs would manifest itself as a missing mass recoiling to the lepton pair. A clear peak would be obtainable unless $M_{\phi^0} \approx M_Z$, in which the aforementioned b–tagging may be applied.

(d) The $\tau\tau q\overline{q}$ channel occurs in 9% of the cases. It proceeds in two ways: $Z \to \tau^+\tau^-$, $\phi^0 \to q\overline{q}$ (3% of the time) and $\phi^0 \to \tau^+\tau^-$, $Z \to q\overline{q}$ (6% of the time). The topology is two energetic, isolated tau leptons, which are defined as 1- or 3 prong slim jets with masses comparable to m_τ, not identified as an electron or muon pair, and associated with a high multiplicity hadron system. The only irreducible background is $e^+e^- \to ZZ \to \tau\tau q\overline{q}$. The Higgs boson would be observed as an accumulation around (M_Z, M_{ϕ^0}) in a two–dimensional distribution of these masses. A reasonable signal to background ratio can be obtained even when $M_\phi \approx M_Z$, which can be improved if a b–tagging requirement is imposed although with the result of a large loss in signal size.

In conclusion we display in Table 3.2 [10] the minimum luminosity needed to discover (5σ signal) or exclude (95% C.L.) ϕ^0 for given values of $\sqrt{s}$ and M_{ϕ^0}.

	Exclusion:		Discovery:	
$\sqrt{s}$ (GeV)	M_{ϕ^0} (GeV)	$\mathcal{L}_{min}$ (pb^{-1})	M_{ϕ^0} (GeV)	$\mathcal{L}_{min}$ (pb^{-1})
175	83	75	82	150
192	98	150	95	150
205	112	200	108	300

Table 3.2: The minimum luminosity needed to discover (5σ signal) or exclude (95% C.L.) ϕ^0 for given values of $\sqrt{s}$ and M_{ϕ^0} (from Ref. [10]).

3.7 Production Processes at the LHC

The LHC is a pp collider with expected centre of mass energy $\sqrt{s} = 14$ TeV, and integrated luminosity $10 \to 100$ fb^{-1}. The production processes at hadron colliders [24] are considerably different to those at an e^+e^- collider, and the backgrounds to searches for the Higgs are more severe. As we shall see the quark decays of ϕ^0, although sometimes the dominant decays, do not present statistically significant signals, and it is necessary to exploit rare decay channels which allow superior signal to background ratios. The main production processes are [24] :

(i) Gluon–gluon fusion: $gg \rightarrow \phi^0$.

(ii) Vector boson fusion: $qq \rightarrow \phi^0 qq$.

(iii) Associated W, Z production: $q\overline{q} \rightarrow W\phi^0$, $Z\phi^0$.

(iv) Associated production with $t\overline{t}$: gg, $q\overline{q} \rightarrow t\overline{t}\phi^0$.

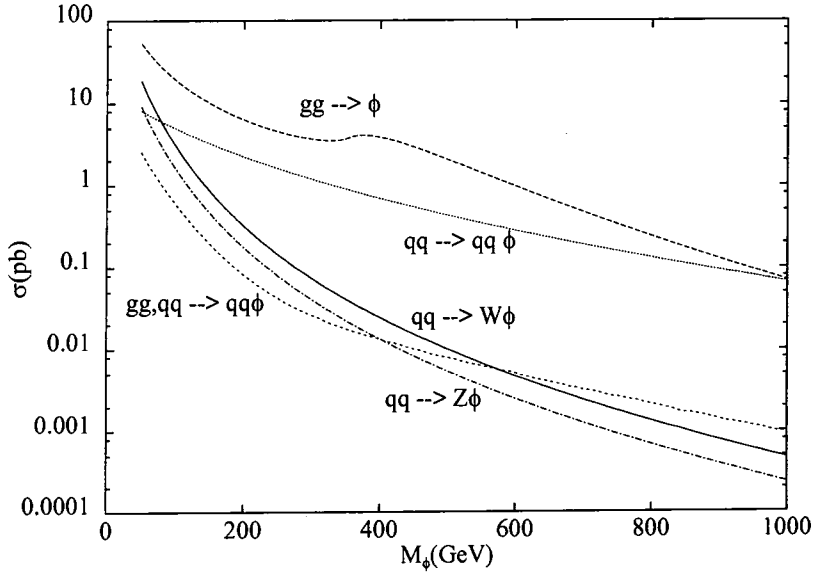

Figure 3.10: Production cross–sections of ϕ^0 at the LHC.

All cross–sections are displayed in Figure 3.10 as a function of M_{ϕ^0} for $\sqrt{s} = 14$ TeV. Gluon–gluon fusion [25] proceeds via a top quark loop and the cross–section increases with increasing m_t. It is the dominant process mainly due to the large value of m_t. Vector boson fusion [26] is the next largest channel, becoming roughly equal to the gg fusion process for larger values of M_{ϕ^0}. The cross–sections for the associated production with W and Z bosons [27] are not large but may be useful for detecting an intermediate mass Higgs if high luminosity is possible, since the Higgs can be tagged by triggering on the lepton decay of the vector boson. The cross–section associated with the W is larger than that associated with the Z due to the stronger coupling of the former to $q\overline{q}$. Associated

production with top quarks [28] depends sensitively on m_t. Larger m_t is favourable from the point of view of the Higgs–top quark coupling, although there will be some kinematical suppression from producing a heavier final state.

3.8 Experimental Search at the LHC

The three channels that offer the best chance of discovery are:

(i) $gg \rightarrow \phi^0 \rightarrow \gamma\gamma$.

(ii) $gg \rightarrow \phi^0 \rightarrow ZZ^{(*)} \rightarrow llll$.

(iii) $q\overline{q} \rightarrow W\phi^0 \rightarrow l\gamma\gamma X$; $gg, q\overline{q} \rightarrow t\overline{t}\phi^0 \rightarrow l\gamma\gamma X$.

These channels will be considered again in later chapters in the context of non–minimal Higgs sectors. Therefore we shall delay displaying the expected event numbers for ϕ^0, and present them later in order to give a direct comparison with the signal from non–minimal Higgs sectors). For now we shall give an outline of the selection process. The following analysis is taken from the ATLAS studies [11]→ [14], [29]. which have simulated the above three channels.

3.8.1 $gg \rightarrow \phi^0 \rightarrow \gamma\gamma$

This process [11], [12], [29] is to be used for the range 100 GeV$\leq M_{\phi^0} \leq$ 150 GeV. It exploits the rare decay $\phi^0 \rightarrow \gamma\gamma$ and despite the low branching ratio (BR=0.1% → 0.2%) it has the advantage of a strongly suppressed QCD background. The irreducible backgrounds consist of the Born ($q\overline{q} \rightarrow \gamma\gamma$), box ($gg \rightarrow \gamma\gamma$) and bremsstrahlung ($qg \rightarrow q\gamma \rightarrow q\gamma\gamma$) processes. Reducible backgrounds include jet–jet and γ–jet events in which one or both jets are mistaken as photons, as well as $Z \rightarrow e^+e^-$ decays which fake photons. The cross–sections of these reducible backgrounds are many orders of magnitude larger than than the signal cross–sections and so excellent photon identification is required.

Signal events were counted in a mass bin of $m \pm 1.4\sigma_m$ (defined in Eq. (3.21)),

$$\sigma_m = \sqrt{(\Gamma_{\phi^0}/2.36)^2 + (0.02M_{\phi^0})^2}\,, \tag{3.21}$$

which contains approximately 80% of the total signal. The criteria for the signal are two photons, satisfying respectively $p_T \geq 40$ GeV and $p_T \geq 25$ GeV, $|\eta| \leq 2.5$. Additional contributions to the signal will come from the other Higgs production processes (with $\phi^0 \rightarrow \gamma\gamma$) although the dominant contribution is from gluon–gluon fusion. The reducible background is potentially dangerous. The ATLAS reports study jet events faking photons which pass the same cuts as those applied to the signal. The ratio of the jet–jet and γ–jet cross–sections to the irreducible $\gamma\gamma$ cross–section was found to be 2×10^6 and 10^3 respectively. Therefore rejection powers of up to 2×10^7 and 10^4 respectively are needed to bring the reducible background to less than 20% of the irreducible background.

The background from $Z \rightarrow e^+e^-$ decays, with the electrons faking photons must also be considered. An electron veto efficiency of 99.8% is needed to bring this background to less than 10% of the signal size.

3.8.2 $gg \rightarrow \phi^0 \rightarrow ZZ^{(*)} \rightarrow llll.$

This channel is often dubbed the 'gold plated' channel [11], [12]. The signal appears as a peak in the invariant 4–lepton mass distribution above a background that is small. The dominant backgrounds are the irreducible $ZZ^{(*)}/Z\gamma^*$ and the reducible $t\bar{t}$ and $Zb\bar{b}$. The process $q\overline{q}$, $gg \rightarrow ZZ^{(*)}/Z\gamma^* \rightarrow llll$ has a small cross–section but is irreducible. The reducible backgrounds have very large cross–sections. This channel can be used if $M_{\phi^0} \geq 2M_Z$ (in which case both Z bosons will be on–shell) and also if $M_{\phi^0} < 2M_Z$ (one Z boson being off–shell). For the latter case the irreducible continuum is dominated in the 4–electron channel by the contributions from the virtual photons, $Z\gamma^*$, which can be greatly reduced by requiring that the dilepton mass corresponding to the off–shell particle (Z^* or γ^*) be larger than a certain threshold. All the signal and background events are collected in a mass bin of $\pm 2\sigma_m$ around M_{ϕ^0}. The reducible background is expected to be at a level well below that of the irreducible background. A statistically significant signal is possible for $M_{\phi^0} \geq 130$ GeV, and we shall present the detailed event table in a later chapter.

For 180 GeV$\leq M_{\phi^0} \leq$ 800 GeV the $\phi^0 \rightarrow llll$ channel is most promising way of searching for ϕ^0 at the LHC. As M_{ϕ^0} increases, the width grows rapidly and so does the momenta of the leptons to be detected. Two lepton candidates are required to have $p_T \geq 20$ GeV, and the remaining two are requested to satisfy $p_T \geq 7$ GeV, and to be within $|\eta| \leq 2.5$. The variable Higgs mass bin (Eq. (3.21)) is used because the Higgs width changes rapidly over the range being considered. A signal acceptance of 95%(90%) was assumed for a mass bin $M_{\phi^0} \pm 2\sigma_m(\pm 1.64\sigma_m)$. Due to the Z bosons from ϕ^0 decay being produced by the 2–body decay of a heavy object, one can achieve a significant background rejection by requiring that the transverse momentum of the Z bosons is larger than a given threshold.

3.8.3 $q\bar{q} \rightarrow W\phi^0 \rightarrow l\gamma\gamma X$; $gg, q\bar{q} \rightarrow t\bar{t}\phi^0 \rightarrow l\gamma\gamma X$.

Selected here is a $\gamma\gamma$ event with an isolated lepton [11], [29]. Smaller backgrounds are present than in the $\gamma\gamma$ channel, although the production cross–section is also smaller since the gg fusion is not relevant. The lepton originates either from $W^{\pm}$ decay in the process $pp \rightarrow W^* \rightarrow W\phi^0$, or from $t \rightarrow Wb \rightarrow l\nu_l b$ in the process $pp \rightarrow t\bar{t}\phi^0$. For the signal it is demanded that p_T(lepton) > 25 GeV, $p_T(\gamma) > 25$ GeV $|\eta| < 2.0$. The size of the mass bin is taken as the same as in the $\gamma\gamma$ channel.

For the background there are irreducible contributions from $W\gamma\gamma$ and $t\bar{t}\gamma\gamma$. Reducible backgrounds originate from a variety of sources and include:

(a) $b\bar{b}\gamma\gamma$ with $b\bar{b} \rightarrow lX$.

(b) $t\bar{t}$ with two jets faking photons and $t\bar{t} \rightarrow lX$.

(c) $W\gamma$ with $W \rightarrow l\nu_l\gamma$.

(d) $Z\gamma$ with $Z \rightarrow l\bar{l}\gamma$.

Other backgrounds, which include jets faking photons and leptons, were shown to be negligible by the ATLAS studies if one assumes rejection factors of 1000 for a jet

faking a photon, 7 for an isolated lepton from b decay and 10^5 for a jet faking lepton. The backgrounds from processes c) and d) can be reduced by demanding that $|M(\text{lepton, photon}) - M(Z)| > 10$ GeV for each photon, and $M(\text{lepton, photon}) > 25$ GeV for each photon. A reasonable signal to background ratio can be obtained in this channel although the signal number is not large.

Chapter 4

Non–minimal Higgs Sectors

4.1 Introduction

Thus far we have described the properties and phenomenology of ϕ^0, the single neutral Higgs boson predicted by the minimal SM. Such a particle is a remnant of the electroweak–symmetry breaking mechanism of adding a $T = 1/2$, $Y = 1$ scalar doublet to the Lagrangian with the neutral Higgs field chosen to have a VEV of magnitude $v/\sqrt{2}$. So far no such Higgs particle has been discovered, and this null–result is usually attributed to the fact that ϕ^0 is too heavy to be produced in sufficient quantities. Due to the lack of experimental evidence for ϕ^0 it is clearly prudent to explore other ways in which Higgs scalars can break the electroweak symmetry [30]; such studies will be of importance to experimentalists.

When constructing an extended Higgs sector one must not violate current experimental precision measurements. The two major experimental constraints on any Higgs sector are:

(i) The measured value of the ρ parameter, $\rho = M_W^2/M_Z^2 \cos^2\theta_W$, must be very close to 1.

(ii) There must be strong suppression of flavour changing neutral currents (FCNCs).

In the minimal SM both these requirements are obeyed. The ρ parameter is found to be exactly equal to 1 at tree–level (see Eqs. (2.23), (2.24) and (2.27)). Radiative

corrections are usually small and will be discussed shortly. The suppression of FCNCs is also predicted since the operations that diagonalize the mass matrix automatically diagonalize Higgs–fermion couplings (Eq. (2.38)). Any non–minimal Higgs sector will also be required to break the $SU(2)_L \times U(1)_Y$ symmetry down to $U(1)_Q$, to provide masses for fermions, and to preserve unitarity in vector boson scattering at high energies. We shall see that all these requirements can be fulfilled in non–minimal models, and thus such models are both theoretically and experimentally viable. The only 'criticism' would be that they enlarge the Higgs sector and thus introduce new unknown parameters such as Higgs masses and mixing angles. However, this 'criticism' is in my opinion rather hollow and unfair. It is true that one should strive for the simplest theory, with the least number of arbitrary parameters, but nature may not be in accordance with this conjecture. The SM is the current most compatible theory and this contains many arbitrary parameters; well–motivated extensions (such as supersymmetry, left–right symmetric models) nearly always require enlarged Higgs sectors, extra gauge particles etc, and so it would seem that introducing new particles/parameters is not so unaesthetic. Such introductions cancel divergences, keep theories self–consistent, and also enable other desirable features to be realized (e.g. extra CP violating phases). In this thesis we shall be advocating the study of non–minimal Higgs sectors since we believe that such a structure will be present if/when an improved version of the SM is found.

4.2 The Structure of Non–minimal Higgs Models

Thus far we have referred to 'non–minimal Higgs sectors'. What structure would these models take? What quantum numbers would the new particles possess? The main constraint on the possible quantum numbers of a non–minimal Higgs representation comes from the ρ parameter. The general formula at tree level is given by:

$$\rho = \frac{M_W^2}{M_Z^2 \cos^2\theta_W} = \frac{\sum_{T,Y}[4T(T+1) - Y^2]|V_{T,Y}|^2 c_{T,Y}}{\sum_{T,Y} 2Y^2 |V_{T,Y}|^2} \,. \tag{4.1}$$

Here $V_{T,Y}$ is the vacuum expectation value of the neutral Higgs field member of the particular representation with total isospin T and hypercharge Y. The parameter $c_{T,Y}$ is 1 (1/2) for a complex (real) representation. This formula is derived from considering the

Higgs boson interaction with the gauge bosons which is given by the kinetic energy part of the Lagrangian. The relevant term is:

$$\left|\frac{g}{\sqrt{2}}(T^+W_\mu^+ + T^-W_\mu^-)\phi_0^i + (gT^3W_\mu^3 + \frac{g'}{\sqrt{2}}YB_\mu)\phi_0^i\right|^2 . \tag{4.2}$$

The symbols are defined in Chapter 2, with ϕ_0^i defined by

$$\phi_0^i = \begin{pmatrix} 0 \\ v_i \end{pmatrix} , \tag{4.3}$$

i.e. v_i is the VEV of the particular representation ϕ^i. From Eq. (4.2) one can obtain the relationship in Eq. (4.1), noting that for a neutral scalar $T^3 = Y/2$.

One can see that $\rho = 1$ requires (assuming $c = 1$)

$$(2T+1)^2 - 3Y^2 = 1 . \tag{4.4}$$

The simplest non–trivial solution to this equation is provided by $Y = \pm 1$, $T = 1/2$ doublets. Note that any number of doublets with these quantum numbers will satisfy $\rho = 1$, with the minimal SM possessing one such doublet. The trivial solution ($T = Y = 0$) is also possible (together with at least one doublet representation) and corresponds to neutral Higgs isospin singlet fields; these representations will not be discussed in this thesis. The next highest representation that satisfies Eq. (4.4) possesses $T = 3$ and $Y = \pm 4$, although this possibility is not usually pursued due to its complexity.

Thus far we have considered the tree–level prediction of ρ. One–loop corrections originate from virtual fermion loops affecting the gauge boson propagators. The contribution of a fermion doublet (U, D) to ρ is given by [31]:

$$\frac{\Delta\rho}{\rho} = \frac{g^2 N_c}{64\pi^2 M_W^2}\left[m_U^2 + m_D^2 - \frac{2m_U^2 m_D^2}{m_U^2 - m_D^2}\ln\left(\frac{m_U^2}{m_D^2}\right)\right] . \tag{4.5}$$

This correction is always positive and grows in magnitude with increasing mass splitting. If $m_U = m_D$ then $\Delta\rho = 0$. We recall that the current measured value is $\rho = 1.0004 \pm 0.0022 \pm 0.002$ [32], and so constraints on the mass splitting of any heavy fermion doublet can be obtained. With the current values of $m_t = 174$ GeV and $m_b = 4.5$ GeV we find $\frac{\Delta\rho}{\rho} = 0.0094$. This is a 3σ deviation, although it is possible that extra Higgs bosons

and/or new physics would contribute with negative $\Delta\rho$. For ϕ^0 the contribution to $\Delta\rho$ in the limit of a large Higgs mass is of the form [33]

$$\Delta\rho^{\text{Higgs}} \sim \ln \frac{M^2_{\phi^0}}{M^2_W}, \tag{4.6}$$

and thus being a logarithmic dependence $\Delta\rho^{\text{Higgs}}$ is not sizeable. Corrections to ρ from extended Higgs models will be discussed later.

One can see from Eq. (4.4) that Higgs representations other than doublets and singlets would cause deviations from $\rho = 1$ at tree–level. To show this let us consider the next simplest representation which is a triplet ($T = 1$). In order to have a neutral member, one is only allowed to have hypercharge values of $Y = 0, \pm 2$, and from Eq. (4.4) it is clear that $\rho = 1$ is not satisfied. However, it is still possible to avoid this problem by a number of means. Consider the case of a doublet together with a triplet. The requirement of $\rho \approx 1$ can be obtained if the vacuum expectation value (VEV) of the triplet is very small compared to that of the doublet. Given the above experimental measurement of ρ, we find that

$$|V_{1,Y}|/|V_{1/2,1}| \leq 0.03\,, \tag{4.7}$$

with $Y = 0, \pm 2$. Therefore the triplet would play a very minor role in electroweak symmetry breaking. An alternative idea would be to combine two or more triplet representations with a doublet, so arranged that the contributions to ρ from the triplets cancel, preserving $\rho = 1$ at tree–level. We shall be discussing a model of this nature in more detail in Chapter 7.

The conclusion of the above analysis is that extended models which include only combinations of doublets and singlets (with at least one doublet representation) most naturally keep $\rho = 1$ at tree–level, although higher representations are also possible. With this in mind, the bulk of this thesis considers extensions of the Higgs sector which only include doublets.

We have studied the restrictions on the nature of the Higgs representation from considering the ρ parameter. Another constraint with which we must comply is the experimental fact that flavour changing neutral currents (FCNCs) are rare, and a sensible theory should provide a way of suppressing these interactions. In the minimal SM the GIM mechanism

eliminates FCNCs at tree–level mediated by Z bosons. In the minimal SM Higgs sector, FCNCs mediated by ϕ^0 are also absent at tree–level due to the fact that the operations which diagonalize the fermion mass matrix simultaneously diagonalize the Higgs–fermion couplings. This was shown explicitly in Eq. (2.38). However, this result ceases to be true for a non–minimal model of k Higgs doublets. In this case the Eq. (2.38) must be changed to

$$M_{ij}^U = \sum_k g_{ijk}^U \frac{v_k}{\sqrt{2}}, \quad M_{ij}^D = \sum_k g_{ijk}^D \frac{v_k}{\sqrt{2}}. \tag{4.8}$$

Clearly when M_{ij} is diagonal, g_{ijk} need not be. Therefore in general one would expect FCNCs in a non–minimal Higgs model with k doublets. An elegant way of keeping FCNCs suppressed is to request that a given fermion type (either up or down) must not couple to more than one Higgs doublet [34]. After imposing this condition the Yukawa couplings are constrained but not unique. We shall see that in a model with two Higgs doublets there exist four distinct versions which only differ in their Yukawa couplings [35].

The final constraint is that of unitarity. We saw earlier that ϕ^0 cancels the bad high energy behaviour in vector boson scattering and so any non–minimal Higgs model is required to reproduce these results. This is possible if the following sum rules are obeyed, with h_i^0 denoting a neutral Higgs boson [36]:

$$\sum_i g_{h_i^0 VV}^2 = g_{\phi^0 VV}^2 \tag{4.9}$$

and

$$\sum_i g_{h_i^0 VV} g_{h_i^0 f\overline{f}} = g_{\phi^0 VV} g_{\phi^0 f\overline{f}}. \tag{4.10}$$

The above equations originate from considering the scattering processes $V_L V_L \to V_L V_L$ and $f_+ \overline{f}_+$ respectively. These sum rules are only appropriate for representations consisting of doublets or singlets. For higher isospin representations there are no simple sum rules. This is because the spectrum of Higgs particles will be more exotic in nature and extra Feynman diagrams will contribute to the above scattering processes, and thus the Higgs bosons will not all contribute in the same channels. Insisting that the unitarity bound is not violated constrains $M_{\phi^0} \leq 700$ GeV. One would expect a mass bound to be obtained in a non–minimal model as well. It can be shown that at least one neutral scalar must have a mass less than 700 GeV, otherwise unitarity will be violated. If the mass of a

neutral scalar is close to this value then this particle must approximately saturate the sum rules above. The remaining neutral Higgs bosons may be much heavier than 1 TeV, and very weakly coupled to vector bosons.

In this section we have discussed that non–minimal Higgs models may certainly be considered. They reproduce all the desirable properties of ϕ^0, differing only in the Higgs particle spectrum. In the the next section we shall focus on the two–Higgs–doublet model (2HDM) which is the minimal extension of the Higgs sector.

4.3 The Two–Higgs–Doublet Model

The 2HDM consists of two complex $SU(2)_L$ doublet scalar fields, ϕ_1 and ϕ_2. The Higgs potential is still required to spontaneously break $SU(2)_L \times U(1)_Y$ down to $U(1)_Q$, and its most general form can be written as [30]:

$$\begin{aligned} V(\phi_1,\ \phi_2) = \lambda_1(\phi_1^\dagger\phi_1 - v_1^2)^2 + \lambda_2(\phi_2^\dagger\phi_2 - v_2^2)^2 \\ \lambda_3\left[(\phi_1^\dagger\phi_1 - v_1^2) + (\phi_2^\dagger\phi_2 - v_2^2)\right]^2 \\ \lambda_4\left[(\phi_1^\dagger\phi_1)(\phi_2^\dagger\phi_2) - (\phi_1^\dagger\phi_2)(\phi_2^\dagger\phi_1)\right] \\ +\lambda_5\left[Re(\phi_1^\dagger\phi_2) - v_1v_2\right]^2 \\ +\lambda_6\left[Im(\phi_1^\dagger\phi_2)\right]^2 . \end{aligned} \tag{4.11}$$

Here λ_i are all real, non–negative parameters. This potential is the most general one subject to gauge invariance and a discrete symmetry, $\phi_1 \rightarrow -\phi_1$, which is only softly violated (by terms of dimension two). This latter symmetry ensures that there is a strong suppression of Higgs mediated FCNCs. The minimum of this potential is at

$$< \phi_1 >= \begin{pmatrix} 0 \\ v_1/\sqrt{2} \end{pmatrix}, \quad < \phi_2 >= \begin{pmatrix} 0 \\ v_2/\sqrt{2} \end{pmatrix} . \tag{4.12}$$

Thus we have the equivalent of a 'Mexican hat' potential, but now as a function of two complex fields, ϕ_1 and ϕ_2, each possessing a VEV. An important parameter is the ratio of the VEVs

$$\tan\beta = \frac{v_2}{v_1}, \tag{4.13}$$

We shall see that $\tan\beta$ plays a significant rôle in the phenomenology of the 2HDM, and in principle can take any value from $0 \rightarrow \infty$. Eight scalar degrees of freedom have been input by introducing two complex Higgs doublets; four carry charge and four are neutral. Three degrees of freedom are required to provide mass for the W^+, W^- and Z. Therefore five remain and manifest themselves as physical particles. The charged goldstone boson is

$$G^{\pm} = \phi_1^{\pm}\cos\beta + \phi_2^{\pm}\sin\beta\,, \tag{4.14}$$

and the physical charged Higgs particle is

$$H^{\pm} = -\phi_1^{\pm}\sin\beta + \phi_2^{\pm}\cos\beta\,, \tag{4.15}$$

with mass $M_{H^{\pm}}^2 = \lambda_4(v_1^2 + v_2^2)$. Since we are assuming CP–invariance the imaginary and neutral parts of the neutral scalar fields decouple. The neutral Goldstone boson is

$$G^0 = \sqrt{2}(Im\phi_1^0\cos\beta + Im\phi_2^0\sin\beta)\,, \tag{4.16}$$

and the neutral physical state is

$$A^0 = \sqrt{2}(-Im\phi_1^0\sin\beta + Im\phi_2^0\cos\beta)\,, \tag{4.17}$$

with mass $M_{A^0}^2 = \lambda_6(v_1^2 + v_2^2)$. The real (CP–even) sector contains two physical Higgs scalars which mix through the following mass–squared matrix:

$$M = \begin{pmatrix} 4v_1^2(\lambda_1+\lambda_3) + v_2^2\lambda_5 & (4\lambda_3+\lambda_5)v_1v_2 \\ (4\lambda_3+\lambda_5)v_1v_2 & 4v_2^2(\lambda_2+\lambda_3) + v_1^2\lambda_5 \end{pmatrix} v^2\,. \tag{4.18}$$

Therefore the 2HDM contains five physical Higgs bosons. A charged pair ($H^{\pm}$); two neutral CP–even scalars (H^0 and h^0 with $M_{H^0} \geq M_{h^0}$); a neutral, CP–odd scalar (A^0), frequently labelled as the 'pseudoscalar'. The four masses are all free parameters, being linked to the λ parameters in the Higgs potential. Also arbitrary are β and α. The VEVs v_1 and v_2 satisfy

$$v_1^2 + v_2^2 = v^2 = (246\text{ GeV})^2. \tag{4.19}$$

This latter relationship is required since $M_W^2 = g^2(v_1^2+v_2^2)/2$ in this model; by comparison with $M_W^2 = g^2v^2/2$, which is the result from the minimal SM, Eq. (4.19) follows easily.

We now investigate the C and P quantum numbers of the Higgs bosons. These quantum numbers will explain the absence of certain couplings. The bosonic sector conserves

C and P separately if the fermions are not included, and thus unique values for these quantum numbers can be assigned. With the inclusion of the fermions CP is still a good symmetry but C and P are not separately conserved. The assignments are shown in Table 4.1.

	J^{PC}		J^P
γ	1^{--}	$W^{\pm}$	$1^-\ 1^+$
Z	$1^{--}, 1^{++}$	$H^{\pm}$	$0^+\ 0^-$
H^0	$0^{--}, 0^{++}$		
h^0	$0^{--}, 0^{++}$		
A^0	$0^{+-}, 0^{+-}$		

Table 4.1: The C and P values of the bosons.

The quantum number assignments for A^0 explain why there is no tree–level coupling to vector boson pairs.

The couplings of the neutral Higgs bosons to W^+W^- and ZZ are automatically forced to obey the sum rule given in Eq. (4.9). Therefore we require

$$g^2_{h^0VV} + g^2_{H^0VV} = g^2_{\phi^0VV} \tag{4.20}$$

for both $V = W$ and Z. By expanding out the covariant derivative, $\sum_i (D_\mu \phi_i)^\dagger (D^\mu \phi_i)$, one finds the following couplings:

$$\begin{aligned} \frac{g_{h^0VV}}{g_{\phi^0VV}} &= \sin(\beta - \alpha), \\ \frac{g_{H^0VV}}{g_{\phi^0VV}} &= \cos(\beta - \alpha), \end{aligned} \tag{4.21}$$

and so the sum rule is obeyed.

Next we analyse the Higgs–fermion couplings. These are not unique in the 2HDM since there is some freedom in how the Higgs doublets are coupled to the fermions. Even after demanding natural flavour conservation, which involves the imposition of discrete symmetries such as $\phi_1 \to -\phi_1$, $\phi_2 \to \phi_2$, there still exist four distinct versions of the 2HDM.

Table 4.2 shows the four different ways with which the 2HDM can be coupled to the fermions (the Yukawa couplings) [35]. The numbers (1 or 2) show which Higgs doublet

	Model I	Model I′	Model II	Model II′
u (up–type quarks)	2	2	2	2
d (down–type quarks)	2	2	1	1
e (charged leptons)	2	1	1	2

Table 4.2: The four distinct structures of the 2HDM (from Ref. [35].

couples to which fermion type, with at most one Higgs doublet coupling to a particular fermion type. In Model I, one of the Higgs doublets decouples from the fermions. For Model II type couplings the Higgs–fermion part of the Lagrangian can be written as:

$$\begin{aligned}\mathcal{L} = &-\frac{g}{2M_W\cos\beta}\overline{D}M_D D(H^0\cos\alpha - h^0\sin\alpha) + \frac{ig\tan\beta}{2M_W}\overline{D}M_D\gamma_5 DA^0 \\ &-\frac{g}{2M_W\sin\beta}\overline{U}M_U U(H^0\sin\alpha + h^0\cos\alpha) + \frac{ig\cot\beta}{2M_W}\overline{U}M_U\gamma_5 UA^0 \\ &+\frac{g}{2\sqrt{2}M_W}(H^+\overline{U}[\cot\beta M_U K(1-\gamma_5) + \tan\beta K M_D(1+\gamma_5)]D + h.c). \qquad (4.22)\end{aligned}$$

Here U and D are column matrices consisting of the three generations of quarks, and K is the CKM matrix. The Higgs–lepton couplings may be obtained by replacing U and D by the corresponding lepton fields, changing the quark mass matrices to lepton mass matrices, and setting $K = 1$. Note that the mass matrices are diagonal and thus the neutral Higgs interactions do not cause FCNCs. The charged Higgs interactions involve the CKM matrix, as is the case for the W charged current interaction. The couplings of the non–minimal neutral Higgs bosons are scaled relative to those of ϕ^0 by trigonometric factors. Table 4.3 shows the couplings for h^0:

	Model I	Model I′	Model II	Model II′
$hu\overline{u}$	$\cos\alpha/\sin\beta$	$\cos\alpha/\sin\beta$	$\cos\alpha/\sin\beta$	$\cos\alpha/\sin\beta$
$hd\overline{d}$	$\cos\alpha/\sin\beta$	$\cos\alpha/\sin\beta$	$-\sin\alpha/\cos\beta$	$-\sin\alpha/\cos\beta$
$he\overline{e}$	$\cos\alpha/\sin\beta$	$-\sin\alpha/\cos\beta$	$-\sin\alpha/\cos\beta$	$\cos\alpha/\sin\beta$

Table 4.3: The fermion couplings of h^0 in the 2HDM relative to those for the minimal SM Higgs boson (ϕ^0).

For the heavier neutral CP–even H^0 one must replace $\sin\alpha$ by $-\cos\alpha$, and $\cos\alpha$ by $\sin\alpha$. Therefore there exists the possibility of significantly different couplings for h^0 and H^0 compared to those of ϕ^0. Note that once M_{ϕ^0} is fixed its cross–sections and

BRs are fixed. This is not the case for the 2HDM, whose couplings also depend on the extra parameters α and β. We shall be considering these possibilities in later chapters, and examining the differences in phenomenology will be a recurring theme of this thesis. Chapter 5 focuses on $H^{\pm}$ and so its couplings/phenomenology are discussed there. We shall not be considering the phenomenology of A^0. Its couplings to the fermions are scaled relative to ϕ^0 by a factor of $\tan\beta$ or $\cot\beta$ (depending on the model in question), although there is also an extra multiplicative γ_5 in the coupling. We note that all these Higgs–fermion couplings obey the unitarity sum rules quoted earlier.

4.3.1 One–loop corrections to ρ in the 2HDM

It was mentioned earlier that a major constraint on any non–minimal Higgs model is the experimental fact that $\rho \approx 1$. In the minimal SM, one loop corrections from ϕ^0 are small since they are logarithmic ($g^2 \ln\frac{M_{\phi^0}}{M_W}$) [37]. Additional contributions to the gauge boson propagators arise in the 2HDM from diagrams of the form displayed in Figure 4.1, where the internal loop is entirely of a scalar nature:

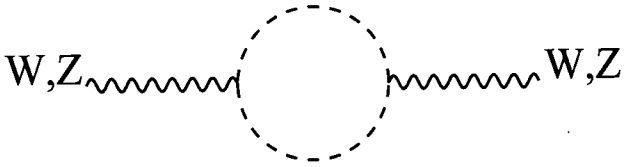

Figure 4.1: 2HDM corrections to the W and Z propagators.

For the $W^{\pm}$ the additional scalar loops will consist of $H^{\pm}A^0$, $H^{\pm}h^0$ and $H^{\pm}H^0$, in addition to the minimal SM type loops consisting of $W^{\pm}h^0$ and $W^{\pm}H^0$. For the Z the purely scalar internal loop consists of H^+H^-, h^0A^0 and H^0A^0, and the minimal SM type loops contain h^0Z and H^0Z. The contribution to ρ is labelled $\Delta\rho$ and is found to be [38]:

$$\Delta\rho = \frac{G_F}{8\pi^2\sqrt{2}}\left[\sin^2(\alpha-\beta)F(M^2_{H^{\pm}}, M^2_{A^0}, M^2_H) + \cos^2(\alpha-\beta)F(M^2_{H^{\pm}}, M^2_{A^0}, M^2_h)\right]. \tag{4.23}$$

where

$$F(a, b, c) = a - \frac{bc}{b-c}\ln\frac{b}{c} - \frac{ab}{a-b}\ln\frac{a}{b} - \frac{ac}{a-c}\ln\frac{a}{c}. \tag{4.24}$$

This contribution can be either positive or negative depending on the values of the Higgs boson masses. If the Higgs masses are ordered as

$$M_{H,h} \leq M_{H^\pm} \leq M_{A^0} \text{ or } M_{A^0} \leq M_{H^\pm} \leq M_{H,h} \tag{4.25}$$

then $\Delta\rho \leq 0$. If the charged Higgs is heavier or lighter than all of the neutral scalars then $\Delta\rho \geq 0$. Due to the top quark contribution to ρ being quite large, $\Delta\rho$ must be either small (if it is positive) or negative. The discovery of the top quark with mass of order 175 GeV means that the top quark correction to ρ is quite sizeable and so the contribution from a 2HDM is preferred to be negative.

4.4 The Minimal Supersymmetric SM

We mentioned at the beginning of this chapter that many extensions/improvements of the SM require an extended Higgs sector. The model of this type which has received the most attention in the literature is the minimal supersymmetric SM (MSSM) [39]. There are various good reasons for its popularity, one of which we now explain. It is desirable to embed the SM in a Grand–Unified Theory (GUT), but once this is done the one–loop corrections to the propagator of ϕ^0, mediated by heavy Higgs bosons which break the GUT symmetry, grow quadratically with the GUT scale:

$$\delta M^2_{\phi^0} = g^4 M_X^2 \approx 10^{24}\ (\text{GeV})^2\,, \tag{4.26}$$

where M_X is the mass of the heavy Higgs bosons. Thus to keep $M_{\phi^0} \leq 1$ TeV (which is required from various indirect constraints on M_{ϕ^0} explained in Chapter 3) the bare mass of ϕ^0 must be tuned to one part in 10^{12}, and this is very unnatural. In the supersymmetric SM one introduces a new super–particle (sparticle) for each particle. The sparticles have the same gauge quantum numbers as their partners but differ by $\frac{1}{2}$ a unit of spin. A consequence of these extra particles is that the aforementioned fine–tuning problem can be solved. To every fermion loop in the Higgs propagator one has an analogous boson (sparticle) loop, and vice versa. Thus one can show

$$\delta M^2_{\phi^0} = \frac{\alpha}{\pi}\left[\Lambda + O(m_b^2) - (\Lambda + O(m_f^2))\right] = \frac{\alpha}{\pi}\left|m_b^2 - m_f^2\right|\,, \tag{4.27}$$

and the one–loop corrections will be small if

$$\left|m_b^2 - m_f^2\right| < O(1\text{ TeV})^2 . \tag{4.28}$$

i.e. the masses of the supersymmetric particles should be of order 1 TeV. Thus the MSSM is a well motivated extension of the SM, and in addition to solving the fine–tuning problem it also allows for gauge coupling constant unification in SUSY-GUTS, and provides an attractive Dark Matter candidate – the lightest sparticle which is expected to be stable.

4.5 The Higgs structure of the MSSM

Supersymmetric theories keep Higgs bosons as elementary spin–0 particles [30], [39]. In this subsection we briefly review the Higgs sector of the MSSM and show that it is a constrained version of the general 2HDM described previously.

In the minimal SM one Higgs doublet is sufficient to provide the mass for the quarks and leptons. Down–type fermions are given mass by coupling to Φ while up–type quarks couple to $i\sigma_2\Phi^*$. Supersymmetric theories forbid the appearance of Φ^* and so one must use a second Higgs doublet (Φ_2) to give mass to the up–type quarks. The presence of a second Higgs doublet also eliminates anomalies in the theory. It is sufficient to require that the sum of all fermion charges vanishes, and so the fermionic partners of one Higgs doublet ($\tilde{H}_1^0$, $\tilde{H}_1^-$) must have their charges balanced by the partners of a second Higgs doublet ($\tilde{H}_2^+$, $\tilde{H}_2^0$). Therefore the Higgs sector of the MSSM is a 2HDM with the additional constraint of supersymmetry. In this thesis we are concerned with the phenomenology of the Higgs sector of the MSSM, and how it may differ from that of a general, non–SUSY 2HDM. Therefore we shall go into detail concerning the exact structure of the full MSSM Lagrangian. We shall see that the results derived earlier for the non–SUSY 2HDM are fully applicable for use in the MSSM, although there are new constraints which arise from imposing supersymmetry.

The Higgs potential for the MSSM can be written in terms of the general 2HDM potential displayed in Eq. (4.11), with the following constraints:

$$\lambda_2 = \lambda_1 ,$$

$$\begin{aligned}
\lambda_3 &= \frac{1}{8}(g^2+g'^2) - \lambda_1 \,, \\
\lambda_4 &= 2\lambda_1 - \frac{1}{2}g' \,, \\
\lambda_5 = \lambda_6 &= 2\lambda_1 - \frac{1}{2}(g^2+g'^2) \,, \\
m_1^2 &= -|\mu|^2 + 2\lambda_1 v_2^2 - \frac{1}{2}M_Z^2 \,, \\
m_2^2 &= -|\mu|^2 + 2\lambda_1 v_1^2 - \frac{1}{2}M_Z^2 \,, \\
m_{12}^2 &= -\frac{1}{2}v_1 v_2 (g^2+g'^2-4\lambda_1) \,.
\end{aligned} \tag{4.29}$$

Here m_{12}, m_1 and m_2 are soft SUSY breaking parameters. Thus one arrives at the following potential.

$$\begin{aligned}
V = (m_1^2+|\mu|^2)H_1^{i*}H_1^i + (m_2^2+|\mu|^2)H_2^{i*}H_2^i - m_{12}^2(\epsilon_{ij}H_1^i H_2^j + h.c) \\
+\frac{1}{8}(g^2+g'^2)\left[H_1^{i*}H_1^i - H_2^{j*}H_2^j\right]^2 + \frac{1}{2}|H_1^{i*}H_2^i|^2 \,.
\end{aligned} \tag{4.30}$$

Using these relations and the expressions for the mass eigenstates of the general 2HDM one can obtain the following mass relations:

$$M_{A^0}^2 = M_{H^\pm}^2 - M_W^2 \,, \tag{4.31}$$

$$M_{H^0,\,h^0}^2 = \frac{1}{2}\left[M_{A^0}^2 + M_Z^2 \pm \sqrt{(M_{A^0}^2)+M_Z^2)^2 - 4M_Z^2 M_{A^0}^2\cos^2\beta}\right] \,. \tag{4.32}$$

The mixing angles are found to be:

$$\cos 2\alpha = -\cos 2\beta \left(\frac{M_{A^0}^2 - M_Z^2}{M_{H^0}^2 - M_{h^0}^2}\right) \,, \tag{4.33}$$

$$\sin 2\alpha = -\sin 2\beta \left(\frac{M_{H^0}^2 + M_{h^0}^2}{M_{H^0}^2 - M_{h^0}^2}\right) \,. \tag{4.34}$$

From the equations one can derive the following important relations:

$$\begin{aligned}
M_{H^\pm} &\geq M_W \,, \\
M_{H^0} &\geq M_Z \,, \\
M_{A^0} &\geq M_{h^0} \,, \\
M_{h^0} \leq M|\cos 2\beta| &\leq M_Z \quad (M \equiv \min(M_Z,\, M_{A^0})) \,.
\end{aligned} \tag{4.35}$$

The last relationship is phenomenologically very important since it implies that h^0 must be of order M_Z which would make it accessible at LEP2. We notice from the above equations that only two of the parameters (β, α, M_{A^0}, M_{h^0}, $M_{H^\pm}$, and M_{H^0}) are independent. The literature usually chooses $\tan\beta$ and M_{A^0} as being independent variables, from which the values of α, M_{h^0}, $M_{H^\pm}$ and M_{H^0} may be inferred. We note that in the general 2HDM five of these six parameters are independent variables. Returning to the MSSM, as $M_{A^0} \to \infty$ all the Higgs masses except M_{h^0} likewise grow large and effectively decouple. Thus one is left with a Higgs sector that closely resembles that of the minimal SM (the couplings of h^0 are identical to those of ϕ^0 in this limit).

Up until now all the quoted mass relations are at the tree–level only. It is important to check if radiative corrections can cause significant enhancements. In this thesis we shall be concerned with these corrections for the case of h^0 and $H^\pm$. For $H^\pm$ it has been shown that the 1–loop corrections to Eq. (4.31) are small over most of the parameter space and thus the tree–level relation remains a very good approximation [40]. For h^0 the situation is very different and the diagrams of the form in Figure 4.2 cause a correction $\delta M^2_{h^0}$ [41].

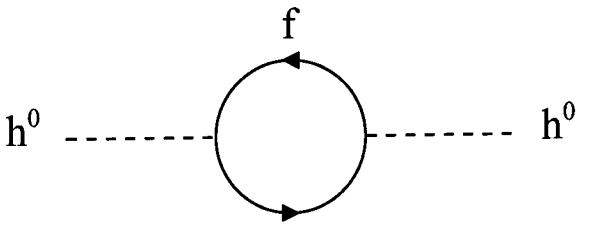

Figure 4.2: Fermion and sfermion corrections to the h^0 propagator.

This correction can be written as (the dominating term only):

$$\delta M^2_{h^0} = \frac{3g^2 m_t^4}{8\pi^2 M_W^2}\left[\ln\left(\frac{m_{\tilde{t}}^2}{m_t^2}\right)\right]. \tag{4.36}$$

Here $m_{\tilde{t}}$ is the mass of the stop particle. This 1–loop correction can significantly increase M_{h^0}, thus violating the bound $M_{h^0} \leq M_Z$. The phenomenological consequence is that h^0 may not be within the discovery range of LEP2, this collider being able to search up to $M_{h^0} \approx 95 \to 100$ GeV. The radiatively corrected M_{h^0} depends on the exact value of $\tan\beta$ and various SUSY parameters such as the squark masses and mixings.

We now turn our attention to the couplings of the Higgs bosons in the MSSM to the fermions and gauge bosons. In this thesis we shall be concerned with Higgs decays to non–SUSY particles, since the predictive power is greater. The Yukawa couplings are of Model II type and so from Table 4.3 we can automatically read off values relative to those of ϕ^0. As we have already mentioned the Higgs sector of the MSSM is a constrained version of the general 2HDM and so the couplings (which are functions of M_{A^0} and $\tan\beta$) are likely to be constrained. Turning our attention first to the couplings to gauge bosons one finds a dramatic suppression in the predicted value of $\cos^2(\beta-\alpha)$ (i.e. the coupling of H^0 to the gauge bosons). Over the vast majority of the experimentally allowed (M_{A^0}, $\tan\beta$) parameter space one find $\cos^2(\beta-\alpha) \leq 0.1$. This implies that the corresponding coupling of h^0 will be very close to ϕ^0 strength. Moreover, in this scenario the fermion couplings of h^0 will also be close to ϕ^0 strength, resulting in h^0 and ϕ^0 being very difficult to distinguish. This problem is discussed in Ref. [42]. We shall not be addressing this topic, but instead will be comparing the phenomenological properties of non–SUSY, non–minimal Higgs bosons to those of ϕ^0 and h^0, assuming that the latter two have very similar signatures.

It is worth mentioning here that the presence of the sparticle spectrum must be taken into account when one considers the phenomenology of the Higgs sector of the MSSM. In particular, virtual sparticles must be included in one–loop diagrams; this is of importance when one considers rare one–loop mediated decays, or production processes that proceed via loops. Examples include the $gg \rightarrow h^0$ fusion production process at hadron colliders which proceeds predominantly via a top quark loop although squark loops must be considered. This has been considered in Ref. [43] and the squarks loop contributions were found to be small. This is because the squark masses are expected to be large (≈ 1 TeV) and thus they decouple, their coupling not behaving as $m_{\tilde{q}}^2/M_W$. The $\gamma\gamma$ decay mode of h^0 will be important to enable detection at hadron colliders, and additional contributions in the this loop mediated decay originate from $H^\pm$, squarks and charginos, the latter being the SUSY partners of $W^\pm$ and $H^\pm$. Contributions from the latter particles are the most sizeable. The chargino coupling grows weaker as its mass increases, and so a light chargino would be needed to cause a reasonable contribution. Effects from the scalar loops are smaller. In many studies (e.g. the ATLAS studies) various assumptions are made concerning the the SUSY parameters, e.g. squark mixing and the masses of the

sparticles. Often squark mixing is assumed to be zero and decays involving sparticles are assumed to have little contribution to overall decay widths. Some studies instead consider the whole SUSY parameter space, showing that significant deviations from the above scenario are possible [44]. In this thesis we shall not be considering Higgs boson decays to SUSY particles, and we generally assume that h^0 has a very similar phenomenology to ϕ^0. If there is a possibility of a significantly different signal in a particular channel then this will be mentioned at the appropriate time.

4.6 The aims of this Thesis

This concludes our account of the Higgs sector of the MSSM. Of all of the extensions of the SM which require an extended Higgs sector the MSSM is the model which receives most phenomenological attention in the literature. It is sometimes suggested that searching for the Higgs bosons of the MSSM is a good way to find supersymmetry, whose sparticles may be rather heavy. However we have shown the Higgs sector of the MSSM is merely a constrained version of the general 2HDM. If a Higgs boson(s) is found in the future (charged or uncharged) with properties roughly corresponding to those of a Higgs boson of the MSSM it would be imprudent to assume that the MSSM is the correct theory. Higgs bosons from the general 2HDM can mimic those from the MSSM since the latter is a constrained version of the former. One should wait for harder evidence of the MSSM, that is the detection of the sparticles, whether from direct production or via decays from Higgs bosons. One can naively infer that the general 2HDM should possess properties that cannot be mimicked by the Higgs sector of the MSSM, since there are no tree–level mass relations and the couplings will not be as constrained. This thesis sets out to find these distinct signatures and to ascertain whether they are phenomenologically observable. The colliders considered are LEP2 and the LHC; the former is already taking data at a lower centre of mass energy, with the latter having been approved and expected to operate early next century. Since the phenomenology of h^0 is expected to be very similar to that of ϕ^0, any conclusions concerning one of these bosons will be applicable to the other. The Higgs sector of the MSSM and ϕ^0 have received the most attention in the literature with relatively little given to the general 2HDM; we shall show that the latter

may possess distinct and sometimes spectacular phenomenological signatures not possible in the MSSM or for ϕ^0.

Our work is organized as follows:

(i) In Chapter 5 we consider the charged Higgs sector of the general 2HDM and its phenomenology at LEP2 and higher energy e^+e^- colliders. The motivation here is that a charged Higgs is unambiguous proof of physics beyond the minimal SM. Moreover, the mass relationships in the MSSM practically forbid the detection of $H^\pm$ of the MSSM at LEP2. This may not be the case for the $H^\pm$ of the general 2HDM.

(ii) In Chapter 6 the phenomenology of the neutral Higgs sector of the non–minimal SM is studied, first in the context of LEP2 and then at the LHC. The couplings of ϕ^0 to matter, and thus its production cross–sections and BRs, can be precisely calculated once M_{ϕ^0} is known. Any serious deviations from these predictions will be indicative of an extended Higgs sector, and this chapter explores the regions of parameter space that may present phenomenologically distinct signatures.

(iii) Chapter 7 considers a higher Higgs representation, namely those with isospin triplets ($I = 1$). We study one such model in the context of LEP2 and show that it predicts exotic Higgs bosons, some of which are not possible in extended models with only doublets.

(iv) Chapter 8 continues a theme introduced in Chapter 7 – 'fermiophobia' – and explores the phenomenology of fermiophobic Higgs bosons at the Fermilab Tevatron and at the LHC.

Chapter 5

Light charged Higgs scalars at e^+e^- colliders

5.1 Introduction

This chapter concerns the detection of light charged Higgs scalars ($H^\pm$) at high energy e^+e^- colliders. In Chapter 4 we showed that extended Higgs models may be considered and one prediction of the 2HDM is the existence of charged Higgs bosons.

One particular form of the 2HDM has received substantial attention in the literature, mainly due to the fact that it is the structure of the MSSM. However, there are four variants of the 2HDM, differing in their couplings to the fermions (see Table 4.2). These are referred to as Models I, I′, II and II′ with Model II appropriate for the MSSM. The phenomenology of these four types of models can be quite different. We will show, for example, that the charged Higgs bosons $H^\pm$ of Models I and I′ can be within the reach of the LEP2 e^+e^- collider ($\sqrt{s} \sim 200$ GeV), while those of Models II and II′ cannot.

In this chapter we shall study the phenomenology of non–minimal Higgs models containing doublet representations in the context of high–energy e^+e^- colliders. The analysis only considers models with the following important assumptions:

(i) natural flavour conservation [34] is imposed at all times.

(ii) when studying decay channels we assume no other new particles apart from Higgs bosons (i.e. non–minimal SM), *cf.* MSSM with extra SUSY particles.

In particular we give emphasis to the general Multi–Higgs–Doublet–Model (MHDM), which has received relatively little attention in the literature. It has been shown that there are significant phenomenological differences between the MHDM and the 2HDM [46]. Particularly important in this respect is the detection of the lightest charged scalar of the MHDM, a theme which we shall cover in this chapter. We note that detection of a charged Higgs boson would provide unambiguous evidence of a non–minimal Higgs sector. In contrast to the 2HDM of, for example, the MSSM, the lightest charged scalar of the MHDM has essentially no theoretical constraint on its mass (Eq. (4.31)) and could therefore be in the discovery range of LEP2.

For all the charged scalars that we will consider there exists an experimental lower bound from LEP of 41.7 GeV [32], obtained from a lack of signal in the processes $e^+e^- \rightarrow \gamma^*, Z^* \rightarrow H^+ H^- \rightarrow \tau\,\nu_\tau\tau\,\nu_\tau$, $cs\tau\nu_\tau$ and $cscs$. With higher energy colliders, distinguishing between the various models and the special cases of $M_H \approx M_W$ or $M_H \approx M_Z$ pose potential problems. We shall show that the possibility of a large branching ratio for the decay channel $H^\pm \rightarrow cb$ (which is possible in the MHDM but not in the 2HDM that is relevant at LEP2) goes some way to overcoming these difficulties.

This chapter is organized as follows. In (5.2) we describe the general features of the charged Higgs sector of the 2HDM and MHDM. In (5.3) we discuss existing constraints on the various models and compute some relevant branching ratios. Sections (5.4) and (5.5) discuss the production of charged Higgs scalars at LEP2 and higher energy e^+e^- colliders respectively. Finally, (5.6) contains our conclusions.

5.2 The Models

The theoretical structure of the 2HDM was described in Chapter 4. Eq. (4.22) showed the charged Higgs interaction Lagrangian for Model II type couplings. For the MHDM it has been shown [45] that the couplings of the charged scalars to the fermions depend on the three complex parameters X, Y and Z. These originate from the mixing matrix

for the charged scalar sector. We will assume, as is conventionally done in the literature, that one of the charged scalars is much lighter than the others and thus dominates the low–energy phenomenology. The relevant part of the Lagrangian is [46]:

$$\mathcal{L} = (2\sqrt{2}G_F)(X\overline{U}_L V M_D D_R + Y\overline{U}_R V M_U D_L + Z\overline{N}_L M_E E_R)H^+ + h.c. \qquad (5.1)$$

Here U_L, U_R (D_L, D_R) denote left– and right–handed up (down) type quark fields, N_L is the left–handed neutrino field, and E_R the right–handed charged lepton field. M_D, M_U, M_E are the diagonal mass matrices of the down–type quarks, up–type quarks and charged leptons respectively. V is the CKM matrix. For the 2HDM the charged Higgs interaction Lagrangian has the same form Eq. (5.1) with the replacements for X, Y and Z shown in Table 5.1 [35]. In the MHDM X, Y and Z are *arbitrary* complex numbers.

	Model I	Model I′	Model II	Model II′
X	$-\cot\beta$	$-\cot\beta$	$\tan\beta$	$\tan\beta$
Y	$\cot\beta$	$\cot\beta$	$\cot\beta$	$\cot\beta$
Z	$-\cot\beta$	$\tan\beta$	$\tan\beta$	$-\cot\beta$

Table 5.1: The values of X, Y and Z in the 2HDM.

It follows that combinations of parameters like XY^* have different values depending on the model under consideration. In particular, we will see in the following section that such a combination appears in loop corrections involving charged scalars, giving rise to important phenomenological differences between the models. For a full review see for example Ref. [46].

5.3 Constraints and Branching Ratios

Precision measurements of the process $b \to s\gamma$ impose the severest constraints on the mass of the charged scalar of the 2HDM (Models II and II′). For a general review of how new physics affects this decay see Ref. [47]. The diagrams which contribute to the process are essentially the same as those for the SM with the $W^\pm$ replaced by $H^\pm$, see Figure 5.1. The photon may be attached to any charged line.

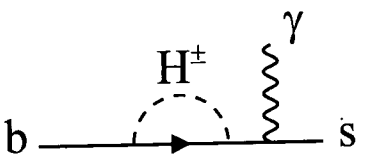

Figure 5.1: Contribution to $b \to s\gamma$ from $H^{\pm}$.

It has been shown [48, 49, 50, 51] that

$$\mathrm{BR}(b \to s\gamma) = C \left| \eta_2 + G_W(x_t) + (|Y|^2/3) G_W(y_t) + (XY^*) G_H(y_t) \right|^2 , \tag{5.2}$$

where

$$C = \frac{3\alpha\eta_1^2 BR(B \to X_c l\nu)}{2\pi F_{\mathrm{ps}}(m_c^2/m_b^2)} \approx 3 \times 10^{-4} . \tag{5.3}$$

Here $F_{\mathrm{ps}} \approx 0.5$ is a phase space factor, $\eta_1 \approx 0.66$ and $\eta_2 \approx 0.57$ are QCD correction factors, and the G functions are positive increasing:

$$\begin{aligned} G_W(x) &= \frac{x}{12(1-x)^4}\left[(7-5x-8x^2)(1-x) + 6x(2-3x)\ln(x)\right] , \\ G_H(x) &= -\frac{x}{6(1-x)^3}\left[(3-5x)(1-x) + 2(2-3x)\ln(x)\right] , \\ F_{\mathrm{ps}} &= 1 - 8x + 8x^3 - x^4 - 12x^2\ln(x) . \end{aligned} \tag{5.4}$$

The dimensionless parameters x_t and y_t are defined by $x_t = m_t^2/M_W^2$ and $y_t = m_t^2/M_H^2$ with M_H being the mass of the charged Higgs. This calculation is purely 'SM + charged Higgs' and so assumes no SUSY particles in the loops. The CLEO collaboration has recently obtained the value [52]

$$\mathrm{BR}(b \to s\gamma) = (2.32 \pm 0.51 \pm 0.29 \pm 0.32) \times 10^{-4} , \tag{5.5}$$

which corresponds to

$$\cdot 1 \times 10^{-4} \leq \mathrm{BR}(b \to s\gamma) \leq 4 \times 10^{-4} \ \ (95\%\ cl) . \tag{5.6}$$

Now in the 2HDM (Models II and II') we have

$$XY^* = \tan\beta(\cot\beta)^* = 1 , \tag{5.7}$$

and so there is a $G_H(y_t)$ contribution to the branching ratio which does not depend on $\tan\beta$. Hence to keep the theoretical branching ratio below the bounds from experiment, the Higgs mass M_H (which appears in G_H) must be constrained. We therefore obtain a lower bound of $M_H > 260$ GeV for the $H^\pm$ of the 2HDM (Models II and II'). However this is *not* the case in 2HDM (Models I and I'). Here $XY^* = -\cot^2\beta$, and so the 2HDM contribution to the decay is $[G_W(y_t)/3 - G_H(y_t)]\ \cot^2\beta$. This is negative for all values of y_t and so no bound on M_H independent of $\tan\beta$ can be found. Hence this $H^\pm$ could be in the range of LEP2.

In the MHDM, the combination XY^* which appears in Eq. (5.2) is an arbitrary complex number. Hence there is the possibility of cancellation between the terms that depend on the MHDM parameters, and therefore no bound on M_H. With the expected energy of LEP2 ($\sqrt{s} = 180 \rightarrow 200$ GeV), $H^\pm$ of the conventional version of the 2HDM (i.e. Model II) as well as $H^\pm$ of Model II' are both inaccessible, while the lightest $H^\pm$ of the MHDM and the charged scalars of the 2HDM (Models I and I') could possibly be found.

The parameter $\tan\beta$ is ubiquitous in the phenomenology of the 2HDM, and therefore we must be aware of any experimental bounds. The most stringent bound can be obtained from considering the effects of $H^\pm$ on the $Z \rightarrow b\bar{b}$ vertex. One–loop corrections mediated by charged Higgs exchange are shown in Figures 5.2 and 5.3:

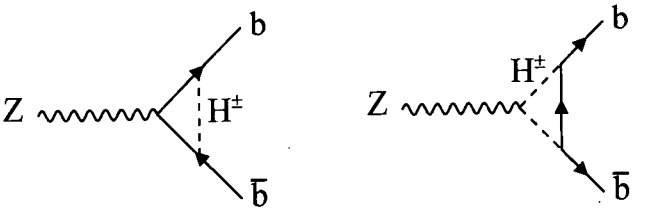

Figure 5.2: Virtual $H^\pm$ corrections to $Z \rightarrow b\bar{b}$.

The $H^\pm$ contribution ($\delta\Gamma$) to the minimal SM decay width can be expressed as [53]:

$$\delta\Gamma = \frac{\alpha^2 N_c M_Z}{48\pi s^2 c^2 M_W^2}\left[m_t^2\cot^2\beta F_1 + m_b^2\tan^2\beta F_2\right]. \tag{5.8}$$

Here F_1 and F_2 are functions of m_t and $M_{H^\pm}$. The cross terms are negligible and only the potentially dominant terms are shown. This contribution is always negative and the term

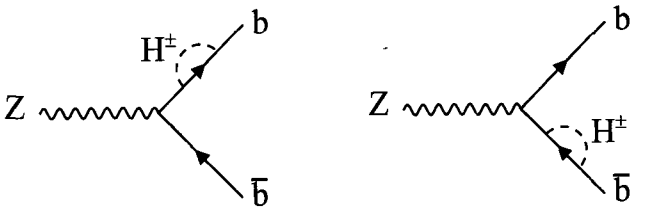

Figure 5.3: Virtual $H^\pm$ corrections to $Z \to b\bar{b}$.

proportional to $m_t^2 \cot^2\beta$ dominates for $\tan\beta \leq 5$. One can therefore constrain $\cot\beta$ and obtain the bound for $M_H \leq 200$ GeV [46]:

$$\tan\beta \geq 1.25\,. \tag{5.9}$$

We next consider the branching ratios for the decays of the $H^\pm$, which will differ from model to model, and are displayed in Table 5.2 (with BRs for $W^\pm$ shown for comparison) In the 2HDM (Models I and I'), for Higgs masses in the range of LEP2, the dominant decay modes are to $\tau\nu_\tau$ or cs [30, 35]. In Model I the branching ratios are independent of $\tan\beta$. In Model I', $\tau\nu_\tau$ starts to dominate for $\tan\beta \geq 1.2$. Given the current constraint

	cs	cb	$\tau\nu_\tau$
$H^\pm$ (Model I)	66%	1%	33%
$H^\pm$ (Model I')	$\leq 45\%$	$\leq 1\%$	$\geq 54\%$
$H^\pm$ (MHDM)	$0 \to 100\%$	$0 \to 100\%$	$0\% \to 100\%$
$W^\pm$	67%	$\approx 0.05\%$	11%

Table 5.2: The branching ratios for $H^\pm$ and $W^\pm$.

that $\tan\beta \geq 1.25$ [46] we find the $\tau\nu_\tau$ rate is $\geq 54\%$. The cb channel never exceeds a few percent ($\approx 1\%$ in Model I and $\leq 0.9\%$ in Model I') due to heavy CKM matrix suppression, although in the MHDM it can be significantly enhanced due to the greater freedom in X, Y and Z. Such an enhancement could have two important uses. It could increase the chance of detection if $M_H \approx M_W$ (when $W^\pm$ decays form a large background),[1] and also indicate that any detected $H^\pm$ is from the MHDM rather than from the 2HDM. Also, we note that another distinctive signature of the MHDM is a lack of $\tau\nu_\tau$ decays ($\ll 33\%$).

[1]This was first observed in [46], but we will perform a full analysis of detection prospects in this difficult mass region.

The actual calculation of the decay widths for the three channels $H^\pm \to \tau\nu_\tau$, $H^\pm \to cb$ and $H^\pm \to cs$ is straightforward. Note that these are the only channels we need consider for Higgs masses in the energy range of LEP2; decays to lighter fermions are negligible because the charged Higgs–fermion coupling is in proportion to mass. The decay channels $H^\pm \to tb$ and $H^\pm \to W^\pm h$ (where h is a light neutral Higgs boson) would dominate for much heavier charged scalars.

The Feynman rule for the $H^+u\bar{d}$ vertex is given by [30, 46]

$$\frac{igV_{ud}}{2\sqrt{2}M_W}[m_d X(1+\gamma_5) + m_u Y(1-\gamma_5)] , \tag{5.10}$$

and that for the $H^+\tau^+\nu_\tau$ vertex is

$$\frac{ig}{2\sqrt{2}M_W} m_\tau Z(1+\gamma_5) . \tag{5.11}$$

With these rules we can readily construct the invariant amplitude $-i\mathcal{M}$ and the corresponding decay width. For the lepton decay channel we obtain

$$\Gamma(H^\pm \to \tau\nu_\tau) \approx \frac{G m_\tau^2 M_H |Z|^2}{4\pi\sqrt{2}} , \tag{5.12}$$

and for the quark decay channels one has

$$\Gamma(H^\pm \to ud) \approx \frac{3G m_d^2 M_H |V_{ud}|^2 |X|^2}{4\pi\sqrt{2}} + \frac{3G m_u^2 M_H |V_{ud}|^2 |Y|^2}{4\pi\sqrt{2}} . \tag{5.13}$$

Here we have used the approximations $M_H^2 \gg m_u^2$, m_d^2 , m_τ^2. The decay widths for the 2HDM are obtained by replacing X, Y and Z with the corresponding values in Table 5.1.

The next step is to study the variation of the decay widths with the parameters X, Y, Z. Before doing so, however, we note that in the MHDM there are various experimental bounds on these parameters which we must respect:

(i) for a top quark mass of 180 GeV and a charged scalar mass of below 200 GeV, there is a bound $|Y| \leq 0.8$ from considering the $Z \to b\bar{b}$ vertex (Eq. (5.9));

(ii) the strictest bound on $|XY^*|$ comes from the aforementioned process $b \to s\gamma$, see Eq. (5.2). The weakest upper bound is obtained for arg $(XY^*) = \pi$, and Ref. [46]

shows that in this case $|XY| < 4$, again for $m_t = 180$ GeV and $M_H < 80$ GeV. As M_H grows the constraint lessens;[2]

(iii) there are very weak bounds on the other MHDM parameters $|X|$ and $|Z|$ and combinations of them such as $|XZ|$ and $|YZ|$ [46], and none are relevant for the analysis which follows.

For the calculation of the decay widths we use the following mass values: $m_s = 180$ MeV, $m_c = 1.5$ GeV, $m_b = 5$ GeV, $m_t = 180$ GeV, $m_\tau = 1.8$ GeV. For the CKM matrix elements we take [32]: $|V_{cs}| = 0.975$ and $|V_{cb}| = 0.040$. Figures 5.4 and 5.5 show

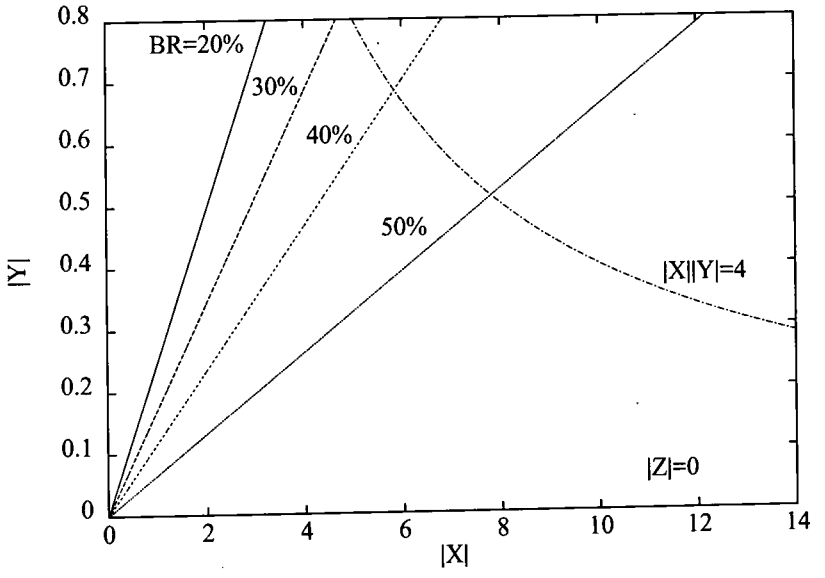

Figure 5.4: Lines of constant branching ratio for the decay $H^+ \to c\bar{b}$ with $|Z| = 0$. The experimentally allowed region lies beneath the curve $|X||Y| = 4$.

lines of constant BR in the $|X|$, $|Y|$ plane for the $H^\pm \to cb$ channel, in the range 20% to 50%. For $M_H = 80$ GeV (which suffers from large $W^\pm$ backgrounds), regions below the curve $|XY| = 4$ are allowed by current experimental data. In Figure 5.4 we have

[2]This bound is based on a previous (95%*cl*) upper limit for $b \to s\gamma$ (5.4×10^{-4}) since superseded by the new measurement from Eq. (5.5).

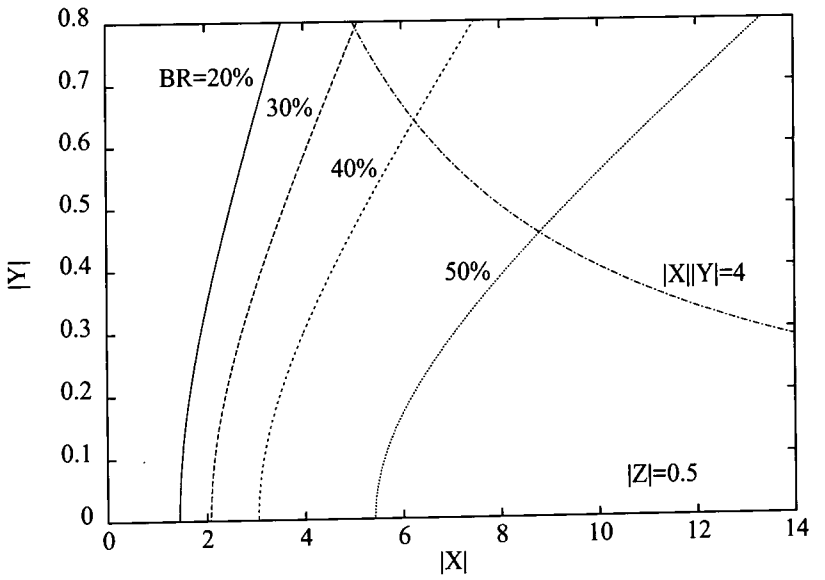

Figure 5.5: Same as Figure 5.4 but with $|Z| = 0.5$.

set $|Z| = 0$, and in Figure 5.5 $|Z| = 0.5$. We see that there is a significant parameter space for large BR ($H^\pm \to cb$), with low values of $|Y|$ and $|Z|$ being more favourable. Table 5.3 shows the maximum obtainable BR($H^\pm \to cb$) using input values for $|Y|$ and $|Z|$, and taking $|X|$ ten times larger than the smallest of these.[3] The important point

	$\|Y\| = 0.2$	$\|Y\| = 0.5$	$\|Y\| = 0.8$
$\|Z\| = 0.2$	39%	19%	10%
$\|Z\| = 0.6$	21%	37%	28%
$\|Z\| = 1.0$	11%	30%	24%

Table 5.3: Maximum values of the branching ratio for $H^\pm \to cb$ assuming $|X| = 10 \min(|Y|, |Z|)$.

here is that sizeable BRs for the decay $H^\pm \to cb$ are obtainable, whether we impose 'naturalness' or not. This is in contrast to the charged scalars of the 2HDM (Models I and I') which never reach more than BR$\sim$1% in the cb channel (Table 5.2). Thus a significant BR ($H^\pm \to cb$) signal would be a signature of the MHDM. Furthermore,

[3]We assume that 'naturalness' requires the parameters to be of the same order of magnitude.

because the $W^\pm \not\to cb$ decay is negligible (BR$\sim$0.05%), there is more chance in the MHDM of overcoming the W^+W^- background when $M_H \approx M_W$. There is also a sizeable parameter space for a low BR ($H^\pm \to \tau\nu_\tau$) in the MHDM. We find using Eqs. (5.12) and (5.13) and that this branching ratio is (not including cb decays for the moment)

$$\approx \frac{|Z|^2}{|Z|^2 + 2|Y|^2} . \tag{5.14}$$

Therefore if $|Y| \geq 2|Z|$, the BR is $\leq 11\%$. The inclusion of the cb channel would decrease this further, and so we conclude that it is very possible to have a low number of $H^\pm \to \tau\nu_\tau$ decays in the MHDM i.e. leptophobia. Recalling that the same BR for Model I and Model I′ must be greater than 33% and 54% respectively (Table 5.2), this is in principle another way of distinguishing the MHDM from the other models.

5.4 Production of $H^\pm$ at LEP2

If for any of the above models M_H *does* lie in the discovery range of LEP2, how would one search for it? Production in top decay, i.e. $e^+e^- \to \gamma^*, Z^* \to t\bar{t} \to H^+H^-b\bar{b}$, is obviously kinematically forbidden at LEP2. Therefore we must rely on the annihilation process $e^+e^- \to \gamma^*, Z^* \to H^+H^-$. This has been studied extensively in the literature for the case of the 2HDM. It is straightforward to show that the $Z\,H^+H^-$ and $\gamma\,H^+H^-$ couplings have the same strength in both the 2HDM and MHDM, with respective Feynman rules [30]

$$\frac{-ig\cos 2\theta_W}{2\cos\theta_W}(p' - p)^\mu \quad \text{and} \quad -ie(p' - p)^\mu , \tag{5.15}$$

where p', p are the 4–momenta of the H^+, H^-. Therefore the analysis of Ref. [54] is relevant for the MHDM. The production cross section is

$$\sigma_{H^+H^-} = \frac{1}{4}\sigma_0\,\beta^3\,F(s, M_Z, \Gamma_Z, \theta_W) , \tag{5.16}$$

where $\sigma_0 = 4\pi\alpha^2/3s$, $\beta = \sqrt{(1 - 4M_H^2/s)}$ and $F(s, M_Z, \Gamma_Z, \theta_W)$ is given by

$$1 - 2C_V C_V' \frac{s(s - M_Z^2)}{(s - M_Z^2)^2 + M_Z^2\Gamma_Z^2} + C_V'^2(C_V^2 + C_A^2)\frac{s^2}{(s - m_Z^2)^2 + M_Z^2\Gamma_Z^2} . \tag{5.17}$$

The couplings C are

$$C_A = \frac{-1}{4\sin\theta_W\cos\theta_W},\quad C_V = \frac{1-4\sin^2\theta_W}{4\sin\theta_W\cos\theta_W},\quad C'_V = \frac{-1+2\sin^2\theta_W}{2\sin\theta_W\cos\theta_W}. \tag{5.18}$$

In the calculations which follow we use the parameter values: $M_Z = 91.18$ GeV, $M_W = 80.30$ GeV, $\alpha = 1/128$, $\Gamma_Z = 2.49$ GeV, $\sin^2\theta_W = 0.225$. From Eqs. (5.16)-(5.18) we can compute the expected total number of H^+H^- events. This is shown in Figure 5.6

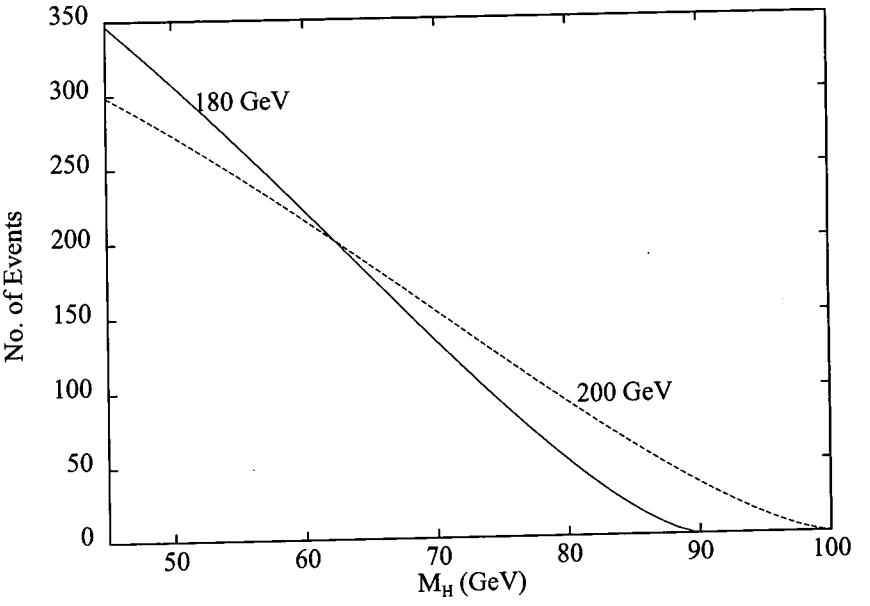

Figure 5.6: Expected number of H^+H^- pairs produced with $\int \mathcal{L} = 500$ pb^{-1} at LEP2 as a function of M_H, for $\sqrt{s} = 180$ and 200 GeV.

as a function of M_H, where we have assumed an integrated luminosity of 500 pb^{-1} and two values for the collider energy. For $\sqrt{s} = 180$ GeV we expect approximately 350 events for M_H=45 GeV, decreasing to 51 events for M_H=80 GeV. Ref. [55] studies the production of $H^\pm$ at LEP2, using L3 detector simulations. Although this analysis only considers the 2HDM (Model II), the results can be extended to the other models. We shall now summarize the detection channels and backgrounds [55]. For $H^\pm$ of Model II the main decay channels are to cs and $\tau\nu_\tau$, with the latter process becoming dominant

for $\tan\beta \geq 3$. Hence Ref. [55] considers three detection channels, although we stress that $H^\pm$ of Model II is out of the discovery range of LEP2. The channels are:

(i) $H^+H^- \to c\bar{s}\,\bar{c}s$.

(ii) $H^+H^- \to cs\tau\nu_\tau$.

(iii) $H^+H^- \to \tau^+\nu_\tau\tau^-\bar{\nu}_\tau$.

5.4.1 $H^+H^- \to c\bar{s}\bar{c}s$

The signal here is a 4–jet event, with the main backgrounds being $q\bar{q}$, WW and ZZ. The $q\bar{q}$ background is removed by a cut on the thrust ($T \leq 0.9$), followed by a cut on $|M^{rec}_{H^+} - M^{rec}_{H^-}| = \Delta M^{rec}$. The parameter ΔM^{rec} is minimized for each 4–jet event combination, and events with $\Delta M^{rec} \geq 5$ GeV are rejected. The WW background is removed by a cut on the invariant mass of the jets, although this cut will remove the signal if $M_H \approx M_W$. For $M_H \leq M_W$ a reasonable signal is expected with event numbers/efficiencies given in Table 5.4. The product of the signal efficiency and the number of H^+H^- events in a particular channel determines the number of events surviving the selection and acceptance cuts.

Process	Eff. or No. of backg. evts
$H^\pm$ (60 GeV)	7%
$H^\pm$ (70 GeV)	7%
$q\bar{q}$	2
W^+W^-	3
ZZ	0

Table 5.4: Expected signal efficiency and background event numbers in the cscs channel for $\sqrt{s} = 175$ GeV (from Ref. [55]).

5.4.2 $H^+H^- \to cs\tau\nu_\tau$

The signature here is an isolated τ and missing energy recoiling against a hadronic system. Demanding a very spherical event removes most of the $q\bar{q}$ background. To remove the

W^+W^- background the invariant masses of the cs and $\tau\nu_\tau$ systems are reconstructed, thus significantly reducing the background if $M_H \leq M_W$. The expected event numbers/efficiencies are given in Table 5.5.

Process	Eff. or No. of backg. evts
$H^\pm$ (60 GeV)	5.6%
$q\bar{q}$	0
W^+W^-	2
ZZ	0
$\tau^+\tau^-$	0

Table 5.5: Expected signal efficiency and background event numbers in the $cs\tau\nu_\tau$ channel for $\sqrt{s} = 175$ GeV (from Ref. [55]).

5.4.3 $H^+H^- \rightarrow \tau^+\nu_\tau\tau^-\overline{\nu}_\tau$

In this channel one searches for two low–multiplicity τ jets, associated with large missing energy. The main backgrounds are from $\tau^+\tau^-$, $q\bar{q}$, W^+W^- and ZZ. Demanding low particle multiplicity removes most hadronic events. The $\tau^+\tau^-$ background is reduced by acoplanarity cuts. The W^+W^- background is strongly suppressed by a imposing a cut on the most energetic τ. In the simulations a cut of $E_\tau \leq 25$ GeV removed most of the W^+W^- background. The expected event numbers and efficiencies are given in Table 5.6.

Process	Eff. or No. of backg. evts
$H^\pm$ (60 GeV)	12%
$H^\pm$ (70 GeV)	12%
$q\bar{q}$	0
W^+W^-	1
ZZ	0
$\tau^+\tau^-$	0

Table 5.6: Expected signal efficiency and background event numbers in the $\tau\nu_\tau\tau\nu_\tau$ channel for $\sqrt{s} = 175$ GeV (from Ref. [55]).

To conclude this analysis, with 500 pb^{-1} of luminosity a 3σ signal should be obtainable for $M_H \leq 70$ GeV, independent of the decay channel. The $\tau\nu_\tau\tau\nu_\tau$ channel is capable of probing close to $M_H = 80$ GeV, if BR($H^\pm \rightarrow \tau\nu_\tau$) $\rightarrow 100\%$. The potential problem arises

when $M_H \approx M_W$. The W^+W^- production cross-section (≈ 20 pb) is considerably larger than that for H^+H^-, see Figure 5.7, and so the $H^\pm \to cs$, $\tau\nu_\tau$ decays will be overwhelmed

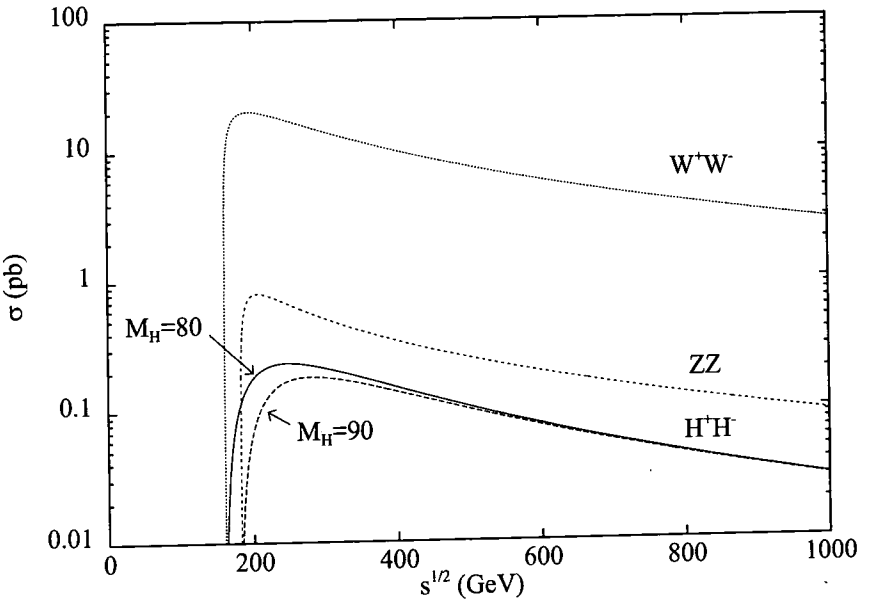

Figure 5.7: Cross sections for the pair production of $W^\pm$, Z and $H^\pm$ at e^+e^- colliders, as a function of $\sqrt{s}$.

by the much more numerous $W^\pm \to cs$, $\tau\nu_\tau$. Table 5.7 shows the expected number of events for 500 pb^{-1} integrated luminosity and two different values of the collider energy ($\sqrt{s}$).[4] Clearly detection of a $H^\pm$ will be very difficult in the region $M_H \approx M_W$, partly due

	$\sqrt{s} = 180$ GeV	$\sqrt{s} = 200$ GeV
W^+W^-	9727	10191
ZZ	0	397
$H^+H^-(M_H = 80$ GeV)	51	91
$H^+H^-(M_H = 90$ GeV)	0	35

Table 5.7: The expected number of W^+W^-, ZZ and H^+H^- events for 500 pb^{-1} integrated luminosity at LEP2.

to the lack H^+H^- pair production events for this mass region, and partly due to the fact

[4]We ignore below-threshold ZZ production at the lower energy.

that invariant mass cuts which reduce the WW background also remove the signal. We must search for another way of reducing the WW background for the region $M_H \approx M_W$ which keeps sufficient signal events. To start we therefore consider the number of events before cuts in particular channels for both signal and background, in order to find the channel with the least background. Using the SM branching ratios for Z decay [32]:

$$b\bar{b} = 15.1\%, \quad c\bar{c} = 12.0\%, \quad s\bar{s} = 15.4\%, \quad \tau\bar{\tau} = 3.4\%, \quad \sum_{i=1}^{3} \nu_i\bar{\nu}_i = 20.1\% , \tag{5.19}$$

and for $W^{\pm}$ [32]:

$$cs = 31.8\%, \quad cb = 0.05\%, \quad \tau\nu_\tau = 10.8\% , \tag{5.20}$$

we show in Table 5.8 the expected numbers of events for the various decay channels. The H^+H^- numbers are the maximum and minimum values. The actual numbers depend on the parameters of the particular model. We see that exploiting the $cb\tau\nu_\tau$ channel has

	$cbcb$	$cbcs$	$cb\tau\nu_\tau$	$cscs$	$cs\tau\nu_\tau$	$\tau\nu_\tau\tau\nu_\tau$
W^+W^-	0.0	3.1	1.1	983.6	668.1	113.5
H^+H^-	$0 \rightarrow 51$	$0 \rightarrow 51$	$0 \rightarrow 51$	$0 \rightarrow 51$	$0 \rightarrow 51$	$0 \rightarrow 51$

Table 5.8: The expected number of W^+W^- and H^+H^- ($M_H = 80$ GeV) induced events for 500 pb^{-1} integrated luminosity at LEP2 ($\sqrt{s} = 180$ GeV).

the advantage of almost negligible background from WW and ZZ events. In addition we will be able to use the selection criteria as for the $cs\tau\nu_\tau$ channel. For the 2HDM (Model I and I'), this is not an option since BR($H^{\pm} \rightarrow cb$) $\leq 1\%$, and so the signal would be negligible. For the MHDM the prospects are much better due to the possibility of a significant branching ratio for the cb decay channel. The number of signal events (before cuts) in the $cb\tau\nu_\tau$ channel is given by:

$$N_{H^+H^-} \times f(\mathrm{BR}) , \tag{5.21}$$

where $N_{H^+H^-}$ is the number of pair produced $H^{\pm}$ events, and f(BR) is defined by

$$f(\mathrm{BR}) = 2 \times \mathrm{BR}(\mathrm{H}^{\pm} \rightarrow \mathrm{cb}) \times \mathrm{BR}(\mathrm{H}^{\pm} \rightarrow \tau\nu_\tau) . \tag{5.22}$$

In order to isolate these final states b–tagging will be necessary. Since this a standard technique for searching for the SM Higgs at LEP2, the efficiency, e_b, will be quite high

($\approx$ 70%) in practice, see for example Ref. [56]. For the $cb\tau\nu_\tau$ channel we shall use the optimistic values BR($H^\pm \to cb$) =BR($H^\pm \to \tau\nu_\tau$) = 50% which maximizes f(BR). We note that in the $cs\tau\nu_\tau$ channel (5.4.2) the invariant mass cut was the last cut applied, and all other non–WW backgrounds had already been removed. When it is applied for the mass region $M_H \approx M_W$ it will remove the signal as well. Our aim is to replace this latter cut with a b tag requirement, which will reduce the WW background to negligible proportions while preserving most of the signal. One can infer from the figures in Ref. [55] that the invariant mass cut reduces the Higgs signal by $\approx 2/3$. Therefore we shall assume a selection efficiency (e_H) of 8.4% for the Higgs signal[5], obtained by scaling the value of 5.6% in Table 5.5. One can obtain the following formula for the number of signal events (N_{sig}) in the $cb\tau\nu_\tau$ channel.

$$N_{H^+H^-} \times e_H \times e_b \times f(\mathrm{BR}) . \tag{5.23}$$

The background from WW is 1.1 event (Table 5.8) *before* any cuts have been applied. Before the b tag requirement the cuts have a selection efficiency considerably below 100% ($\approx$ 10% $\to$ 20%) and therefore the background is entirely negligible (if one ignores false tags due to c quarks from the W^+W^- background). We then require 3 or more signal events for detection, and we see from the Eq. (5.2.3) that the number of events for $M_H = 80$ GeV and $\sqrt{s} = 180$ GeV is equal to 2.1. Therefore detection is certainly marginal. At the higher collider energy, $\sqrt{s} = 200$ GeV, ZZ production becomes a background. The corresponding number of events in the various channels is given in Table 5.9.[6] Due to the greater $N_{H^+H^-}$ we find that $N_{sig} = 3.8$.

All this analysis is with optimistic choices for e_b and f(BR). With greater luminosity, which would be available at a next generation collider (see (5.5)), one could probe a greater parameter space of f(BR). For $M_H \approx M_Z$ one may still use the above detection channel, but with the reduced number of events (35 for $\sqrt{s} = 200$ GeV) we would find 1.4 events and so detection is not possible at LEP2.

Although the $cb\tau\nu_\tau$ channel is promising and provides a chance of overcoming the difficult $M_W \approx M_H$ region in the MHDM, it only probes a small parameter space of

[5]Ref. [57] shows that the efficiency varies little with different values of M_H.

[6]The $ZZ \to \tau\nu_\tau\tau\nu_\tau$ number corresponds to $Z \to \tau\bar{\tau}$ and $Z \to \sum_i \nu_i\bar{\nu}_i$.

$f(\mathrm{BR})$ at LEP2 since $N_{H^+H^-}$ is rather small. $\mathrm{BR}(H^\pm \to cb) \geq 30\%$ is needed, although this is certainly possible – see Figures 5.4 and 5.5. With greater luminosity, which would be available at a next generation collider one could probe a lower values of $f(\mathrm{BR})$.

	$cbcb$	$cbcs$	$cb\tau\nu_\tau$	$cscs$	$cs\tau\nu_\tau$	$\tau\nu_\tau\tau\nu_\tau$
W^+W^-	0.0	3.2	1.1	1030.6	700.0	118.9
ZZ	14.4	0	0	14.7	0	5.4
H^+H^- (80)	$0 \to 91$	$0 \to 91$	$0 \to 91$	$0 \to 91$	$0 \to 91$	$0 \to 91$
H^+H^- (90)	$0 \to 35$	$0 \to 35$	$0 \to 35$	$0 \to 35$	$0 \to 35$	$0 \to 35$

Table 5.9: The expected number of W^+W^-, ZZ and H^+H^- ($M_H = 80,\ 90$ GeV) induced events for 500 pb^{-1} integrated luminosity at LEP2 ($\sqrt{s} = 200$ GeV).

If a $H^\pm$ is found then can we infer the underlying Higgs model? As mentioned before, a sizeable $H^\pm \to cb$ signal would be a signature of the MHDM. For a mass comfortably below M_W a reasonable number of $H^\pm$ pairs will be produced and we shall require three tagged $cb\tau\nu_\tau$ events to conclude that a detected $H^\pm$ originates from the MHDM. From Eq. (5.22) we can obtain Eq. (5.24), from which the values of $f(\mathrm{BR})$ needed to produce the distinctive signature of three tagged $cb\tau\nu_\tau$ events can be found.

$$f(\mathrm{BR}) \times N_{H^+H^-} = 36\,. \tag{5.24}$$

Thus for $N_{H^+H^-} = 100$ (corresponding to $M_H = 75$ GeV at $\sqrt{s} = 180$ GeV), one finds $f(\mathrm{BR}) = 0.36$, and thus $\mathrm{BR}(H^\pm \to cb) \geq 20\%$ is required. For lower masses $\mathrm{BR}(H^\pm \to cb) \approx 10\%$ (or even less) would be sufficient. We note that for the 2HDM Eq. (5.24) shows that the above values would predict ≤ 0.1 events, which is unobservable.

In addition, we recall that a lack of $H^\pm \to \tau\nu_\tau$ decays i.e. leptophobia with $\mathrm{BR}(H^\pm \to jets \to 100\%$, is in principle another indicator of the MHDM. Eq. (5.14) shows that quite a large region of parameter space is available for a BR $\leq 10\%$ and this could be a good discriminator. For the extreme case of $\mathrm{BR}(H^\pm \to jets) \to 100\%$ one would find a twofold increase in the number of events in the $c\bar{s}cs$ channel compared to Model I, and a fourfold increase compared to Model I′; this would be distinctive. Thus we see that when $N_{H^+H^-}$ is larger it is possible to exploit the distinctive signatures of $H^\pm$ of the MHDM. In the next section we turn our attention to higher energy e^+e^- colliders.

5.5 High–Energy e^+e^- Colliders

Prospects for a very high energy e^+e^- linear collider have recently been discussed, see for example Ref. [57], with collision energy $\sqrt{s} = 500 \rightarrow 1000$ GeV, and integrated luminosity of the order $1 \rightarrow 10$ fb^{-1}. The increased centre–of–mass energy would of course enable heavier H^+H^- pairs to be created, should M_H be beyond the reach of LEP2. The charged scalars of the 2HDM (Model II and II') may also be in range now, with $M_H \geq 260$ GeV from the $b \rightarrow s\gamma$ constraint (Eq. (5.2)). We will again focus on the pair production process, although if $\sqrt{s} > 2\,m_t \approx 350$ GeV and $m_t > M_H + m_b$, an additional production mechanism becomes available, *viz.* $t \rightarrow H^{\pm}b$. The phenomenology of the 2HDM at these colliders has been studied [57]. The backgrounds for the LEP2 will still be relevant although the magnitudes of the cross–sections will differ; in particular the main backgrounds ($q\overline{q}$ and WW) are smaller in magnitude. One new background is the production of $t\bar{t}$ pairs. This may cause difficulties if $M_H \approx m_t$ and this scenario is discussed later. This background can usually be removed by an invariant mass cut on the $t\bar{t}$ jets. For $M_H \geq m_t + m_b$ the channel $H^{\pm} \rightarrow tb$ is open. Very large hadronic activity is required for the signal, and the $t\bar{t}$ background is substantially reduced by demanding events with large b quark content; the signal consists of $W^+W^-b\overline{b}b\overline{b}$ final states compared to the $t\bar{t}$ final state of $W^+W^-b\bar{b}$. A charged Higgs with $M_H \leq 0.4\sqrt{s}$ may be detected straightforwardly with a luminosity of 10 fb^{-1} if its decays are dominated by SM fermion or $W^{\pm}h^0$ channels [57].

Figure 5.8 shows the expected number of events for $\sqrt{s} = 500$ GeV and $\sqrt{s} = 1000$ GeV, corresponding to an integrated luminosity of 3 fb^{-1}. Is it possible to detect the charged Higgs when $M_H \approx M_W$ or $M_H \approx M_Z$ at these colliders? Table 5.10 shows the expected number of charged scalar pairs for the two collider energies and an integrated luminosity of 3 fb^{-1}. Using the $\tau\nu_\tau\tau\nu_\tau$ channel it is possible [57], [58] to detect a charged

	$\sqrt{s} = 500$ GeV	$\sqrt{s} = 1000$ GeV
H^+H^- ($M_H = 80$ GeV)	317	89
H^+H^- ($M_H = 90$ GeV)	303	88

Table 5.10: Number of $e^+e^- \rightarrow H^+H^-$ pairs for $\int \mathcal{L} = 3$ fb^{-1}.

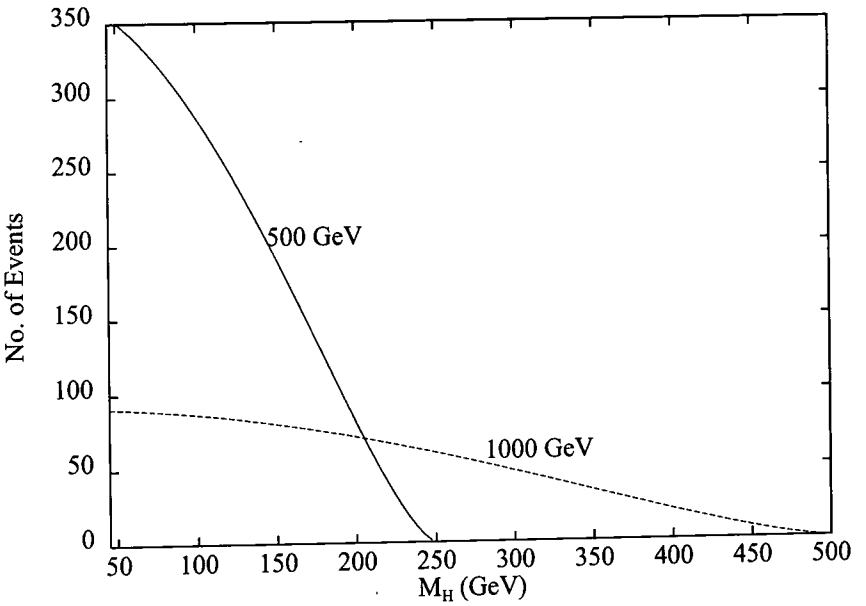

Figure 5.8: As for Figure 5.6, but for $\sqrt{s} = 500$ and 1000 GeV with $\int \mathcal{L} = 3$ fb^{-1}.

Higgs of $M_H \approx M_W$ with $\mathcal{L} = 10\,\text{fb}^{-1}$ provided that BR $(H^\pm \to \tau\nu_\tau)$ is at least 30%. From Table 5.2 this is certainly the case for the 2HDM (Models I and I'). For the MHDM this may not be the case due to the possibility of suppressed lepton decays. Enhanced $H^\pm \to cb$ decays would again allow detection and, as we have already stressed, provides a way of distinguishing between the 2HDM and MHDM.[7]

There are however two caveats to this discussion. First, if a light h exists then the decay $H^\pm \to W^\pm h$ needs also to be considered. In 2HDM models the $W^\pm H^\pm h$ coupling depends on $\cos(\beta - \alpha)$, where α is a mixing angle arising from the diagonalization of the CP–even sector of the Higgs mass matrix. If this factor is not small, the Wh channel can dominate the fermion decay modes [30] (assuming that the tb channel is kinematically forbidden). With the expectation that $h \to b\bar{b}$, this would lead to a new source of b quarks feigning the signal coming from an enhanced MHDM cb channel. However this

[7]We note that in the 2HDM (Model II') a large cb decay is also possible if $\tan\beta$ is large, see Table 5.1. However, due to the constraint $M_H \geq 260$ GeV, the $H^\pm \to tb$ channel will always be available and thus becomes the dominant quark decay mode.

should not be a problem in practice, since the $W^\pm h$ final state has a very different topology (dominantly 4–jet) from that of $H^\pm \to cb$ (dominantly 2–jet). Note that the mere presence of $H^\pm \to W^\pm h$ inevitably reduces BR ($H^\pm \to cb$) somewhat.

The second caveat is that when $H^\pm \to tb$ is allowed, it usually dominates over all fermion decay modes in both 2HDM and MHDM. The decay $H^\pm \to W^\pm h$ can compete depending on the value of the suppression factor from the Higgs sector mixing angles (which is $\cos(\beta-\alpha)$ in the 2HDM), and the mass of the neutral h boson; see Ref. [30]. Can we distinguish between the MHDM and 2HDM for this higher mass region, $M_H > m_t+m_b$? In the MHDM, large values of $|Z|$ and small values of $|X|$, $|Y|$ could enhance $\tau\nu_\tau$ decays sufficiently so that they compete with the tb channel. However, asymmetric choices such as $|X| = 0.1$, $|Y| = 0.1$, $|Z| = 10$ would be needed and this seems somewhat unnatural. The enhancement is also possible in Model I′ for $\tan\beta \geq 10$, a condition perhaps more natural than that needed for the MHDM. Of course, the discovery of a second charged scalar would provide conclusive proof of a MHDM (notwithstanding the existence of more exotic Higgs sectors containing triplets – see Chapter 7).

A suppressed $H^\pm \to \tau\nu_\tau$ decay mode would still be a signature of the MHDM, in principle. However, this method requires the Model I and I′ branching ratios to have a lower bound. This is the case (see earlier) for M_H in the range of LEP2, but for heavier Higgs bosons the $W^\pm h$ and/or tb channels must be included. Hence no lower bound is possible and the $\tau\nu_\tau$ decays are usually negligible. This distinguishing method is therefore only relevant *before* the $W^\pm h$ and/or tb channels open up.

Table 5.11 shows the various backgrounds to the H^+H^- signal from W^+W^- and ZZ production at $\sqrt{s} = 500$ GeV, assuming an integrated luminosity of 3 fb^{-1}. Using the

	$cbcb$	$cbcs$	$cb\tau\nu_\tau$	$cscs$	$cs\tau\nu_\tau$	$\tau\nu_\tau\tau\nu_\tau$
W^+W^-	0.0	7.2	2.4	2284.0	1551.4	263.4
ZZ	27.3	0.0	0.0	27.9	0.0	10.3
$H^+H^-(80)$	$0 \to 317$	$0 \to 317$	$0 \to 317$	$0 \to 317$	$0 \to 317$	$0 \to 317$
$H^+H^-(90)$	$0 \to 303$	$0 \to 303$	$0 \to 303$	$0 \to 303$	$0 \to 303$	$0 \to 303$

Table 5.11: The expected number of W^+W^-, ZZ and H^+H^- ($M_H = 80$, 90 GeV) induced events for 3 fb^{-1} integrated luminosity at 500 GeV.

formulae from the previous section, Eqs. (5.21) $\rightarrow$ (5.24), and with e_H staying roughly the same as the LEP2 case [57], we can see that the increased $N_{H^+H^-}$ enables a greater parameter space of $f(\mathrm{BR})$ to be covered, i.e. for $N_{sig} = 3$ at $M_H = 80$ GeV one requires $f(\mathrm{BR}) \geq 0.11$. The background is again well below 1 event. The same channel also allows $H^\pm$ of the MHDM to be distinguished, and using Eq. (5.24) we see that the coverage of $f(\mathrm{BR})$ is better than at LEP2, as is expected due to the increased values of $N_{H^+H^-}$ over a wider range of masses. For example, with $M_H = 150$ GeV (corresponding to $N_{H^+H^-} = 200$) one finds that $\mathrm{BR}(H^\pm \rightarrow cb) \geq 10\%$ is sufficient.

The region $M_H \approx M_Z$ is not a problem at the higher energy collider due to the tenfold increase in event number, and the ZZ cross–section being an order of magnitude smaller than the WW cross–section.

The situation when $M_H \approx m_t \approx 180$ GeV needs special consideration. Here there exists a background from $e^+e^- \rightarrow Z^*, \gamma^* \rightarrow t\bar{t}$. The literature has dealt with this case for the 2HDM (see for example Ref. [57]) and the analysis holds again for the MHDM. The best chance of eliminating the $t\bar{t}$ background is by exploiting the $H^+H^- \rightarrow c\bar{c}s\bar{s}$ channel. Because the $t\bar{t}$ decays primarily to $W^+W^-b\bar{b}$, the process of anti–b–tagging can single out the Higgs bosons. This idea will in general work better for the 2HDM where the $H^\pm$ rarely decays to b quarks.

5.6 Conclusions

In this chapter we have studied the detection prospects of light charged Higgs scalars of the MHDM and 2HDM (Models I, I′, II, II′) at e^+e^- colliders. It is theoretically possible that the masses of these particles for the MHDM and 2HDM (Model I and I′) lie within the discovery range of LEP2. For $H^\pm$ of the above models, with $\sqrt{s} = 180$ GeV, masses from 41.7 GeV (current LEP lower bound) to $M_H < M_W$ will be covered successfully. The region $M_H \approx M_W$ is problematic, partly due to the lower number of H^+H^- events, and partly due to the fact that a invariant mass cut on reconstructed jets will eliminate the signal as well as the background. A possible way of obtaining a signal in this difficult region is to use the $cb\tau\nu_\tau$ channel which is almost totally free of background. A significant

BR ($H^\pm \to cb$) is required and this is only possible in the MHDM. For $\sqrt{s} = 200$ GeV, a BR ($H^\pm \to cb$) of 30% would be sufficient if $M_H \approx M_W$, but for $M_H \approx M_Z$ too few charged scalars are produced. We showed that branching ratios of these magnitudes (or greater) *are* allowed, which is in contrast to the 2HDM. Away from this mass region, a distinctive signature of $H^\pm$ from the MHDM would be BR ($H^\pm \to cb$) $\geq 10\%(20\%)$ for $M_H = 75$ GeV (60 GeV). Another distinct signature of the MHDM would be BR($H^\pm \to \tau\nu_\tau$) $\leq 10\%$, i.e. leptophobia. In the case of BR($H^\pm \to jets$) $\to 100\%$, the signal in the 4-jet channel would be double that possible in the 2HDM.

For the $H^\pm$ of the various 2HDM considered (Model I and I′) the mass regions $M_H \approx M_W$ and $M_H \approx M_Z$ are inaccessible as there is no significant $H^\pm \to cb$ decay to exploit.

We have also considered higher energy e^+e^- colliders with increased luminosity. These would enable heavier charged scalars to be produced, including those of the 2HDM (Model II and II′), and create more events for the difficult $M_H \approx M_W$ and $M_H \approx M_Z$ regions. For both the 2HDM and MHDM detection is fairly straightforward for $2M_H < 0.8\sqrt{s}$. The only potential problem would be for $M_H \approx M_W$, but Ref. [58] has shown that a sizeable $\tau\nu_\tau$ branching ratio would be sufficient for detection. A significant $H^\pm \to cb$ channel in the MHDM would provide an alternative signal for this region and would again provide a way of distinguishing between the 2HDM and the MHDM as long as $M_H < m_t + m_b$. If $H^\pm \to tb$ is allowed then this channel (along with a possible $H^\pm \to W^\pm h$) generally dominates for both models and thus they would be virtually indistinguishable. However, there does exist a small region of parameter space ($\tan\beta \geq 10$ or equivalent in MHDM which would produce a higher BR ($H^\pm \to \tau\nu_\tau$) for the MHDM and 2HDM (Model I′) than is ever possible in the other models.

Chapter 6

Non–minimal neutral Higgs bosons.

6.1 Introduction

This chapter considers the neutral Higgs sectors of the 2HDM and the MHDM, and their phenomenology at LEP2 and the LHC. As was described in Chapter 4, the 2HDM predicts two CP–even neutral scalars, and our aim now is to ascertain whether it may be possible to distinguish between ϕ^0 and the neutral bosons of extended models. We note that the couplings of ϕ^0 to matter, and thus its production cross–sections and BRs, are fixed theoretically once M_{ϕ^0} is known. Therefore if a Higgs signal is found with strong deviations from the phenomenology of ϕ^0, this may suggest a non–minimal Higgs model. We shall explore the parameter space of β and α to see if such deviations are indeed possible. Of interest to us is the lightest CP–even Higgs boson of the 2HDM and MHDM, labelled as h_1, and we will consider in turn its phenomenology at LEP2 and at the LHC. We stress that if a neutral Higgs boson is detected at a future collider it is important to ascertain from which model it originates. Our convention is that h^0 labels the lightest CP–even Higgs boson in the MSSM. The chapter is organized as follows. In (6.2) we introduce the relevant non–minimal Higgs models and investigate their couplings. Section (6.3) examines their phenomenology at LEP2 in the case of distinctive branching ratios not possible for ϕ^0 and h^0, with the conclusions given in (6.4). Section (6.5) studies the analogous phenomenology at the LHC, with its conclusions given in (6.6).

6.2 Couplings of the Models

We shall focus on the lightest CP–even neutral scalar (h_1); for the analysis at LEP2 we assume that this Higgs particle is the only one in range at this collider. Our analysis at the LHC will again only consider h_1, although it is quite possible that this collider will detect the other Higgs bosons of the model.

The theoretical structure of the 2HDM is well known [30], and was reviewed in Chapter 4. The MHDM [46], [59], has received substantially less attention. In particular, when the MHDM is considered in the literature the focus is nearly always on the charged Higgs sector, see Chapter 5. We shall be investigating the properties of h_1 of the MHDM, and for simplicity assume no mixing between CP–even and CP–odd scalars. It has been shown in Chapter 5 and in Ref. [46] that significant differences can exist between the 2HDM and MHDM in the case of the charged Higgs sector, and we anticipate an analogous result in the neutral Higgs sector. We shall focus on the 2HDM and give mention to the MHDM where appropriate.

Table 4.2 shows the four different ways with which the 2HDM can be coupled to the fermions (the Yukawa couplings). The numbers (1 or 2) show which Higgs doublet couples to which fermion type. The Higgs sector of the MSSM requires Model II type couplings and thus the phenomenology of Model II has received the most attention of the four. Models I′ and II′ are rarely mentioned, and only then in the context of the charged Higgs sector [35]. For a MHDM there are more permutations of the Yukawa couplings, although it is conventional to couple each fermion type to a distinct doublet, e.g. in a 3HDM doublets 1, 2, 3 would couple to d, u, e respectively. We shall be considering the lightest CP–even Higgs scalar (h_1) of the above models, and for the 2HDM its couplings to the fermions are given in Table 6.1.[1]

We recall that α is the mixing angle used to diagonalize the CP–even mass matrix and β is defined by $\tan\beta = v_2/v_1$ (v_i is the VEV of the i^{th} doublet and $v_1^2 + v_2^2 = 246^2$ GeV^2). In the MSSM, which is a constrained version of the 2HDM (Model II), the angles α and β are related (see (4.5)). For the models that we shall consider α and β are independent.

[1]For Higgs masses in the range of LEP2, branching ratios to vector bosons are negligible.

	Model I	Model I′	Model II	Model II′
$hu\overline{u}$	$\cos\alpha/\sin\beta$	$\cos\alpha/\sin\beta$	$\cos\alpha/\sin\beta$	$\cos\alpha/\sin\beta$
$hd\overline{d}$	$\cos\alpha/\sin\beta$	$\cos\alpha/\sin\beta$	$-\sin\alpha/\cos\beta$	$-\sin\alpha/\cos\beta$
$he\overline{e}$	$\cos\alpha/\sin\beta$	$-\sin\alpha/\cos\beta$	$-\sin\alpha/\cos\beta$	$\cos\alpha/\sin\beta$

Table 6.1: The fermion couplings of h_1 in the 2HDM relative to those for the minimal SM Higgs boson (ϕ^0).

From Eq. (5.9) there exists the bound of

$$\tan\beta \geq 1.25\,, \tag{6.1}$$

obtained from considering the effects of the charged Higgs scalar on the $Z \to b\overline{b}$ decay [46].

For the MHDM there exist N doublets with the VEVs (v_i) obeying the relationship

$$v^2 = \sum_{i=1}^{N} v_i^2\,. \tag{6.2}$$

The lightest CP–even mass eigenstate is a linear combination of the Lagrangian eigenstates, and can be written as

$$h_1 = \sum_{i=1}^{N} X_{i1}^{*}\phi_i^0\,. \tag{6.3}$$

The parameters X_{i1}^{*} originate from the mixing matrix for the CP–even neutral Higgs sector defined by

$$\phi_i^0 = \sum_{j=1}^{N} X_{ij}h_j\,. \tag{6.4}$$

They are therefore analogous to $\sin\alpha$ and $\cos\alpha$ in the 2HDM. Our convention is that ϕ_i^0 is the real part of the neutral Higgs field of the i^{th}doublet; h_j are the mass eigenstates with h_1 taken to be the lightest. The unitarity of the matrix forces the relationship

$$\sum_{i=1}^{N} |X_{i1}|^2 = 1\,. \tag{6.5}$$

The Yukawa couplings in the MHDM are not as correlated as in the 2HDM. Therefore a MHDM can always feign a 2HDM but might possibly possess a distinctive signature. We shall now quantify the above statement. In the 2HDM there exists the relation

$v^2 = v_1^2 + v_2^2$. Since the strength of a Yukawa coupling is proportional to $1/v_i$, for small v_i the coupling is significantly enhanced relative to the minimal SM Higgs boson (ϕ^0). We see that if v_1 (say) is small, then $v_2 \approx v$ is automatic. Therefore any Yukawa coupling which is proportional to v_2 cannot be enhanced significantly compared to ϕ^0. However in the MHDM one has the relation in Eq. (6.2). This is a weaker constraint on the v_i and therefore it is entirely possible that several v_i are simultaneously small and hence a significantly different phenomenology may be possible. The Yukawa couplings for a MHDM (relative to ϕ^0) are of the form

$$vX_{i1}^*/v_i\,, \tag{6.6}$$

and so the enhancements possible in the 2HDM are attainable if $v_i \ll v$.

6.3 Phenomenology at LEP2

As a prerequisite to studying the phenomenology of h_1 at LEP2 we must next study its BRs for the range $M_{h_1} \leq 100$ GeV (i.e. the LEP2 discovery range). The important decays are to $b\bar{b}$, $\tau^+\tau^-$, $c\bar{c}$ and gg. For ϕ^0 with $M_{\phi^0} = 50$ GeV the ratios of the respective BRs (from Figures 3.6 and 3.7) are approximately:

$$b\bar{b} : \tau^+\tau^- : c\bar{c} : gg = 0.87 : 0.08 : 0.03 : 0.02\,. \tag{6.7}$$

For $M_{\phi^0} = 100$ GeV one has:

$$b\bar{b} : \tau^+\tau^- : c\bar{c} : gg = 0.80 : 0.09 : 0.03 : 0.07\,. \tag{6.8}$$

Here the BRs for $b\bar{b}$ and $c\bar{c}$ are evaluated by summing the Feynman diagrams in Figure 6.1, with the replacements $q = b$ and $q = c$ respectively. The virtual QCD corrections have not been displayed in the figures although they are included in Eqs. (6.7) and (6.8). The BR for gg represents the summation of all diagrams which give light quark jets i.e. all diagrams in Figure 6.1 with $q = u$, d, s, and both diagrams in Figure 6.2. We note that decays via a quark loop proceed predominantly by a top quark loop.

In Eq. (6.8) decays to WW^* (where $*$ denotes an off–shell particle) are at the 1% level. It is apparent from Eqs. (6.7) and (6.8) that decays to $b\bar{b}$ dominate, and this property

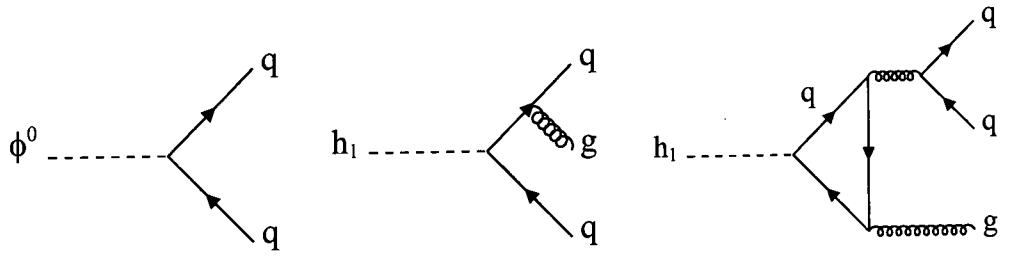

Figure 6.1: Decays of $h_1 \to q\bar{q}$, $q\bar{q}g$.

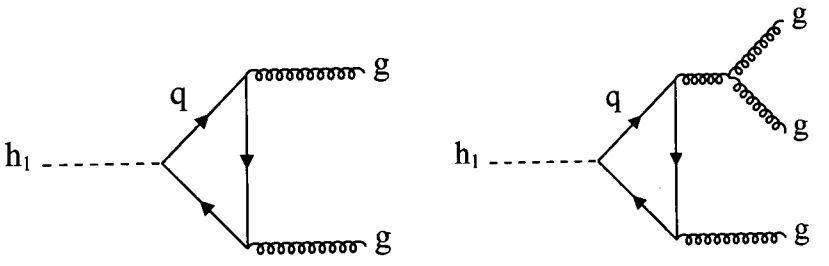

Figure 6.2: Decays of $h_1 \to gg(g)$.

allows light quark backgrounds to the Higgs signal to be reduced by b–tagging. For h^0 one has very similar BRs for masses in the LEP2 range [11]. Distinguishing ϕ^0 from h^0 provides a challenge for future colliders and is discussed elsewhere [42]. It is the aim of this section to study the phenomenology of the 2HDM and MHDM at LEP2, in the case of extreme BRs not possible for ϕ^0 and h^0. The phenomenology at the LHC will be discussed later (6.5). From Table 6.1 one can vary the angles α and β independently to see if parameter spaces exist for such extreme BRs. We can summarize as follows:

(i) Model I′: BR $(h_1 \to \tau^+\tau^-)$ large if $\tan\beta \gg 1$ and $\sin\alpha$ moderate[2] to maximal.

(ii) Model II′: BR $(h_1 \to \tau^+\tau^-)$, BR $(h_1 \to c\bar{c})$ and BR $(h_1 \to gg)$ share domination for small $\sin\alpha$ and $\tan\beta$ moderate.

(iii) Model II: BR $(h_1 \to c\bar{c})$ and BR $(h_1 \to gg)$ share domination for small $\sin\alpha$ and $\tan\beta$ moderate.

[2]We take 'moderate' to mean the angle is approximately $\pi/4$.

(iv) Model I: Has exactly the same BRs as ϕ^0, unless $\cos\alpha \to 0$ (fermiophobia) which will be discussed in Chapter 8.

One must be aware of the bound $\tan\beta \geq 1.25$ from Eq. (6.1) when varying the angles. It is apparent that distinctive BRs *are* possible in the 2HDM, the general requirement being that one of the angles has an extreme value. Most noticeably the $b\bar{b}$ decays can be suppressed and/or made negligible[3]. This is in contrast to ϕ^0 and h^0 which will decay predominantly to $b\bar{b}$ for masses in range at LEP2 – see Eqs. (6.7) and (6.8). It is our aim to exploit these enhanced BRs at LEP2. On first viewing it seems that BR $(h_1 \to \tau^+\tau^-) \gg 10\%$ would provide a clear signal of Model I′, since searching for $\phi^0 \to \tau^+\tau^-$ in conjunction with $Z \to hadrons$ is one of the proposed techniques at LEP2 and gives a reasonable signal [10]. However, the production cross–section $\sigma(e^+e^- \to Z^* \to Zh_1)$ is suppressed relative to that of ϕ^0 by a factor of $\sin^2(\beta-\alpha)$. Therefore we must investigate whether the parameter choices needed to obtain a distinctive BR simultaneously decrease the production cross–section at LEP2. We shall now address this problem, as well as applying the proposed search techniques for ϕ^0 to h_1 of the 2HDM and MHDM.

The phenomenology of ϕ^0 at LEP2 has been extensively covered in the literature, most recently in Ref. [10], and was reviewed in Chapter 3. The dominant production mechanism for ϕ^0 if M_{ϕ^0} is in the range of LEP2 ($M_{\phi^0} \leq \sqrt{s} - M_Z$ GeV) is the Higgs–strahlung process [20]

$$e^+e^- \to Z\phi^0, \tag{6.9}$$

in which ϕ^0 is emitted from a virtual Z boson. This cross–section is shown in Figure 3.9. We shall be interested in the case of $\sqrt{s} = 192$ GeV, since it is at this energy that the computer simulations in Ref. [10] have been carried out. The cross–section for ϕ^0 is $\sigma = 1.06$ (0.51) pb for $M_{\phi^0} = 60$ (90) GeV. For $M_{\phi^0} = 99$ GeV, which is the mass generally considered to be at the limit of the LEP2 range for $\sqrt{s} = 192$ GeV, $\sigma = 0.21$ pb. Experimental simulations have been performed for the following event types:

(i) $Z \to e^+e^-;\ \mu^+\mu^-,\ \phi^0 \to$ anything.

[3]We note that the width of the third diagram in Figure 6.1 (with $q = b$) would be boosted if the coupling to up–type quarks is enhanced. However, this diagram has a very small width [63] and so heavily suppressed $h_1 \to b\bar{b}$ decays are still possible.

(ii) $Z \rightarrow \tau^+\tau^-$, $\phi^0 \rightarrow$ hadrons and vice versa.

(iii) $Z \rightarrow \nu\overline{\nu}$, $\phi^0 \rightarrow$ hadrons.

(iv) $Z \rightarrow$ hadrons, $\phi^0 \rightarrow b\overline{b}$.

Events (iii) and (iv) require b–tagging to reduce the light quark background, and since we shall be considering Higgs bosons with suppressed $b\overline{b}$ decays these will not be relevant to our analysis. Events of the form (i) are independent of the Higgs BRs, and require a pair of energetic leptons with an invariant mass compatible with M_Z. The Higgs signal appears as a peak in the missing mass distribution. Events of the form (ii) are characterized by two energetic, isolated τ's associated with two hadronic jets. The existence of a Higgs boson would then be observed as an accumulation around (M_{ϕ^0}, M_Z) in the invariant mass distributions of the τ's and jets. Table 6.2 (from Ref. [10]) shows the simulated effective cross–sections in the four channels for $M_{\phi^0} = 90$ GeV and $\sqrt{s} = 192$ GeV:

	$\phi^0 l^+ l^-$	$\tau^+\tau^- q\overline{q}$	$\phi^0 \nu\overline{\nu}$	$\phi^0 q\overline{q}$
ALEPH	12:12	8:5	24:13	58:33
DELPHI	6:2	4:6	25:18	46:36
L3	13:7	–	28:21	36:23
OPAL	8:30	–	17:13	34:36

Table 6.2: Effective cross–sections for signal (first number) and background (second number) in fb, at LEP2 for $M_{\phi^0} = 90$ GeV and $\sqrt{s} = 192$ GeV, taking into account acceptances and efficiencies (from Ref. [10]).

All the above analysis has been for ϕ^0, with BRs given by Figures 3.6 and 3.7. It is our aim now to extrapolate these results for use in the 2HDM and MHDM. As shown earlier these models may possess vastly different BRs to those of ϕ^0. However, the production cross–section for h_1 is suppressed relative to that for ϕ^0 (denoted by σ_{ϕ^0}) by $\sin^2(\beta - \alpha)$. A possible consequence of this suppression is that a very light h_1 ($M_{h_1} \approx 10$ GeV) would have escaped detection at LEP1 if $\sin^2(\beta - \alpha) \ll 0.1$. This possibility has recently been considered in Refs. [60], [61] and these papers consider making use of non–suppressed production channels. For h^0 of the MSSM the relations between the masses and mixing angles, enables one to obtain the lower bound $M_{h^0} \geq 44$ GeV [62]. Therefore the detection

of a neutral CP–even Higgs boson with a mass between 10 GeV and 40 GeV would indicate h_1. However, it would be impossible to infer from which specific model it originates unless it displays a distinctive BR.

To start our analysis let us now take the case of Model I′ with a dominant BR ($h_1 \to \tau^+\tau^-$). One would therefore use detection channel (ii), and the event cross–section (before applying efficiencies and acceptances) would be given by $\sigma_{\phi^0} \times \sin^2(\beta - \alpha)$ multiplied by:

$$\left[\mathrm{BR}(Z \to q\bar{q}) \times \mathrm{BR}(h_1 \to \tau^+\tau^-) + \mathrm{BR}(h_1 \to q\bar{q}) \times \mathrm{BR}(Z \to \tau^+\tau^-)\right] . \qquad (6.10)$$

Eq. (6.10) shows that for h_1 the dominant term is the first term since BR $(Z \to q\bar{q}) = 70\%$, while BR $(Z \to \tau^+\tau^-) = 3.4\%$. After inputting the values for the BRs one finds for ϕ^0 a cross–section equal to

$$0.086 \times \sigma_{\phi^0} . \qquad (6.11)$$

For Model I′ this may be greatly enhanced, e.g. for BR $(h_1 \to \tau^+\tau^-) = 80\%$ and BR $(h_1 \to$ jets$)=20\%$ we have the following cross–section:

$$0.57 \times \sigma_{\phi^0} \times \sin^2(\beta - \alpha) . \qquad (6.12)$$

Hence there could be a considerable increase in the signal size for this channel, as much as an order of magnitude. It is now necessary to see if the values of β and α needed to give a large BR $(h_1 \to \tau^+\tau^-)$ cause a suppression in the $\sin^2(\beta - \alpha)$ term. We note from the couplings in Table 6.1 that $\alpha \to \pi/2$ would further enhance $\tau^+\tau^-$ decays while suppressing the $b\bar{b}$ channel. However, from Eq. (6.12) we see that allowing both $\alpha \to \pi/2$ and $\beta \to \pi/2$ would cause strong suppression from $\sin^2(\beta - \alpha)$ in the cross–section. We shall now derive the value of α that maximizes the number of events.

To obtain a large BR $(h_1 \to \tau^+\tau^-)$ we showed earlier that $\tan\beta$ must be large and $\sin\alpha$ must be moderate to maximal. In Eq. (6.10) the dominant term is the first one and so we shall neglect the second. The first term is proportional to $\sin^2\alpha/\cos^2\beta$, and so we wish to maximize $f(\beta,\ \alpha)$ defined by:

$$f(\beta,\ \alpha) = \sin^2(\beta - \alpha) \times \sin^2\alpha/\cos^2\beta . \qquad (6.13)$$

In Figure 6.3 we plot $f(\beta,\ \alpha)$ with $\beta = 1.5$ rads (86°) since large BR $(h_1 \to \tau^+\tau^-)$ requires small $\cos\beta$.

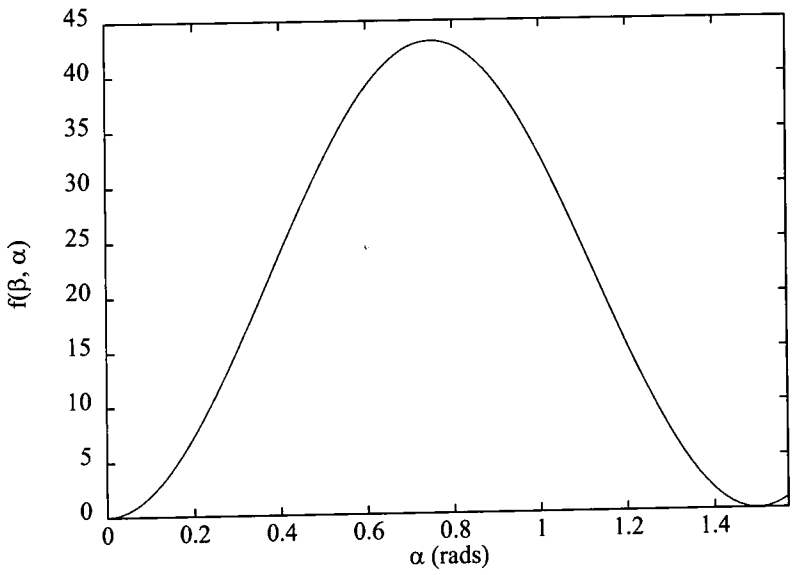

Figure 6.3: $f(\beta,\ \alpha)$ as a function of α for $\beta = 1.5$ rads.

It is apparent from Figure 6.3 that moderate values of α ($\approx \pi/4$) allow the largest values of $f(\beta,\ \alpha)$. We see that $\alpha = \pi/4$ and $\beta \approx \pi/2$ would give $\sin^2(\beta - \alpha)$=0.5. Therefore the suppression of the cross–section in Eq. (6.12) is not so severe, and the distinctive signature of a large number of $\tau^+\tau^-$ plus 2 jet events is certainly possible in Model I′. Moreover, a large $\tau^+\tau^-$ peak will be centered at M_{h_1} with almost no peak at M_Z, which is in contrast to the ϕ^0 case which will have small $\tau^+\tau^-$ peaks centered at M_ϕ and M_Z (since the two terms in Eq. (6.10) are of roughly equal magnitude). Hence, even if there is significant suppression from the $\sin^2(\beta - \alpha)$ term, the relative heights of the peaks will be different for h_1. However there may not be enough events to notice this pattern unless M_{h_1} is considerably lighter than 90 GeV, i.e. when the cross–section is larger. Table 6.2 shows that for the ALEPH detector with 500 pb^{-1} of integrated luminosity one would expect the number of signal (background) events to be 4 (2). This is for ϕ^0 with $M_{\phi^0} = 90$ GeV. For $M_{\phi^0} = 60$ GeV (say) the improved cross–section would double the number of events.

For h_1 of Model I, Table 6.1 shows that its couplings to the fermions are scaled by the

same factor and so will be identical to those of ϕ^0 if this scaling is not too small; the special case of fermiophobia ($\cos\alpha \to 0$) will be covered in Chapter 8. Hence no distinct BR is possible. We recall that h^0 of the MSSM also feigns ϕ^0 over a large parameter space, but h_1 of Model I could have a suppressed production rate due to the factor $\sin^2(\beta-\alpha)$; hence a neutral CP–even Higgs boson with identical BRs to ϕ^0 but a suppressed cross–section and/or $M_{h_1} \leq 44$ GeV would be indirect evidence[4] for Model I′. Alternative distinctive signatures of Model I would be a fermiophobic Higgs (Chapter 8) and/or a light charged scalar ($M_{H^\pm} \leq 80$ GeV) – see Chapter 5.

For Model II′ we stated earlier that the decays $h_1 \to \tau^+\tau^-$, $h_1 \to gg$ and $h_1 \to c\bar{c}$ would share the domination for small $\sin\alpha$ and $\tan\beta$ moderate, i.e. $h_1 \to b\bar{b}$ may be heavily suppressed. The decay $h_1 \to gg$ proceeds via a top quark loop and so is boosted since the above parameter choices enhance couplings to up–type quarks. From Eqs. (6.7) and (6.8) we see that the ratio of the $\tau^+\tau^-$ partial width to the jet ($c\bar{c}$ and gg) partial width would be 8:5 for $M_{h_1} = 50$ GeV, and 9:10 for $M_{h_1} = 100$ GeV. Therefore in contrast to Model I′ the $\tau^+\tau^-$ decays can never saturate the total width (i.e. BR $\approx 100\%$). Hence it would appear that Model II′ could be mimicked by Model I′, although in this case Model I′ would have accompanying $b\bar{b}$ decays while Model II′ would be accompanied by $c\bar{c}$ and gg. If the $b\bar{b}$ decays are of sufficient magnitude then Model I′ would also register a signal in detection methods (iii) and (iv) (which require b–tagging), while Model II′ would not. Therefore it is possible that h_1 of Model II′ has a distinct signature.

Model II is the structure that is most considered in the literature since it is the form required for the MSSM. For suitable parameter choices (see earlier) the $b\bar{b}$ channel may be suppressed and the decays $h_1 \to gg$ and $h_1 \to c\bar{c}$ could dominate. We do not believe that this scenario has been considered before, and any detection technique that requires b–tagging or $\tau^+\tau^-$ decays will fail. However, the missing mass technique is Higgs BR independent and so there is still a chance of a signal, provided that the cross–section suppression is not too great. Figure 6.4 plots the suppression $\sin^2(\beta-\alpha)$ as a function of α for $\beta = \pi/4$ (moderate $\tan\beta$ is required for an enhancement of $c\bar{c}$ and gg decays) and shows that for very small α (i.e. $\sin\alpha \approx 0$, which is of interest to us) the cross–section suppression is only of order 0.5. Therefore we anticipate that a reasonable signal could be

[4]Of course, another 2HDM or a MHDM could mimic the BRs of ϕ^0 for carefully chosen couplings.

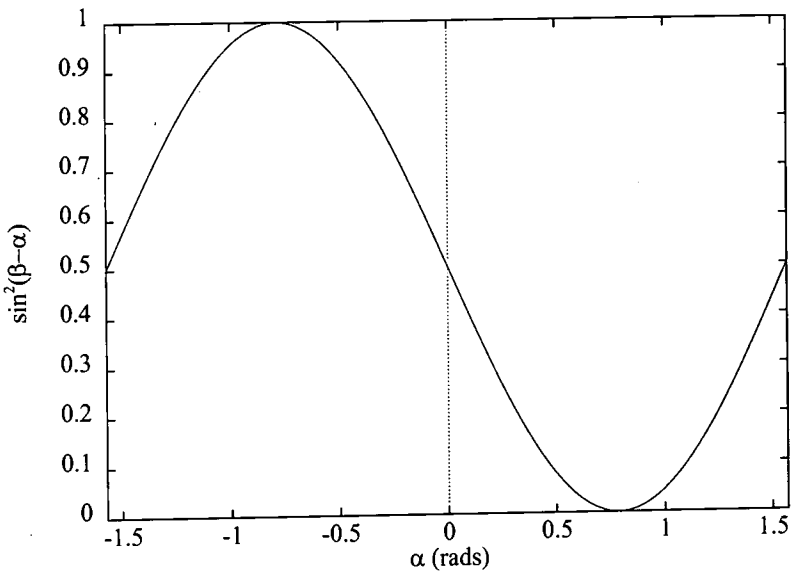

Figure 6.4: $\sin^2(\beta - \alpha)$ as a function of α for $\beta = \pi/4$ rads.

obtained for the scenario of $c\bar{c}$ and gg decays dominating; see Table 6.2 for an indication of event numbers. We stress that the non–observance of a Higgs signal in the other three detection channels (which make use of $b\bar{b}$ and $\tau^+\tau^-$ decays), but a positive signal using the missing mass technique would be evidence for h_1 of Model II with $h_1 \to c\bar{c}$, gg decays dominating. Moreover, if such a signal is observed there would then be motivation to search for charm rich jets originating from h_1. We conclude that Model II does possess a distinctive signature.

Having completed our account of the 2HDM at LEP2 we now address the MHDM. As mentioned earlier, a MHDM can always feign a 2HDM but there may be a chance of it possessing a distinctive signature. Concerning decay channels, the 2HDM can exhibit extreme BRs for the decays to up–type quarks, down–type quarks and leptons. Of course the MHDM can possess identical enhancements (Eq. (6.6)) but this is not distinctive. However, if the production cross–section of h_1 from the MHDM has less suppression than h_1 from the 2HDM, as well as having an extreme BR, then this would be a distinguishing trait. The coupling of the MHDM neutral scalars to Z (which is $\sin^2(\beta-\alpha)$ in the 2HDM)

is given by

$$\frac{\sigma_{h_1}}{\sigma_{\phi^0}} = \frac{|\sum v_i X_{i1}|^2}{v^2} . \tag{6.14}$$

We recall that the scenario of an extreme BR in the 2HDM is often accompanied by a cross–section suppression of ≤ 0.5. From Eq. (6.14) one can show that the suppression in the MHDM could be less. This is the case if a particular v_i^2 is much larger than the others ($v_i^2 \rightarrow 246^2$ GeV^2), as well as possessing $|X_{i1}^2|$ close to 1. Therefore there exist parameter spaces for

$$0.5 \leq \frac{\sigma_{h_1}}{\sigma_{\phi^0}} \leq 1. \tag{6.15}$$

6.4 Conclusions for LEP2

We have studied the phenomenology of the lightest CP–even neutral Higgs boson (h_1) of the 2HDM and MHDM at LEP2. We considered the four versions of the 2HDM and a general MHDM, and showed that h_1 could possess branching ratios (BRs) significantly different to those of the minimal SM Higgs boson (ϕ^0) and h^0 of the MSSM. For masses in the range of LEP2 ϕ^0 and h^0 decay predominantly to $b\bar{b}$. It is assumed that h_1 is the only Higgs boson in range at LEP2. The production cross–section of $e^+e^- \rightarrow Zh_1$ is suppressed relative to that of ϕ^0 by a factor $\sin^2(\beta - \alpha)$ in the 2HDM and an analogous factor in the MHDM; a consequence of this suppression is that a very light h_1 with 10 GeV $\leq M_{h_1} \leq$ 44 GeV may have escaped detection at LEP1. We showed that Model I′ may exhibit a large BR ($h_1 \rightarrow \tau^+\tau^-$) which would register a clear signal. Model II may decay predominantly to $c\bar{c}$ and gg; this would provide a distinctive signature since it could only be observed as missing mass recoiling against a lepton pair (from $Z \rightarrow l^+l^-$), with no signal in the other detection channels. For Model I, h_1 possesses the same BRs as ϕ^0 and so does not have a distinctive signature. Model II′ may decay predominantly to a mixture of $\tau^+\tau^-$, $c\bar{c}$ and gg; the enhanced $\tau^+\tau^-$ channel could be mimicked by Model I′, but these latter decays would be accompanied by b quark jets, in contrast to the light quark/charm rich jets which would accompany the enhanced $\tau^+\tau^-$ channel in Model II′. Therefore it is possible that Model II′ possesses a distinct signature. In the MHDM, h_1 can feign any of the above extreme BRs but may be distinguished in this scenario from h_1 of the 2HDM if its production cross–section is close to that of ϕ^0.

6.5 Phenomenology at the LHC

We now consider the phenomenology of h_1 at the LHC in order to ascertain whether detection/distinctive signatures are possible, assuming that h_1 escaped detection at LEP2 and therefore its mass is constrained, $M_{h_1} \geq 100$ GeV; this bound is for h_1 with couplings to vector bosons of ϕ^0 strength. However, we must remember that a relatively light h_1 may escape detection at LEP1 and LEP2 if the vector boson (h_1VV) coupling is very suppressed, and we shall mention this possibility. We shall again focus on the 2HDM, with mention given to the MHDM where appropriate. We recall from (6.2) that h_1 from the MHDM may mimic h_1 from the 2HDM.

At the LHC one must consider the range 100 GeV$\leq M_{h_1} \leq$ 800 GeV. Before we consider its BRs we first recall the decays of ϕ^0 and h^0. Figures 3.6 $\rightarrow$ 3.8 show that for ϕ^0 the decays to vector bosons dominate over most of the parameter space i.e. for $M_{\phi^0} \geq 150$ GeV. One can see that $\phi^0 \rightarrow t\bar{t}$ decays peak at around 20% and then fall as M_{ϕ^0} increases (in the figures we take $m_t = 175$ GeV). For h^0 (which is expected to be lighter than 150 GeV) one has almost exactly the same BRs, although production processes involving the b quark coupling may be enhanced for large values of $\tan\beta$. In addition decays and production processes that proceed via loops receive extra contributions from SUSY particles, although over the bulk of the SUSY parameter space the effects are small [30]. The ATLAS reports assume $m_{\tilde{q}} = 1$ TeV and zero squark mixing ($\tilde{q}$ denotes a squark), for which the squark contributions are small. For a review of how SUSY particles may alter the phenomenology of h^0 see Ref. [44]. Throughout this chapter, and indeed this thesis, we shall be assuming that h^0 has roughly similar properties to ϕ^0. We now turn our attention to the BRs of h_1. There are differences here from the LEP2 scenario due to the rapid strengthening of the VV^* channel for $M_{h_1} \geq 100$ GeV, these decays being negligible at LEP2.

One must be aware of the bound on $\tan\beta$ from Eq. (6.1) when varying the angles. Distinctive BRs are still possible in the 2HDM for the heavier mass region, the general requirement again being that one of the angles has an extreme value. The $\tau^+\tau^-$ decays may be boosted as before in Model I', although for $M_{h_1} \geq 150$ GeV this enhanced channel will have strong competition from vector boson decays. As in the LEP2 case, the $b\bar{b}$ decays

of h_1 can be suppressed in contrast to those of ϕ^0 and h^0, the latter two particles decaying predominantly to $b\bar{b}$ for masses up to 140 GeV, at which stage the $VV^{(*)}$ channel takes over. Conversely, $b\bar{b}$ decays can be enhanced over the $VV^{(*)}$ decays in some models for the heavier Higgs mass region ($M_{h_1} \geq 150$ GeV). It is also possible to suppress the vector boson decay channels for $\alpha \approx \beta$, i.e. $\sin^2(\beta - \alpha) \to 0$. This would allow $h_1 \to t\bar{t}$ decays to dominate (unless another channel like $\tau^+\tau^-$ or $b\bar{b}$ was sufficiently enhanced). The rare decay $h_1 \to \gamma\gamma$ is an important process at hadron colliders and this may have a larger BR if the $b\bar{b}$ decays are sufficiently suppressed. In conclusion, there is scope for enhanced/suppressed BRs for h_1 with respect to ϕ^0 and h^0 at the LHC. It is our aim to study these distinct BRs, in order to see whether such distinct signatures could be observable. Again we must investigate whether the parameter choices needed to obtain a distinctive BR for h_1 also cause a strong suppression in its production cross-section at the LHC. We shall address this problem, as well as applying to h_1 the proposed search techniques for ϕ^0 (which were reviewed in Chapter 3).

At the LHC the dominant production process for ϕ^0 is that of gg fusion (see Figure 3.10), which proceeds via a top quark loop [24], [25], [63]. Other production channels are considerably smaller, with the next largest being WW fusion. Vector boson fusion [26] is always suppressed in a 2HDM by a factor $\sin^2(\beta - \alpha)$, while gg fusion can be enhanced by up to a factor of two. If the gg fusion process is absent then the cross-section $\sigma(pp \to h_1 X)$ is heavily diminished, and this is the case for a fermiophobic Higgs (Chapter 8). The Higgs bremsstrahlung off a b quark is small for ϕ^0 but in Model II and II′ it can be boosted for large values of $\tan\beta$ and may become the dominant production channel.

We note that the LHC is capable of probing Higgs masses up to 800 GeV [11], [24]. Therefore there is a reasonable chance of detecting more than one if not all of the Higgs bosons at the LHC; we must be aware of this whenever h_1 is shown to be hidden due to suppressed production processes, since the other Higgs bosons may have enhanced or ϕ^0 strength couplings which enable detection.

The most studied channels in the literature for detecting ϕ^0 are [11], [24]:

(i) $\phi^0 \to \gamma\gamma$ for 80 GeV$\leq M_{\phi^0} \leq$ 130 GeV.

(ii) $\phi^0 \to ZZ^{(*)} \to llll$ for 130 GeV$\leq M_{\phi^0} \leq$ 800 GeV.

Other channels are considered to give a lesser chance of detection, e.g. channels which make use of $\phi^0 \to b\bar{b}$ decays are swamped by backgrounds. For the models that we shall consider there are four possible ways which could distinguish h_1 from ϕ^0 or h^0:

(i) An enhanced signal in the channel $h_1 \to \gamma\gamma$ for 80 GeV$\leq M_{h_1} \leq$ 130 GeV.

(ii) An enhanced or suppressed signal in the decay $h_1 \to ZZ^{(*)} \to llll$ for 130 GeV$\leq M_{h_1} \leq$ 800 GeV.

(iii) An enhancement of the decay $h_1 \to t\bar{t}$ or $b\bar{b}$.

(iv) An enhancement of the decay $h_1 \to \tau^+\tau^-$.

In the subsections that follow we shall see that some of the above signatures are exclusive to a particular extended model, while others only suggest that a detected neutral Higgs boson would be of a non–minimal nature. Each of the above event types will be examined in the context of pp collisions at $\sqrt{s} = 14$ TeV and $\mathcal{L} = 30$ or 100 fb^{-1}. We shall focus on the four distinct versions of the 2HDM, remembering that h_1 from the MHDM can mimic any h_1 from the 2HDM. However, a feature of the 2HDM is the fact that once α and β have been chosen to obtain a distinctive BR, the production cross–section is constrained and often suppressed compared to ϕ^0. This is due to the fact that a large $\tan\beta$ automatically forces a coupling proportional to $\cot\beta$ to be reduced, or $\cos\alpha \to 1$ forces $\sin\alpha \to 0$ (see Table 6.1). In the MHDM this correlation is relaxed, as explained earlier in (6.2). Hence it is possible to have a larger production cross–section in the MHDM than in the 2HDM, together with an enhanced BR, resulting in more signal events overall. This result was shown in (6.3) for the LEP2 case.

We now discuss four ways with which h_1 of a 2HDM can distinguish itself from ϕ^0 and h^0 of the MSSM. Figure 3.10 shows the production cross–sections of ϕ^0 at the LHC for $\sqrt{s} = 14$ TeV. As mentioned earlier, the gg fusion process dominates, and since this proceeds via a top quark loop the action of decreasing the $h_1 t\bar{t}$ coupling is unfavourable for the total cross–section. When one varies α and β, all the individual production cross–sections (i.e. gg fusion, WW fusion etc) and BRs will be altered with respect to ϕ^0. The

overall event number will be proportional to the product of the total cross–section and the BR.

6.5.1 $h_1 \to \gamma\gamma$

For ϕ^0, the decay to $\gamma\gamma$ proceeds via charged particle loops (Figure 6.5), i.e. fermions and W bosons. For h^0 there are additional contributions from squarks, charged Higgs bosons and charginos. Contributions from charginos may be sizeable in certain regions of parameter space. The ATLAS reports [11] assume no squark mixing and that the sparticles do not contribute significantly to the phenomenology of h^0. It is shown there that the signal for $(h^0 \to \gamma\gamma)$ is suppressed considerably compared to that of ϕ^0 over the vast majority of the parameter space. Other studies [44] show that over the full SUSY parameter space there can be significant deviations from the results in the ATLAS reports. We shall not consider this possibility and instead we shall use the assumptions and results of the ATLAS reports. Therefore any enhanced signal in this channel for h_1 compared to ϕ^0 is to be interpreted as an indication of the 2HDM or MHDM.

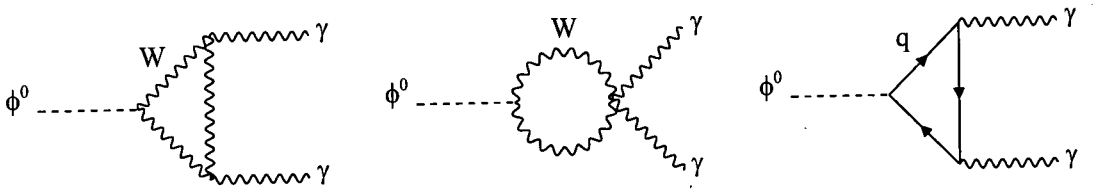

Figure 6.5: Decays of $\phi^0 \to \gamma\gamma$.

We thus concentrate on the decay $\phi^0 \to \gamma\gamma$ and look for ways of enhancing $h_1 \to \gamma\gamma$. For ϕ^0 the vector boson loops dominate and contribute with opposite sign to the fermion loops. One–loop corrections are small [63], and the tree–level width can be written as [30]:

$$\Gamma(\phi^0 \to \gamma\gamma) = \frac{G_F \alpha^2 M_{\phi^0}^3}{128\sqrt{2}\pi^3} \left| \sum_f N_c Q_f^2 A_f(\tau_f) + A_W(\tau_W) \right|^2 , \tag{6.16}$$

where N_c is the colour factor, Q_f is the electric charge of the fermion, and the τ variables

are defined by

$$\tau_f = \frac{M_{\phi^0}^2}{4m_f^2} \quad \text{and} \quad \tau_W = \frac{M_{\phi^0}^2}{4M_W^2} \,. \tag{6.17}$$

The amplitudes A_f and A_W can be expressed as

$$\begin{aligned} A_f(\tau) &= 2[\tau + (\tau - 1)f(\tau)]/\tau^2 \,, \\ A_W(\tau) &= -[2\tau^2 + 3\tau + 3(2\tau - 1)f(\tau)]/\tau^2 \,, \end{aligned} \tag{6.18}$$

with the function $f(\tau)$ given by

$$\begin{aligned} f(\tau) &= (\arcsin\sqrt{\tau})^2 \qquad \tau \leq 1 \,, \\ f(\tau) &= \frac{1}{4}\left[\log\frac{1+\sqrt{1-\tau^{-1}}}{1-\sqrt{1-\tau^{-1}}} - i\pi\right]^2 \qquad \tau > 1. \end{aligned} \tag{6.19}$$

The above equations show that the dominant fermion loop is that of the t quark (i.e. $f = t$). Since we are considering $M_{h_1} \leq 130$ GeV [5] we are therefore interested in the region $\tau \leq 1$. In this region the amplitudes (A) are real and vary as follows: $A_W = -7(-12)$ for $\tau = 0(1)$, $A_f = 4/3(2)$ for $\tau = 0(1)$. Hence the W loops are dominant. For the minimal SM Higgs, BR $(\phi^0 \to \gamma\gamma) \approx 0.1\% \to 0.2\%$ for 80 GeV $\leq M_{\phi^0} \leq 130$ GeV (Figure 3.7). To increase this BR for h_1 one would naively wish to enhance $\Gamma(h_1 \to \gamma\gamma)$ significantly, but this is not an option since:

(i) The W loop contributes the most, and the h_1WW vertex is suppressed relative to ϕ^0WW by a factor $\sin^2(\beta - \alpha)$.

(ii) It is possible to reduce the $t\bar{t}$ vertex, and so cause less destructive interference. However, since the t loop is not the dominant contribution to $\Gamma(h_1 \to \gamma\gamma)$, this does not increase the width much, and the corresponding reduction in $\sigma(gg \to h_1)$ markedly diminishes the total cross-section.

A better way of increasing BR $(h_1 \to \gamma\gamma)$ is to suppress other decay channels such as $b\bar{b}$ (which dominates in the relevant mass region). This suppression can be achieved in

[5] For $M_{h_1} \geq 130$ GeV the $\gamma\gamma$ channel becomes less important since VV^* decays are becoming stronger and usually give a better signature.

Models II and II' for small $\sin\alpha$ and $\tan\beta$ moderate, although in Model II the above parameter choices suppress $b\bar{b}$ and $\tau^+\tau^+$ decays simultaneously, thus further enhancing BR $(h_1 \to \gamma\gamma)$. In the extreme case of BR $(h_1 \to b\bar{b}) \to 0$ $(\sin\alpha \to 0)$, one finds that enhancements of a factor two (relative to ϕ^0) are possible for BR $(h_1 \to \gamma\gamma)$. With the main production cross-section $gg \to h_1$ at twice ϕ^0 strength (since $\cos^2\alpha/\sin^2\beta \approx 2$) one would find sizeable enhancements in the number of $\gamma\gamma$ events relative to the process $pp \to \phi^0 \to \gamma\gamma$. The detection methods and selection criteria were described in Chapter 3.

Table 6.3 (from Ref. [12]) shows the expected signal for ϕ^0 for $\mathcal{L}$=30 fb^{-1} with the significance being rather low in the range 80 GeV$\leq M_{\phi^0} \leq$ 100 GeV. For h_1 the enhancement of $\gamma\gamma$ events by a factor up to 5 would provide a spectacular signature, and Table 6.4 shows the signal numbers for Model II with $\alpha = 0$ and $\beta = \pi/4$.

M_{ϕ^0} (GeV)	80	100	120
BR $(\phi^0 \to \gamma\gamma)$	0.09%	0.15%	0.23%
$S/\sqrt{B}$	1.5	2.7	4.1

Table 6.3: Signals for process $pp \to \phi^0 X$, $\phi^0 \to \gamma\gamma$, for $\mathcal{L}$=30 fb^{-1} (from Ref. [12]).

M_{h_1} (GeV)	80	100	120
BR $(h_1 \to \gamma\gamma)$	0.22%	0.37%	0.40%
$S/\sqrt{B}$	8.3	13.7	15.8

Table 6.4: Signals for process $pp \to h_1 X$, $h_1 \to \gamma\gamma$, with maximum enhancement, for $\mathcal{L}$=30 fb^{-1}.

In Model I' it is not possible to simultaneously suppress the $h_1 b\bar{b}$ coupling and keep the $h_1 t\bar{t}$ coupling near ϕ^0 strength. A consequence of this is that although similar enhancements of BR $(h_1 \to \gamma\gamma)$ are again possible, the production mechanism $(gg \to h_1)$ will be heavily suppressed. Despite this, a chance of detection remains in the associated production channel $q\bar{q} \to Wh_1$ with subsequent decays $W \to l\nu_l$ and $h_1 \to \gamma\gamma$. The event selection criteria were given in (3.8.3). Enhancing $h_1 \to \gamma\gamma$ would require $\alpha \to \pi/2$, $\beta \approx \pi/4$, and hence $\sin^2(\beta-\alpha) \approx 0.5$; thus the associated production cross-section would be suppressed relative to ϕ^0 by a factor of 0.5. However, with the higher $h_1 \to \gamma\gamma$ one would expect a comparable number of events, and since a reasonable statistical signal in

the associated production channel is possible for ϕ^0 with high luminosity, an analogous signal for h_1 may be obtainable. Table 6.5 uses the results of the simulation done in Ref. [29]. The event numbers for ϕ^0 include contributions from the associated process

M_{ϕ^0} (GeV)	Signal (S)	Background (B)	$S/\sqrt{B}$
80	13.5	10.5	4.2
110	18.3	7.0	6.9

Table 6.5: Signals for process $pp \to \phi^0 lX$, $\phi^0 \to \gamma\gamma$, for $\mathcal{L} = 100$ fb^{-1} (from Ref. [29]).

$pp \to t\bar{t}\phi^0$, $\phi^0 \to \gamma\gamma$, with the lepton trigger originating from $t \to Wb \to l\nu_l b$. This process contains about 60% of the signal in Table 5. For the above mentioned case of h_1, the contribution in this channel would be negligible (since the parameter choice for a larger BR ($h_1 \to \gamma\gamma$) require suppression of the $h_1 b\bar{b}$ and $h_1 t\bar{t}$ coupling). Therefore we would expect around half the number of events shown in Table 5, giving a small signal between 2.5σ and 3.5σ. A null search in the $gg \to h_1 \to \gamma\gamma$ channel but a signal in the associated channel would then be evidence for Model I′.

We recall that a fermiophobic Higgs will possess a sizeable BR ($H_F \to \gamma\gamma$), and would give a clear, distinct signal in the above channel. BR ($H_F \to \gamma\gamma$) has values 20% (1%) for $M_{\phi^0} = 100$ GeV (130 GeV) and this would provide a very strong signal. For example if $M_F = 110$ GeV and $\cos^\beta = 0.39$ (the latter gives the least cross-section suppression) one would find $S/\sqrt{B} \approx 40$; this is due to BR ($H_F \to \gamma\gamma$) being 40 times greater than that for ϕ^0 for the same mass. For $M_F \geq 130$ GeV there will not be much difference between the signal for ϕ^0 and for H_F in this channel since the BRs to two photons become comparable.

6.5.2 $h_1 \to \tau^+\tau^-$

The next channel we wish to consider is $h_1 \to \tau^+\tau^-$. In the mass region of interest this decay falls from BR=8% $\to$ 2% for $M_{\phi^0} = 100 \to 150$ GeV. BR ($h^0 \to \tau^+\tau^-$) is similarly small. We showed in (6.3) that large values of BR ($h_1 \to \tau^+\tau^-$) are possible in Models I′ and II′, and this property can be exploited at LEP2. In this subsection it is our aim to consider the detection prospects of this channel at the LHC, to see if this distinctive signature can be identified. At LEP2 the main production process is $e^+e^- \to Z^* \to Zh_1$.

This relies on the ZZh_1 vertex which is always suppressed by the factor $\sin^2(\beta-\alpha)$. Section (6.3) showed that after choosing β and α to obtain a very large BR $(h_1 \to \tau^+\tau^-)$ this suppression is not so severe (≈ 0.5) at LEP2. At the LHC the dominant production process is by gluon–gluon fusion and so one must check if the choices of α and β needed to enhance BR $(h_1 \to \tau^+\tau^-)$ simultaneously reduce the $t\bar{t}h_1$ vertex which is crucial to the mechanism $gg \to h_1$. One can see from Table 6.1 that the choice of large $\tan\beta$ (thus $1/\cos\beta$ large) will enhance the h_1ll vertex, while $\cos^2\alpha = 0.5 \to 1$ would keep the $t\bar{t}h_1$ vertex near ϕ^0 strength. As M_{h_1} increases the production cross–section obviously decreases, and competition from $VV^{(*)}$ channels is stronger unless we suppress these decays. For example, for ϕ^0 one finds BR $(\phi^0 \to \tau^+\tau^-) \approx 0.1\%$ for $M_{\phi^0} = 170$ GeV. For h_1 it is possible to suppress the $VV^{(*)}$ decays by considering $\sin^2(\beta-\alpha) \to 0$. However, since we require $\beta \to \pi/2$, obtaining the suppression of the $VV^{(*)}$ decays requires $\alpha \to \pi/2$, and this choice of α causes a strong reduction in the production cross–section $\sigma(gg \to h_1)$. We wish to maximize the event number (cross–section times branching ratio) which is proportional to $f(\beta,\, \alpha)$ defined by

$$f(\beta,\, \alpha) = \frac{\cos^2\alpha}{\sin^2\beta}\left[\frac{\Gamma_{h_1}^{\tau^+\tau^-}}{\Gamma_{h_1}^{\tau^+\tau^-}+\Gamma_{h_1}^{VV}}\right], \tag{6.20}$$

where

$$\Gamma_{h_1}^{\tau^+\tau^-} = \sin^2\alpha\Gamma_{\phi^0}^{\tau^+\tau^-}/\cos^2\beta\,, \tag{6.21}$$

and

$$\Gamma_{h_1}^{VV} = \sin^2(\beta-\alpha)\Gamma_{\phi^0}^{VV}\,. \tag{6.22}$$

Contributions from other channels are negligible in Eq. (6.20). We can see that lower values of α (i.e. $\cos\alpha \to 1$) are favourable from the point of view of the cross–section (the first factor in Eq. 6.20), although the effect on $\Gamma^{\tau^+\tau^-}$ is that a smaller $\cos\beta$ is needed to overcome the suppression from $\sin\alpha$ (Eq. (6.21)). In the analysis that follows we shall choose $\beta = 89°$ and $\alpha = \pi/4$ which provides for Model I′:

(i) Enhancement of 1640 for the width of the $\tau^+\tau^-$ channel.

(ii) Some suppression of the WW channel, since $\sin^2(\beta-\alpha) = 0.5$.

(iii) The coupling $h_1t\bar{t}$ is not so suppressed ($\cos^2\alpha/\sin^2\beta \approx 0.5$). Therefore no large reduction of $\sigma(gg \to h_1)$.

Choosing $\cos\alpha \to 1$ in order to maximize the cross-section would require $\cos\beta \to 0$ to enable the $\tau^+\tau^-$ channel to be enhanced over the VV^* channel. We note that a large BR $(h_1 \to \tau^+\tau^-)$ in only possible in Model I'. In Model II' the partial width $\Gamma(h_1 \to \tau^+\tau^-)$ cannot be enhanced significantly since the $h\tau^+\tau^-$ vertex is proportional to $1/\sin\beta$ (see Table 6.1), and $\sin\beta \to 1$ as $\beta \to \pi/2$. However, as stated in (6.3), for masses of h_1 in range at LEP2 one could suppress the $h_1 b\bar{b}$ coupling while keeping $h_1\tau\tau$ near ϕ^0 strength, with the result of increasing BR $(h_1 \to \tau^+\tau^-)$ substantially. This is not the case for h_1 in the mass range relevant at the LHC ($M_{h_1} \geq 100$ GeV), since decays to $VV^{(*)}$ are important and the only way to have a large BR $(h_1 \to \tau^+\tau^-)$ in Model II' would be to heavily suppress $h_1 \to VV^{(*)}$. This would require $\alpha \approx \beta$, conflicting with the requirements for the suppression of $h_1 \to b\bar{b}$, which are $\alpha \to 0$ and $\beta \approx \pi/4$. Hence it is not possible in Model II' to simultaneously suppress $h_1 \to b\bar{b}$ and $h_1 \to VV^{(*)}$. Therefore a large BR $(h_1 \to \tau^+\tau^-)$ in the mass region of interest here ($M_{h_1} \geq 100$ GeV) is only possible in Model I'.

However, obtaining a large BR $(h_1 \to \tau^+\tau^-)$ will require an increasingly small parameter space as M_{h_1} increases over the threshold of real VV decays; over this threshold BR $(h_1 \to \tau^+\tau^-)$ decreases as $M_{h_1}^2$, and therefore the parameter space for a sizeable BR $(h_1 \to \tau^+\tau^-)$ is confined to large values of $\tan\beta$. We shall now consider in detail the detection prospects of h_1 from Model I' in the context of a large BR $(h_1 \to \tau^+\tau^-)$, with the aim of ascertaining up to what value of M_{h_1} this distinct signature can be probed. We shall be using the analysis of the ATLAS reports [11], [13] which consider A^0 and H^0 (the heavier CP-even scalar) of the MSSM and their decays to $\tau^+\tau^-$. For large $\tan\beta$ these particles do not possess a large BR $(h_1 \to \tau^+\tau^-)$ but instead have enhanced production cross-sections due to the Higgs bremsstrahlung off a b quark being strongly boosted (proportional to $\tan\beta$). The $h_1\tau^+\tau^-$ coupling is also boosted by the same amount but BR $(h_1 \to \tau^+\tau^-)$ will always be an order of magnitude $(N_c m_b^2/m_\tau^2)$ less than the $b\bar{b}$ channel (10% at best). It can be shown that $\phi^0 \to \tau^+\tau^-$ decays cannot be observed at the LHC, given the rather low BR. For Model I' one can have a roughly ϕ^0 strength $gg \to h_1$ cross-section and a large BR $(h_1 \to \tau^+\tau^-)$, thus providing significantly more events. The aforementioned A^0 and H^0 have greatly boosted cross-sections for large $\tan\beta$ and so even with their relatively small BRs to $\tau^+\tau^-$ they can produce a strong signal. We

shall show that comparable signals are possible in Model I′ as well. An important way of distinguishing a $\tau^+\tau^-$ signal from h_1 from the combined signal of H^0 and A^0 (which are degenerate for $M_{H,A} \geq 150$ GeV) is the fact that h^0 in the MSSM (which should have a mass less than 150 GeV) could be observable, having SM–like decays and so is possibly detectable in the channel $h^0 \to \gamma\gamma$. Hence the discovery of a neutral Higgs particle with large BR to $\tau^+\tau^-$, and *no* sign of h^0 would be some evidence for Model I′. In addition, there will be a lack of ZZ decays for the combined H^0 and A^0 signal, since $A^0 \to ZZ$ is forbidden and $H^0 \to b\bar{b}$ will be the accompanying (and dominant) decay for the MSSM case. An accompanying signal in the *llll* channel is possible for h_1 in Model I′ but not for the combined A^0 and H^0 signal in the MSSM (see (6.5.4) for a study of the *llll* channel).

The trigger for the channel is the leptonic decay from one of the τ-leptons; the other τ is decayed to hadrons. The main backgrounds consist of [13]:

(i) $t\bar{t}$ production, followed by $t\bar{t} \to WWbb$, and $W \to l\nu_l$, $W \to$ hadrons.

(ii) W plus jets production, with $W \to l\nu_l$.

(iii) $b\bar{b}$ production, with $b \to$ jets, $b \to l + X$.

(iv) Single Z^0 production, with $Z^0 \to \tau^+\tau^-$, and $\tau \to had\ \nu_\tau$, $\tau \to l\nu_\tau\nu_l$.

The backgrounds are suppressed by the following cuts:

(1) An isolated lepton is required with $p_T \geq 24$ GeV (reduces (iii)).

(2) $E_T^{jet} \geq 40$ GeV.

(3) $p_T^{miss} \geq 18$ GeV (reduces (iii)).

(4) $m_{\tau\tau} = M_{h_1} \pm \Delta M$ (reduces (iv) for $M_{h_1} \geq 120$ GeV).

(5) $m_T(l, p_T^{miss}) \leq 25$ GeV (reduces(i) and (ii)).

In the analysis that follows we shall use the values $\alpha = \pi/4$ and $\beta = 89°$ (which corresponds to $\tan\beta = 57$). All individual production cross–sections (i.e. gg fusion,

WW fusion etc) with this choice of parameters are essentially half those for ϕ^0, (since $\cos^2\alpha/\sin^2\beta \approx 0.5$, $\sin^2(\beta-\alpha) \approx 0.5$), resulting in a total cross-section half the magnitude of that for ϕ^0. The BR ($h_1 \to \tau^+\tau^-$) is obtained from appropriate scaling of the BRs for ϕ^0.

M_{h_1} (GeV)	100	120	150	200	300
BR ($h_1 \to \tau^+\tau^-$)	$\approx 100\%$	$\approx 100\%$	98.5%	49.7%	30.5%
$\sigma(pp \to h_1 X)$ (pb)	13.17	10.03	7.57	5.13	3.13
Signal (BR $\times\sigma$) (pb)	13.17	10.03	7.45	2.55	0.95
Signal Events (S)	111	249	541	462	241
Background (B)	810	500	660	540	530
Significance ($S/\sqrt{B}$)	3.9	11.1	21.1	19.9	10.5

Table 6.6: Signals for process $pp \to h_1 X$, $h_1 \to \tau^+\tau^-$, with $\mathcal{L} = 30$ fb^{-1} (from Ref.[11], with rescaling).

Table 6.6 shows the expected number of events at the LHC and the significance of the signal. Our numbers for the backgrounds and acceptances are taken from the ATLAS report [11]. We can see from the table that for $M_{h_1} = 300$ GeV there is still a large signal. Therefore this corner of parameter space ($89° \leq \beta \leq 90°$) provides a strong signal in Model I′ in the $\tau^+\tau^-$ channel, even for relatively large values of M_{h_1}, *and* is exclusive to this particular model. For smaller M_{h_1} there is a larger parameter space of $\tan\beta$ for a strong, distinct signal of Model I′. For example, it can be shown that for $80° \leq \beta \leq 90°$ (or $\tan\beta \geq 5.7$) one would find BR ($h_1 \to \tau^+\tau^-$) $\approx 40\%$, which would give a 8.6σ signal for $M_{h_1} = 150$ GeV. The ATLAS report considers masses below 120 GeV difficult to detect in this channel due to the strong $Z \to \tau^+\tau^-$ background.

We note that the enhancement of the Higgs bremsstrahlung off a b quark at high $\tan\beta$ is possible in the non–SUSY Model II. As in the case of H^0 and A^0 of the MSSM, the BR ($h_1 \to \tau^+\tau^-$) can never be more than 10%, since BR ($h_1 \to b\bar{b}$) decays are similarly enhanced. With values of $\tan\beta \approx 57$ one can obtain a $\tau^+\tau^-$ signal considerably larger than is obtained for h_1 of Model I′ using the same $\tan\beta$ value. However, as mentioned before, the accompanying decays for Model II will be to $b\bar{b}$ with the process $h_1 \to ZZ^* \to llll$ suppressed. For Model I′ the accompanying decays are $h_1 \to WW^*$, ZZ^* and so a signal in the $llll$ channel is still likely, unless BR ($h_1 \to \tau^+\tau^-$) is very large. A positive signal in

both channels would therefore be distinctive of Model I'.

6.5.3 $h_1 \to t\bar{t}$, $h_1 \to b\bar{b}$

Decays of a Higgs boson to quark pairs, although usually dominant for the intermediate mass Higgs boson (i.e. $M_{\phi^0} \leq 2M_W$), are considered difficult at a hadron collider and other channels usually give better chances of detection. For ϕ^0 the most promising signals are rare $\gamma\gamma$ decays for $M_{\phi^0} \leq 130$ GeV, and $ZZ^{(*)} \to llll$ for $M_{\phi^0} \geq 130$ GeV. However, in the 2HDM it is possible that the quark decays ($t\bar{t}$ or $b\bar{b}$) dominate the vector boson channels over a wider range of Higgs masses and therefore it is important to infer whether these quark decays can indeed present a signature, or if h_1 would be hidden.

In any 2HDM it is possible for $h_1 \to t\bar{t}$ decays to dominate (for $M_{h_1} \geq 2m_t$) if the VV decays are sufficiently suppressed i.e. $\sin^2(\beta-\alpha) \to 0$. In the extreme case of $\sin^2(\beta-\alpha) = 0$ (i.e. $\beta = \alpha$), $t\bar{t}$ decays would saturate the width unless $\beta \approx \alpha \to \pi/2$, in which case $b\bar{b}$ decays can be strong in Models II and II'; we shall discuss this latter possibility below. For now let us consider the case of $h_1 \to t\bar{t}$ decays dominating, with a reasonable production cross-section. The ATLAS report [11] studies this process for H^0 and A^0 of the MSSM, both of which may possess BR to $t\bar{t} \to 100\%$. We aim to extrapolate these results for use with h_1.

We must first mention a caveat that if $\sin^2(\beta-\alpha) \to 0$ then a light h_1 may have escaped detection at LEP. This is the first time in the chapter that we have implemented $\beta \approx \alpha$. Previous to this the conditions for extreme BRs have required $\sin^2(\beta-\alpha) \approx 0.5$ and so a very light h_1 would certainly have been found at LEP by the standard $e^+e^- \to Z\phi^0$ process. The BRs of the light h_1 can be inferred form Table 6.7 where we have set $\alpha = \beta$; for Models I, II, and II' decays to $b\bar{b}$ would all dominate (recall $\tan\beta \geq 1.25$ when considering the couplings in Table 6.7), while in Model I', decays to $\tau^+\tau^-$ would dominate for $\tan\beta \geq 3$. We shall not be considering the case of a very light h_1 and refer the reader to Refs. [60], [48] for production channels at LEP which do not make use of the suppressed $e^+e^- \to Z\phi^0$ process. We note that these papers only consider Model II.

Returning to the case of $h_1 \to t\bar{t}$, the ATLAS report [11] considers the detection

	Model I	Model I′	Model II	Model II′
$hu\bar{u}$	$\cot\beta$	$\cot\beta$	$\cot\beta$	$\cot\beta$
$hd\bar{d}$	$\cot\beta$	$\cot\beta$	$-\tan\beta$	$-\tan\beta$
$he\bar{e}$	$\cot\beta$	$-\tan\beta$	$-\tan\beta$	$\cot\beta$

Table 6.7: The fermion couplings of h_1 in the 2HDM relative to those for the minimal SM Higgs boson (ϕ^0), with $\beta = \alpha$.

prospects in the $t\bar{t}$ channel for A^0 and H^0 of the MSSM, which may have BR (H^0, $A^0 \to t\bar{t}$) $\to$ 100%. The signal is extracted by searching for $W^+W^-b\bar{b}$ final states, with one $W \to l\nu$ decay providing the trigger, and one hadronic $W \to jj$ decay. The lepton is required to possess $p_T \geq 20$ GeV, with all jets satisfying $p_T \geq 40$ GeV. Both b jets must be tagged, with efficiency assumed to be around 60%. With these cuts the continuum $t\bar{t}$ production is by far the dominant background. The top masses are reconstructed, using a algorithm for reducing the combinatorial background for $l\nu b$ and jjb. The mass resolution for M_{h_1} is quite large and varies from 35 GeV to 80 GeV as M_{h_1} increases from 330 GeV to 500 GeV. Large mass bins are needed to collect the signal. We present the event numbers for h_1 in Table 6.8 by rescaling the ATLAS numbers; we take $\alpha = \beta$, BR ($h_1 \to t\bar{t}$) = 100%, and $m_t = 175$ GeV.

M_{h_1} (GeV)	Signal (S)	Background (B)	$S/\sqrt{B}$
370	1800	68600	6.9
400	1980	85700	6.8
500	1670	127400	4.7

Table 6.8: Statistical signal in the $h_1 \to t\bar{t}$ channel for $\mathcal{L} = 30$ fb^{-1} (from Ref. [11] with rescaling).

The statistical significance of the signal is large but is only meaningful if the theoretical error on $\sigma(pp \to t\bar{t})$ is less than 1%, which is not the case at the present. If the error is reduced then there would be some chance of detection in this channel. It does not seem possible to distinguish $h_1 \to t\bar{t}$ decays from the combined signal of H^0 and A^0 in the MSSM due to roughly equal event numbers, although the MSSM predicts $M_{h^0} \leq 150$ GeV and detection of h^0 along with a signal in the $t\bar{t}$ channel from H^0 and A^0 would be some indication of the MSSM.

The other quark decay that could dominate is that of $h_1 \to b\bar{b}$ in Models II and II' for $\tan\beta \geq 5$ (see Table 6.7). However, it seems that this particle would be hard to find at hadron colliders since the main production processes are gg fusion or radiation off a b quark, these processes giving jet signatures which have large backgrounds. Producing h_1 in association with a W boson via $q\bar{q} \to W^* \to Wh_1$, with $W \to l\nu_l$ (a lepton trigger) and $h_1 \to b\bar{b}$ only probes $M_{h_1} \leq 120$ GeV [11], [14]. Therefore we conclude that the quark decays of h_1 would be difficult to observe at the LHC; prospects are much better in other channels, unless the quark decays saturate the width in which case one has no choice but to study the decays $h_1 \to t\bar{t}$ or $h_1 \to b\bar{b}$.

6.5.4 $h_1 \to ZZ^{(*)}$

The Higgs decay to two Z bosons, with the subsequent decay $ZZ \to llll$ is the 'gold-plated' channel, since it gives a large signal throughout the range 130 GeV$\leq M_H \leq$ 800 GeV. Below the real ZZ threshold one of the vector bosons must be off-shell. In the 2HDM, $\Gamma(h_1 \to VV^{(*)})$ is suppressed by $\sin^2(\beta-\alpha)$ and therefore the width cannot be increased. However, for $M_{h_1} \geq 150$ GeV these decays usually dominate, unless the suppression is large and/or another channel is greatly boosted. Table 6.9 shows the expected signal and background ratio for ϕ^0, which is very large over much of the mass interval 200 GeV$\leq M_{\phi^0} \leq$ 800 GeV, reaching as high as 40 standard deviations. The event selection criteria were given in (3.8). Therefore any strong suppression in this channel, either of the cross-section or branching ratio or both would certainly be noticed. This would indicate an extended Higgs model, although would not provide any information as to which particular model.

For the mass region 100 GeV$\leq M_{\phi^0} \leq$ 130 GeV the $ZZ^* \to llll$ channel does not provide a strong enough signature since the BR $(\phi^0 \to ZZ^*)$ is small. The same is true for h^0. In a 2HDM it is possible to suppress the $b\bar{b}$ channel which may enable the $llll$ signal to be used for lower masses of h_1 than is possible for ϕ^0.

To have a reasonable signal for $M_{h_1} \leq 130$ GeV in the $llll$ channel one needs to find a model which can suppress the $b\bar{b}$ decays (so as to make BR $(h_1 \to ZZ^*)$ larger), *and* keep a reasonable cross-section i.e. the $t\bar{t}$ coupling near ϕ^0 strength. Model I cannot

M_{h_1} (GeV)	Signal (S)	Background (B)	$S/\sqrt{B}$
120	5.2	4.7	2.4
130	24.8	8.2	8.5
150	68.5	10.0	21.7
170	19.9	9.5	6.5
180	51.9	9.0	17.3
200	189	29	35.3
300	314	68	38.2
400	267	56	35.7
500	137	29	25.6
600	70	25	14.1
700	38	21	8.3
800	22	17	5.4

Table 6.9: Statistical signal in the $\phi^0 \to ZZ^{(*)} \to llll$ channel for $\mathcal{L} = 100$ fb^{-1} (from Ref.[12].

do this, and nor can Model I'. The required couplings are possible in Models II and II', although Model II has the possibility of a larger signal since both $b\bar{b}$ and $\tau^+\tau^-$ can be simultaneously suppressed. The choice of $\cos^2\alpha \to 1$ and moderate $\sin^2\beta$ (≈ 0.5) would boost the $t\bar{t}$ coupling and so enhance the $gg \to h_1$ cross–section; these parameter choices would also cause the required suppression of the $b\bar{b}$ and $\tau^+\tau^-$ decays (in Model II' the $\tau^+\tau^-$ cannot be simultaneously suppressed, and so the BR to ZZ^* would be less). This means that although $c\bar{c}$ and gg decays would dominate, BR $(h_1 \to Z^*Z) = 1\%$ is possible (compare BR $(\phi^0 \to Z^*Z) = 0.3\%$ for $M_{\phi^0} = 110$ GeV), and combined with the enhanced cross–section one would find an increase of order 4 for the $llll$ signal. This analysis is for $M_{h_1} = 110$ GeV, although it requires sufficiently good Higgs mass resolution to be sure that one has found a Higgs of 110 GeV with an enhanced $llll$ signature instead of $\phi^0 \to llll$ with $M_{\phi^0} = 130$ GeV (say), the latter giving a similar number of events. In practice sufficient mass resolution should be obtainable.

For the heavier Higgs masses, $M_{h_1} \geq 2M_Z$, the decay to two real Z bosons $h_1 \to ZZ$ is possible. For ϕ^0 the decay process $\phi^0 \to ZZ \to llll$ provides a 'gold plated' signal above the background for $M_{\phi^0} \leq 700$ GeV (see Table 6.9). In the 2HDM it is not possible to enhance these couplings, as the ZZ and WW channels are both scaled by the same $\sin^2(\beta - \alpha)$ suppression. Two signatures remain which could suggest a 2HDM in this

channel:

(i) An enhanced cross–section. Since $gg \to \phi^0$ gives the largest rate, if one enhances the $h_1 t\bar{t}$ coupling it is possible to have more $llll$ events than for the ϕ^0 case.

(ii) A suppression of the $llll$ signal relative to ϕ^0 would be very noticeable, since the ϕ^0 signal can be as large as 40σ.

Case (i) is possible in all 2HDM, for parameter choices such as $\cos^2\alpha \to 1$ and moderate $\sin^2\beta$ (≈ 0.5). This would cause an enhancement of 2 for the gg fusion cross–section, and the overall cross–section would be enhanced by roughly the same factor (since gg fusion gives the largest contribution). Case (ii) is also possible in any 2HDM and therefore the above scenarios do not give any information on which particular model would be present. There are two ways for case (ii) to be realized.

(a) The choice of $\beta \approx \alpha$ forces $\sin^2(\beta - \alpha) \approx 0$ and so the $h_1 \to ZZ$, WW decays are heavily suppressed. Instead the $t\bar{t}$ channel dominates for the heavy Higgs mass region, $M_{h_1} \geq 2M_Z$, unless another channel is significantly boosted.

(b) The BRs to ZZ and WW may be kept dominant, but the production cross–section could be heavily suppressed, i.e. a reduced $h_1 t\bar{t}$ coupling would heavily suppress the fusion process $gg \to h_1$.

Case (b) is true for a fermiophobic Higgs (H_F) which shall be discussed in Chapter 8.

6.6 Conclusions at the LHC

We have studied the phenomenology of the lightest CP–even neutral Higgs boson (h_1) of the 2HDM and MHDM at the LHC. Emphasis is given to the problem of distinguishing h_1 from the SM Higgs boson (ϕ^0) and the MSSM Higgs boson (h^0). This is complementary to our earlier conclusions (6.4) which considered prospects at LEP2. We studied four different decay channels and showed that the following distinct signals are possible:

(i) An enhanced signal in the $pp \to h_1 X$, $h_1 \to \gamma\gamma$ channel would be evidence for Model II or II′, although Model II can produce the greater number of events. A signal in the associated production channel $pp \to h_1 W$, $h_1 \to \gamma\gamma$ and $W \to l\nu_l$ but no signal in the above channel would be evidence for Model I′ or a fermiophobic Higgs (with the latter capable of more signal events – see Chapter 8).

(ii) A large signal from $h_1 \to \tau^+\tau^-$ decays is possible in Model I′, and the accompanying signature would be $llll$, unless the former has a very large BR. In Models II and II′ it is possible to have a comparable enhancement of $\tau^+\tau^-$ events but the accompanying decays would be to hadrons, which could not be separated from the backgrounds.

(iii) Enhanced $h_1 \to t\bar{t}$, $b\bar{b}$ decays in the heavy Higgs region are possible although they are very difficult to detect at the LHC due to the large jet background. A reasonable signal is more likely in the $t\bar{t}$ channel if the theoretical error on the background $pp \to t\bar{t}$ cross–section can be reduced to below 1%.

(iv) A suppressed or enhanced signal in the gold plated $llll$ channel is indicative of a non–minimal Higgs sector, although there would be no information as to the model from which it originates, unless there exists another enhanced BR such as $h_1 \to \tau^+\tau^-$, which would indicate Model I′.

In the MHDM, h_1 may mimic the above signatures, although it has the possibility of larger cross–sections as well as an enhanced BR, thus resulting in more signal events overall.

Chapter 7

A Model with Higgs Triplets

7.1 Introduction

Thus far only extended Higgs models with doublet representations have been considered. These preserve $\rho = 1$ at tree–level, and one–loop corrections from the Higgs sector are small – see Chapter 4. However it is possible that higher Higgs representations exist, and in this chapter we shall study a model with Higgs isospin triplets. We note that many extensions of the SM require triplet Higgs representations (e.g. left–right symmetric models), although triplets can be considered purely in the context of the non–minimal SM, i.e. no other new particles apart from Higgs bosons. The general formula for ρ in the context of general Higgs representations with isospin T and hypercharge Y was displayed in Eq. (4.1), from which it can be shown that a triplet representation on its own cannot maintain $\rho = 1$ at tree–level. A triplet together with a doublet can keep $\rho \approx 1$ if the VEV of the triplet is very small, of order 0.03 that of the doublet VEV (Eq. (4.7)). This is of course possible but leads one to wonder why nature chose such a representation at all; we recall that one of the motivations for the existence of Higgs bosons in the SM is for them to have a non–zero VEV, and so introducing Higgs bosons with very small VEVs seems contradictory and unnatural (this reasoning would not be valid for models which are specifically constructed to produce a small mass for neutrinos).

A more attractive option which has found favour in the literature [30], [64], [65],

[66] is to combine one doublet with one real ($T = 1, Y = 0$) triplet and one complex ($T = 1, Y = 2$) triplet. From Eq. (4.1) it is easily shown that $\rho = 1$ can be maintained at tree level if the VEVs of the triplet fields are equal. Denoting $V_{1,0} = V_{1,2} = b$ and $V_{1/2,1} = a/\sqrt{2}$, [1] we find that $M_W^2 = \frac{1}{4}g^2v^2$ with $v^2 \equiv a^2 + 8b^2 = (246\ \text{GeV})^2$. There is no constraint on b (apart from $8b^2 \leq v^2$) which is in contrast to the previous case of one triplet and a doublet. Therefore it is possible that the triplets play a major role in symmetry breaking and this model (henceforth to be called HTM) seems theoretically more favourable. The rest of the chapter is organized as follows. In (7.2) we present a review of the HTM while (7.3) deals with current constraints on its parameters. In (7.4) we study the prospects for detection at LEP2, using the most natural values for arbitrary parameters. Distinguishing this model from other Higgs representations is an important issue and is thus covered in detail. Finally, (7.5) contains our conclusions.

7.2 The Higgs Triplet Model (HTM)

The HTM in question was first proposed by Georgi and collaborators [64] and a detailed phenomenological account can be found in Ref. [65]. The Higgs fields take the form

$$\phi = \begin{pmatrix} \phi^{0*} & \phi^+ \\ \phi^- & \phi^0 \end{pmatrix}, \quad \chi = \begin{pmatrix} \chi^0 & \xi^+ & \chi^{++} \\ \chi^- & \xi^0 & \chi^+ \\ \chi^{--} & \xi^- & \chi^{0*} \end{pmatrix}. \tag{7.1}$$

i.e. one complex doublet ($Y = 1$), one real triplet ($Y = 0$), and one complex triplet ($Y = 2$). The value $\rho = 1$ is maintained at tree-level by giving the χ^0 and ξ^0 fields the same VEV, $\langle\chi^0\rangle = \langle\xi^0\rangle = b$, and $\langle\phi^0\rangle = a/\sqrt{2}$. The phase conventions are $\phi^- = -(\phi^+)^*$, $\chi^- = -(\chi^+)^*$, $\chi^{--} = (\chi^{++})^*$, $\xi^- = -(\xi^+)^*$ and $\xi^0 = (\xi^0)^*$.

The kinetic energy term is given by:

$$\mathcal{L}_{\text{kin}} = \frac{1}{2}\text{Tr}\left[(D_\mu\phi)^\dagger(D^\mu\phi)\right] + \frac{1}{2}\text{Tr}\left[(D_\mu\chi)^\dagger(D^\mu\chi)\right]. \tag{7.2}$$

Here,

$$D^\mu\phi \equiv \partial^\mu\phi + ig(\mathbf{W}.\tau/2)\phi - ig'\phi B\tau_3/2, \tag{7.3}$$

[1] Where $V_{T,Y}$ is the VEV of a given representation.

and

$$D^\mu\chi \equiv \partial^\mu\chi + ig(\mathbf{W}.\mathbf{t}/2)\chi - ig'\phi B t_3 \,. \tag{7.4}$$

where the $\tau_i/2$ are the usual 2×2 representation matrices of SU(2) and the t_i are a 3×3 representation of $\tau_i/2$. It is convenient to introduce a doublet triplet mixing angle defined by:

$$\cos\theta_H \equiv \frac{a}{\sqrt{a^2+8b^2}}\,,\quad \sin\theta_H \equiv \sqrt{\frac{8b^2}{a^2+8b^2}}\,. \tag{7.5}$$

We will also use the following combinations of fields:

$$\phi^0 \equiv \sqrt{\frac{1}{2}(\phi_R^0 + i\phi_I^0)}\,,\quad \chi^0 \equiv \sqrt{\frac{1}{2}(\chi_R^0 + i\chi_I^0)}\,,$$
$$\psi^\pm \equiv \sqrt{\frac{1}{2}(\chi^\pm + \xi^\pm)}\,,\quad \zeta^\pm \equiv \sqrt{\frac{1}{2}(\chi^\pm - \xi^\pm)}\,.$$

The gauge boson masses are obtained by expanding out the kinetic energy term (Eq. (7.2)). One finds:

$$M_W^2 = M_Z^2\cos^2\theta_w = \frac{1}{4}g^2v^2\,, \tag{7.6}$$

with $v^2 = a^2 + 8b^2$. Thus $\rho = 1$ is predicted at tree–level. There exists a fiveplet $H_5^{++,+,0,-,--}$, a threeplet $H_3^{+,0,-}$ and two singlets, H_1^0 and $H_1^{0'}$, with each member of a particular multiplet being degenerate in mass at tree level. Their respective compositions are (with $c_H = \cos\theta_H$, $s_H = \sin\theta_H$)

$$H_5^{++} = \chi^{++}\,,\quad H_5^{+} = \zeta^{+}\,,\quad H_5^0 = \sqrt{\frac{1}{3}}(\sqrt{2}\xi^0 - \chi_R^0)\,; \tag{7.7}$$

$$H_3^{+} = c_H\psi^+ - s_H\phi^+\,,\quad H_3^0 = c_H\chi_I^0 + s_H\phi_I^0\,; \tag{7.8}$$

$$H_1^0 = \phi_R^0\,,\quad H_1^{0'} = \sqrt{\frac{1}{3}}(\sqrt{2}\chi_R^0 + \xi^0)\,. \tag{7.9}$$

According to the phase conventions $H_5^{--} = (H_5^{++})^*$, $H_5^- = -(H_5^+)^*$, and $H_3^- = -(H_3^+)^*$. Mixing is possible between H_1^0 and $H_1^{0'}$, varying from zero to maximal depending on the parameters in the Higgs potential. It is conventional in the literature [65] to adopt the language of zero mixing purely for the sake of simplicity. However in this chapter we show

that by assuming natural[2] values for the parameters in the Higgs potential, and using the bound on $\sin\theta_H$ (from considering the $Z \to b\bar{b}$ vertex), this mixing is negligible. Hence results will be presented using H_1^0 and $H_1^{0'}$ as mass eigenstates. We will decouple the triplet fields (in the matrix χ) from the fermions in the HTM. The only possible coupling (by gauge invariance) to the fermions would be the $Y = 2$ triplet field to the lepton–lepton channel, via couplings of the form [65]

$$\mathcal{L} = ih_{ij}(\psi_{iL}^T C\tau_2 \Delta \psi_{jL}) + h.c. \tag{7.10}$$

Here i, j are family indices and ψ_{iL} is the usual two–component leptonic doublet field,

$$\psi_{iL} = \begin{pmatrix} \nu_{li} \\ l_i \end{pmatrix}_L \tag{7.11}$$

and Δ is a 2×2 representation of the $Y = 2$ complex triplet field,

$$\Delta = \begin{pmatrix} \chi^+/\sqrt{2} & -\chi^{++} \\ \chi^{0*} & -\chi^+/\sqrt{2} \end{pmatrix}. \tag{7.12}$$

However, when Eq. (7.10) is expanded one finds a mass for neutrinos

$$m_{ij} = \frac{h_{ij} s_H v}{\sqrt{2}}. \tag{7.13}$$

Assuming that the matrix h_{ij} is diagonal, using the current constraints on neutrino masses one finds that $h_{ee} \leq 5.75 \times 10^{-12}/s_H$, and $h_{\tau\tau} \leq 2 \times 10^{-4}/s_H$. Therefore such couplings are only significant phenomenologically for very small values of $\sin\theta_H$ (much less than 0.1) [65]. Recalling that the motivation for this model is that $\sin\theta_H$ should be significant (i.e. the triplet fields play a sizeable role in electroweak symmetry breaking) it seems contradictory to consider the case of a very small $\sin\theta_H$. Hence our point of view is that even if a Higgs–lepton–lepton coupling exists it will have no phenomenological impact. Therefore we will not consider it and decouple the triplet fields from all fermions. It follows that all members of the 5-plet and $H_1^{0'}$ are 'fermiophobic' at tree level, because they consist purely of triplet fields. They will still couple to gauge bosons (from the kinetic energy term in the Lagrangian) and to other Higgs bosons (from the scalar potential). The 3-plet members, $H_3^\pm$ and H_3^0, are respectively equivalent to $H^\pm$ and A^0 of the 2HDM

[2]Here we take 'natural' to mean equal.

(Model I) with the replacement $\cot\beta \to \tan\theta_H$ in the Feynman rules. The H_1^0 plays the role of the minimal SM Higgs in the limit of $\sin\theta_H \to 0$. A full list of Feynman rules for this model appears in Ref. [65].

It is instructive to see how unitarity is preserved in the HTM. It was explained in (4.2) that for a model with Higgs doublets unitarity is preserved if various sum rules are respected (see Eqs. (4.9, 4.10)). In the HTM there are no simple analogous rules; due to the more exotic spectrum of Higgs bosons one finds that the Higgs contribution to a given scattering process may proceed in various different channels, although the net effect must but the same as the ϕ^0 contribution. For example, let us consider the process $ZW^- \to ZW^-$. In the minimum SM the Higgs contribution is a t–channel graph involving ϕ^0, with effective strength proportional to $g^2 M_Z^2$ (i.e. from the $ZZ\phi^0$ and $WW\phi^0$ coupling). In the HTM there are three t–channel graphs for the neutral bosons, and a s–channel and a u–channel for H_5^-. The s– and u–channel graphs combine to give the same result as a t–channel graph except for an overall sign difference. Thus the four contributions have effective strengths proportional to

$$\begin{aligned} H_1^0 &: \; g^2 c_H^2 M_Z^2 \,. \\ H_1^{0\prime} &: \; \frac{8}{3} g^2 s_H^2 M_Z^2 \,. \\ H_5^0 &: \; \frac{-2}{3} g^2 s_H^2 M_Z^2 \,. \\ H_5^- &: \; -g^2 s_H^2 M_Z^2 \,. \end{aligned} \tag{7.14}$$

The sum of all four terms gives the original $g^2 M_Z^2$ of the ϕ^0 t–channel graph in the minimum SM. In $W^+W^+ \to W^+W^+$ scattering, H_5^{++} contributes in the s–channel and again the sum of the HTM contributions is equivalent to that of ϕ^0.

Thus it appears that the HTM can reproduce all the desirable properties of ϕ^0, that is, it preserves unitarity, gives masses to the fermions and bosons, and maintains $\rho = 1$ at tree–level. However we must mention a naturalness problem that arises in the HTM at the one–loop level. Ref. [65] shows that there are quadratically divergent contributions to the ρ parameter. These can be cancelled by counterterms originating from the one–loop Higgs potential, although a certain amount of fine–tuning is required. However, the level of fine–tuning is no more serious than that required in the minimal SM to keep $M_{\phi^0} \leq 1$

TeV.

7.3 Constraints on Parameters

Precision measurements of the process $Z \to b\bar{b}$ impose the strongest bound on $\sin\theta_H$. Virtual charged scalars with tree level fermion couplings contribute to this decay i.e. $H^{\pm}$ in the 2HDM and $H_3^{\pm}$ in the HTM. Ref. [46] shows that this vertex constrains $|\cot\beta| \leq 0.8$ in the 2HDM, which corresponds to $|\tan\theta_H| < 0.8$ (or $|\sin\theta_H| \leq 0.63$) in the HTM. This constraint is for a top quark mass of 180 GeV and $M_{H_3} \leq 200$ GeV. We are not aware that this bound is considered in the literature, and recent papers still consider the case of $|\sin\theta_H| \to 1$. We note that $|\sin\theta_H| \leq 0.06$ is equivalent to $|V_{\text{trip}}|/|V_{\text{doub}}| \leq 0.03$ (see Eq. (4.7)). Therefore it is in the spirit of the model to only consider $|\sin\theta_H| > 0.1$ (say). The maximum value of $|\sin\theta_H| = 0.63$ allows $|V_{\text{trip}}|/|V_{\text{doub}}| = 0.4$, showing that the triplets could still play a significant role in electroweak symmetry breaking.

The other arbitrary parameters in the model are of course the masses of the Higgs bosons. From the Higgs potential we can write down the following tree level values [65] , with λ_i being a Higgs self coupling constant and $v^2 = (246\text{ GeV})^2$:

$$M_{H_5}^2 = 3(\lambda_5 s_H^2 + \lambda_4 c_H^2)v^2 \ , \quad M_{H_3}^2 = \lambda_4 v^2 \ . \tag{7.15}$$

As mentioned earlier, all members of a particular multiplet are degenerate in mass. In general, H_1^0 and $H_1^{0'}$ can mix according to the mass–squared matrix

$$M = \begin{pmatrix} 8c_H^2(\lambda_1+\lambda_3) & 2\sqrt{6}s_H c_H \lambda_3 \\ 2\sqrt{6}s_H c_H \lambda_3 & 3s_H^2(\lambda_2+\lambda_3) \end{pmatrix} v^2 \ . \tag{7.16}$$

There exists two mass eigenstates denoted by ψ_1 and ψ_2 with $M_{\psi_1} > M_{\psi_2}$:

$$M_{\psi_1,\psi_2}^2 = \frac{1}{2}\left[M_{11} + M_{22} \pm \sqrt{(M_{11}-M_{22})^2 + 4M_{12}^2}\right] \ . \tag{7.17}$$

It is clear that the mixing vanishes in the limit of $\lambda_3 \to 0$ and this scenario is usually considered in the literature. However, it is our aim to keep natural values for λ_i and we will present results for the case of them all being equal (we see these as being the *most*

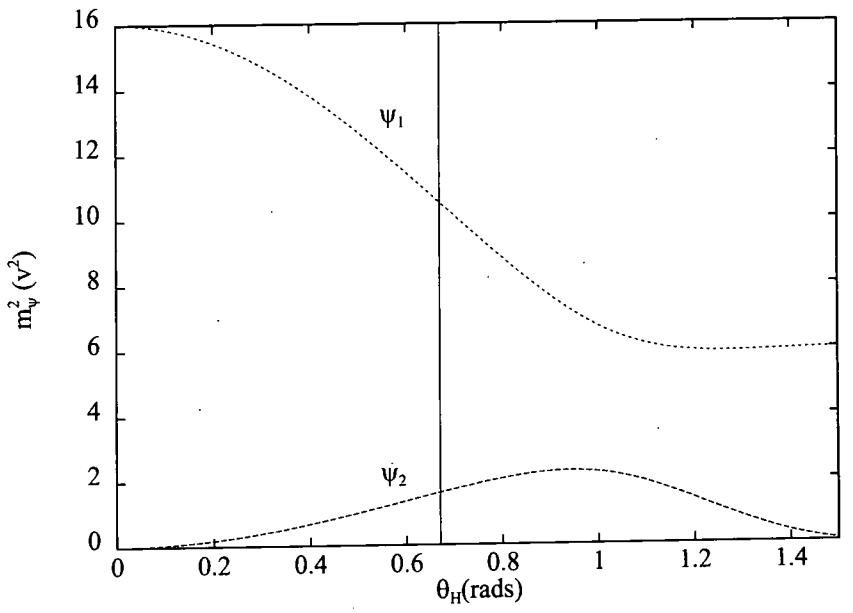

Figure 7.1: The squared masses of ψ_1 and ψ_2 in units of $v^2 = (246\ \text{GeV})^2$ as a function of θ_H ($\lambda_i = 1$ is assumed). The experimentally allowed region lies to the left of the vertical line $\theta_H = 0.67$ rads.

natural values). From now on we will employ a set of units in which $\lambda_i = 1$. Figure 7.1 shows the masses of ψ_1 and ψ_2 in this unit system as a function of θ_H. From the constraint on $\sin\theta_H$, one finds $\theta_H < 0.67$ rads (or 38.7°). From Figure 7.1 it is apparent that $10v^2 \leq M_{\psi_1} \leq 16v^2$, and $0 \leq M_{\psi_2} \leq 1.5v^2$. Hence there exists a natural, tree level hierarchy of masses:

$$M^2_{\psi_1} = 10v^2 \rightarrow 16v^2\ ,\quad M^2_{H_5} = 3v^2\ ,\quad M^2_{H_3} = v^2\ ,\quad M^2_{\psi_2} = 0 \rightarrow 1.5v^2\ . \tag{7.18}$$

The compositions of ψ_1 and ψ_2 are given by:

$$\psi_1 = H_1^{0'} \sin\alpha_T + H_1^0 \cos\alpha_T\ , \tag{7.19}$$

$$\psi_2 = H_1^{0'} \cos\alpha_T - H_1^0 \sin\alpha_T\ , \tag{7.20}$$

with the mixing angle obtained from

$$\sin 2\alpha_T = \frac{2M_{12}}{\sqrt{(M_{11} - M_{22})^2 + 4M_{12}^2}}\ . \tag{7.21}$$

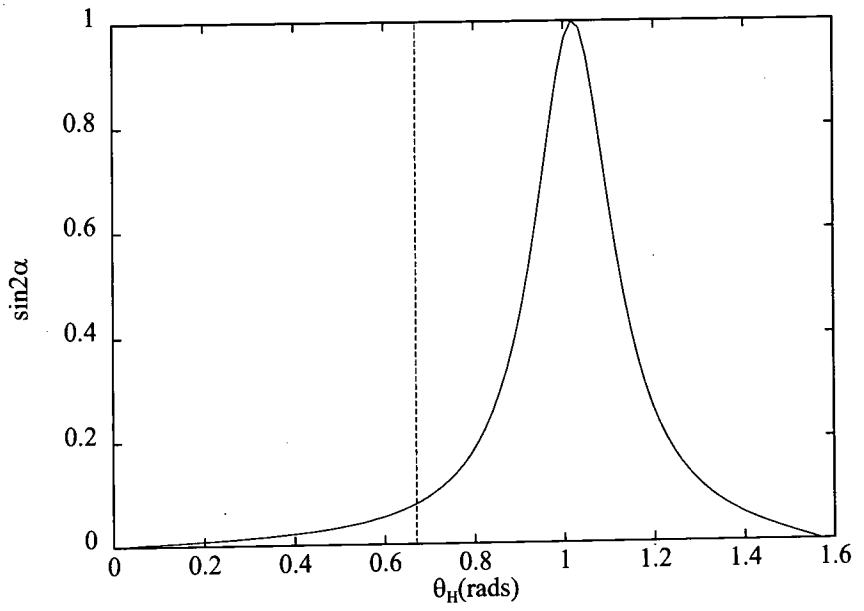

Figure 7.2: The mixing angle $\sin 2\alpha_T$ as a function of θ_H. The experimentally allowed region lies to the left of the vertical line $\theta_H = 0.67$ rads.

Figure 7.2 shows how $\sin 2\alpha_T$ varies with θ_H. It is clear that the bound $\theta_H \leq 0.67$ rads forces the value of $\sin 2\alpha_T$ to be < 0.1. This strongly constrains α_T to the region $\leq 2.9°$ or $\geq 87.1°$. In the former case $\sin \alpha_T \leq 0.05$ and $\cos \alpha_T = 0.999 \rightarrow 1$. From Eqs. (7.19, 7.20) it is then clear that ψ_1 is effectively H_1^0 with ψ_2 equal to $H_1^{0'}$. The converse is true for $\alpha_T \geq 87.1°$. Therefore very little mixing is present and so we can treat $H_1^{0'}$ and H_1^0 as mass eigenstates to a very good approximation.

Now that we know the composition of all the mass eigenstates and their Feynman rules, could some of the Higgs bosons be light enough to lie in the energy range of LEP2 (i.e. an e^+e^- collider with $\sqrt{s} = 175 \rightarrow 200$ GeV)? We must first consider the current lower bounds on their masses from both direct/indirect searches. By 'indirect' searches we mean measuring processes that are sensitive to the Higgs sector. The most important process of this kind is the decay $b \rightarrow s\gamma$ which can proceed by emitting a virtual $H_3^{\pm}$ (for

a general review of how this decay is sensitive to new physics see Ref. [47]). Recently the first measurement of its branching ratio was announced by the CLEO collaboration, with the value [52]

$$\mathrm{BR}(b \to s\gamma) = (2.32 \pm 0.57 \pm 0.35) \times 10^{-4} \,. \tag{7.22}$$

This measurement sets a lower limit ($M_H \geq 260$ GeV) on the mass of $H^\pm$ (2HDM, Model II), taking it out of the range of LEP2. However, from Chapter 5 we recall that no lower bound can be obtained for the $H^\pm$ (2HDM, Model I). Recalling that $H_3^\pm$ obeys the same phenomenology as this latter charged scalar with the substitution $\cot\beta \to \tan\theta_H$, then $H_3^\pm$ may also be in the range of LEP2.

The other charged scalars in this model ($H_5^{\pm\pm}$ and $H_5^\pm$) are fermiophobic at tree level and so do not contribute to this decay. Hence no indirect mass bound can found for them. For neutral scalars, direct bounds from e^+e^- colliders are stronger. The current LEP limits on these particles are as follows [32]:

$$M_{H_5^{\pm\pm}} \geq 45.6 \text{ GeV} \,, \tag{7.23}$$

$$M_{H_5^\pm} \,,\, M_{H_3^\pm} \geq 41.7 \text{ GeV} \,. \tag{7.24}$$

Eqs. (7.23, 7.24) are obtained by searching for $e^+e^- \to \gamma^*,\ Z^* \to H^+H^-,\ H^{++}H^{--}$. Limits for H_1^0, $H_1^{0\prime}$ and H_5^0 (which can couple to vector bosons) are best obtained by searching for $e^+e^- \to Z^* \to ZH_i^0$ (at higher collider energy W^+W^- and ZZ fusion become important). From Ref. [65] we have the following ratios for this cross section, with ϕ^0 being the minimal SM Higgs:

$$H_5^0 : H_1^{0\prime} : H_1^0 : \phi^0 = \frac{4}{3}s_H^2 : \frac{8}{3}s_H^2 : c_H^2 : 1 \,. \tag{7.25}$$

The bound on M_{ϕ^0} is ≥ 63.5 GeV [32], and so the bounds on H_5^0, $H_1^{0\prime}$ and H_1^0 will tend to be less due to $s_H < 0.63$ ($s_H^2 < 0.39$). Ref. [32] states that for a cross-section ≥ 0.1 times that of the ϕ^0, the bound is ≥ 40 GeV.

There is one caveat to the lower limit for $H_5^{\pm\pm}$. The current searches have assumed $H^{\pm\pm} \to l^\pm l^\pm$ [67], [68] which is the decay for a doubly charged scalar of a left–right symmetric theory. The $H_5^{\pm\pm}$ in the model we are studying would decay via W^*W^* to $l^\pm l^\pm \nu\nu$ (for masses in the range of LEP2) [65], [69]. This would provide a way of distinguishing

between the two models, but also suggests that the ≥ 45.6 GeV limit (Eq. (7.23)) may not be relevant for our analysis. However, we expect $H_5^{\pm\pm}$ and $H_5^{\pm}$ to have very similar masses (equal at tree level) and so the ≥ 41.7 GeV bound (Eq. (7.24)) could loosely be used for both.

7.4 Phenomenology at LEP2

We next investigate the prospects for detection of the Higgs bosons at LEP2, for which we will assume $\sqrt{s} = 175 \rightarrow 200$ GeV. Using the mass hierarchy (Eq. (7.18)) as a guide, we will consider in turn the possible combinations of Higgs bosons in range at this collider. Distinguishing the HTM from other models is an important issue and is discussed below. Measuring the value of $\sin\theta_H$ is also desirable, in order to see to what extent the triplets contribute to electroweak symmetry breaking.

Case 1: Here we consider only ψ_2 to be in the discovery range, i.e. $M_{\psi_2} \leq \sqrt{s} - 100$ GeV [3]. As mentioned in (7.3), ψ_2 will be (to a good approximation) entirely $H_1^{0\prime}$ or H_1^0 depending on the value of the mixing angle (α_T).

a) $\psi_2 = H_1^0$: The production process here would be $Z^* \rightarrow ZH_1^0$. From Eq. (7.25) we see that the rate would be quite large ($c_H^2 \geq 0.61$) and so detection should not be a problem ($H_1^0 \rightarrow b\bar{b}$ is expected to be the strongest decay channel for $M_{H_1^0} \leq 100$ GeV). The detection techniques in this channel were covered in (3.6). Its suppressed production rate could be a way of distinguishing it from ϕ^0, although we must remember that a light h^0 from a 2HDM [30] would also have the same signature. However, some evidence that we have a non-minimal Higgs sector could be obtained.

b) $\psi_2 = H_1^{0\prime}$: Again one uses the Higgs *bremsstrahlung* process $Z^* \rightarrow ZH_1^{0\prime}$. The rate (see Eq. (7.25)) is $\sin\theta_H$ dependent but could be slightly above that for ϕ^0 when $s_H^2 = 0.39$ (its maximum value). If produced in sufficient quantities then we must search for the decays of this fermiophobic Higgs. Ref. [70] analyses such decays and concludes

[3] Assuming the production mechanism $e^+e^- \rightarrow Z^* \rightarrow Z\psi_2$.

that the dominant channel for masses below 90 GeV would be to $\gamma\gamma$ induced at one loop. We shall be covering the phenomenology of fermiophobic Higgs bosons in more depth in Chapter 8 and so do not attempt to give a rigorous explanation here. The $\gamma\gamma$ channel would provide an excellent signature and should have a large branching ratio. One would search for $jj\gamma\gamma$ events; the main background would come from initial state and final state radiation, and can be removed by demanding energetic photons.

However, a fermiophobic Higgs is also possible in the 2HDM (Model I) [71] with the mixing angle α fine–tuned to equal $\pi/2$. In principle, there still exists a parameter space that could distinguish between the two. The Z-Z-Higgs coupling for this latter boson is Z-Z-ϕ^0 strength with a suppression factor of $\sin(\beta-\alpha)$. With $\alpha=\pi/2$ one has $\sin(\beta-\alpha)=-\cos\beta$, and from the constraint $|\cot\beta|\leq 0.8$, one finds a production cross section ≤ 0.39 that of the ϕ^0. From Eq. (7.25) we see that this cross section for $H_1^{0\prime}$ is $\sin\theta_H$ dependent and so could be significantly greater than 0.39. This could distinguish $H_1^{0\prime}$, although one could postulate that if such a fermiophobic Higgs is found, it is more likely to be from the HTM (as the 2HDM requires fine-tuning for fermiophobia).

Case 2: Here we consider only the 3–plet to be in range. The $H_3^{\pm}$ would be produced by pair production, $e^+e^-\to\gamma^*, Z^*\to H^+H^-$. Singly charged scalars from the 2HDM (Model I and I') and general multi–doublet model (MHDM) are also possible at this collider and a full phenomenological study appeared in Chapter 5. Distinguishing $H_3^{\pm}$ from $H^{\pm}$ (2HDM, Model I) is impossible due to their identical couplings. However, detection would be proof of a non–minimal Higgs sector. The H_3^0 cannot be produced by $Z^*\to ZH_3^0$, being equivalent to A^0 in the 2HDM (Model I). Its production at e^+e^- colliders must wait until the $Z^*\to H_3^0H_1^0$, $H_3^0H_1^{0\prime}$ processes become available (see Case 3).

Case 3: This case combines the above analyses, considering both the 3–plet and ψ_2 to be accessible.

a) $\psi_2=H_1^0$: A new production channel is now available, that of $Z^*\to H_3^0H_1^0$. The cross–section is well known [30], [65] and a review of the detection techniques appears in Ref. [55]. One searches for a signal of $b\bar{b}b\bar{b}$ (which is the dominant decay of the H_3^0

and H_1^0), and a b–tag requirement heavily reduces the main four jet backgrounds from $q\overline{q}$, WW and ZZ. A good signal is present over a small background if the cross–section is not too suppressed (it is proportional to s_H^2). Detection in this channel would suggest the triplet model i.e. a pair of degenerate Higgs bosons, H_3^0 and $H_3^\pm$. Without this option one would observe just $H_3^\pm$ and H_1^0, which would look like a 2HDM (Model I or I') (as mentioned earlier).

b) $\psi_2 = H_1^{0\prime}$: Again the presence of $Z^* \to H_3^0 H_1^{0\prime}$ is useful in suggesting the triplet model, due to the presence of a pair of degenerate Higgs bosons. The signal will be different to that of case 3(a) due to the $\gamma\gamma$ decays of $H_1^{0\prime}$. Hence one would search for $b\overline{b}\gamma\gamma$ events. This would add to the signal in the $Z^* \to ZH_1^{0\prime}$ channel, although a b–tag requirement would make the $Z^* \to H_3^0 H_1^{0\prime}$ signal more prominent. The cross–section is proportional to c_H^2 and therefore would possess a reasonable rate. Without this option of Higgs pair production, $H_3^\pm$ and $H_1^{0\prime}$ could look like the 2HDM (Model I) with a fine–tuned mixing angle. However, case 1(b) explains that we could perhaps infer the HTM is present.

Case 4: Now we include the members of the 5–plet. This situation has rich phenomenology and should readily identify the HTM. The most spectacular evidence would be that of $H_5^{\pm\pm}$. The pair production cross–section would be four times that of the singly charged Higgs bosons, yielding > 350 events for $M_{H_5} \leq 80$ GeV at $\sqrt{s} = 200$ GeV. The dominant decay channel would be to W^*W^* [65], [69], (the 5–plet members are fermiophobic) yielding a four fermion final state. The cleanest signature would $ll\nu\nu$ and this decay could distinguish $H_5^{\pm\pm}$ from the doubly charged scalar of a left–right symmetric model, the latter decaying to ll. A review of the detection techniques can be found in Refs. [67], [68], although these searches were for the decay $H^{++}H^{--} \to llll$. The backgrounds to the $llll$ channel are very small, and the signal number is large due to the sizeable production cross–section.

Many other production processes become available with the introduction of the 5–plet. These are $H_5^+ H_5^-$, $H_5^\pm H_3^\mp$, $H_5^0 H_3^0$, ZH_5^0 and $H_5^\pm W^\mp$. The $H_5^\pm$ would be produced in pairs (standard process for charged scalars), singly by the exotic vertex $H_5^\pm W^\mp Z$, and by $Z^* \to H_5^\pm H_3^\mp$. Ref. [72] shows that the dominant decay of $H_5^\pm$ would be to $W^{\pm *} Z^*$. This

vertex is exclusive to higher Higgs representations and is not present in models with just doublets. The H_5^0 would be produced by $Z^* \to ZH_5^0$, $H_5^0 H_3^0$. Being fermiophobic also, its decays are similar to those of $H_1^{0\prime}$.

The best processes for measuring the contribution of the triplets to electroweak symmetry breaking will be $\cos\theta_H$ dependent (recalling that $c_H^2 \geq 0.61$). The ones likely to give most events are $Z^* \to ZH_1^0$ (which is proportional to c_H^2) and $Z^* \to H_3^0 H_1^{0\prime}$ (proportional to $\frac{8}{3}c_H^2$).

7.5 Conclusions

We have studied the most popular model containing Higgs triplets (HTM) in the context of the non–minimal Standard Model. Such a representation is possible, not being in conflict with current experimental data (most notably the measurement of $\rho \approx 1$).

Various exotic Higgs bosons with reasonable cross–sections are predicted (i.e. doubly charged and fermiophobic bosons), all of which escape the mass bounds from $b \to s\gamma$. Therefore they can be searched for at LEP2. Making use of a natural mass hierarchy obtained from the Higgs potential, we considered in turn the possible combinations of Higgs bosons in range at this collider. If light enough ($\leq$ 80 GeV), detection of $H_5^{\pm\pm}$ would be straightforward and a strong signature of the HTM. Otherwise, distinguishing this model from other non-minimal representations is not so easy. The discovery of one of the fermiophobic Higgs bosons (the lightest likely to be ψ_2 composed mainly of $H_1^{0\prime}$), and/or a pair of bosons roughly degenerate in mass (H_3^0 and $H_3^\pm$) would be indicators but not conclusive evidence.

A Next Linear Collider (NLC) with $\sqrt{s} = 500 \to 1000$ GeV would enable heavier Higgs bosons to be produced, should LEP2 be insufficiently energetic. Decays to lighter Higgs bosons would no longer be negligible and so detection methods must change accordingly. However, all the production processes mentioned above would be relevant, with new ones also becoming significant (such as vector boson fusion for both neutral and charged scalars). A general outline of detection prospects at such a collider appears in Ref. [65]. Ref. [73] examines production processes using the exotic $H_5^\pm W^\mp Z$ vertex as an alternative

way of distinguishing the HTM. However, $s_H^2 \approx 1$ is required to detect this vertex, and given the constraint $s_H^2 \leq 0.39$ this method seems difficult.

Prospects at high energy hadron colliders have also been discussed, see for example Ref. [65]. Usually such work focuses on $H_5^{\pm\pm}$ [74], with relatively little attention given to the fermiophobic neutral Higgs bosons ($H_1^{0\prime}$, H_5^0). We recall that discovery of one of these latter scalars would suggest the HTM, though the main production process of gluon fusion via a fermion loop would be absent. The topic of fermiophobia is coverered in more depth in the next chapter.

Chapter 8

Fermiophobic Higgs bosons

8.1 Introduction

In Chapter 7 the concept of a fermiophobic Higgs boson (H_F) was introduced, and we discussed how such particles are required (due to experimental data) in the HTM. It was also mentioned that a H_F is possible in the 2HDM for values of $\alpha \approx \pi/2$. We concluded in Chapter 7 that the phenomenology of H_F is rarely covered in the literature, although it may possess very distinct signatures; in addition, the discovery of such a particle would shed important light on the underlying Higgs representation. In particular, fermiophobia is not possible in the MSSM, and hence searching for H_F is well motivated. In this chapter we aim to provide a full analysis of the phenomenology of H_F at hadron colliders (Tevatron and LHC), with mention given to its phenomenology at LEP2. The fermiophobic Higgs bosons that we shall cover are $H_1^{0\prime}$ and H_5^0 of the HTM, and the lightest CP–even scalar of the 2HDM (Model I) which was referred to as h_1 in Chapter 6. Our nomenclature in this chapter is such that H_F refers to general fermiophobic Higgs of mass M_F, while h_1^F refers to the H_F of the 2HDM (Model I) i.e. with $\alpha = \pi/2$.

8.2 Fermiophobia

Fermiophobia can arise naturally in models with Higgs triplets. In the HTM the hypercharge values of the triplets ($Y = 2$ and $Y = 0$) together with the requirement of gauge invariance severely restrict their couplings to the fermions. As explained in Chapter 7, the only possible triplet–fermion coupling would be to the lepton–lepton channel, but the current limits on neutrino masses render this interaction phenomenologically irrelevant (see Eq. (7.13)) For the 2HDM one can see from the couplings in Table 6.1 that Model I is the only structure which can display fermiophobia, the requirement being $\cos\alpha \to 0$. The heavier CP–even Higgs boson (H) would itself be fermiophobic if $\cos\alpha \to 1$, although since this particle may be much heavier than h_1^F we shall concentrate on the latter. Of course, a H_F may also be possible in the MHDM if a mixing angle is tuned to zero (see Eq. (6.6)). It is clear that the discovery of a H_F imposes strong constraints on the structure of the underlying Higgs model, since fermiophobia requires either a fine–tuned mixing angle or a Higgs triplet representation. In this chapter we shall not consider a charged H_F; for recent studies we refer the reader to Refs. [72], [73].

In Chapter 7 we analysed the HTM using a natural argument of equating all Higgs self couplings (λ_i) to 1; it was shown that $H_1^{0'}$ can be taken as a physical mass eigenstate and we also obtained the natural mass hierarchy given by Eq. (7.18). This natural argument predicts $H_1^{0'}$ to be either the lightest or the heaviest of the bosons in the HTM, depending on the exact value of the mixing angle α_T. We shall be concentrating on the scenario of it being the lightest but detection prospects will be mentioned if this is not the case. Chapter 7 constrains α_T by using the bound $\sin\theta_H \leq 0.63$. This result is for $M_{H_3} \leq 200$ GeV which we see as being justified if one wishes to search for $H_1^{0'}$ at the Tevatron; from the mass ratios in Eq. (7.18) we see that $M_{H_3} \leq 200$ GeV would imply $0 \leq M_{\psi_2} \leq 245$ GeV, which is the mass range that is relevant at the Tevatron. The other neutral H_F in the HTM is H_5^0, and we shall see that it is harder to produce at the Tevatron due its more suppressed couplings to vector bosons. In this chapter we shall apply the above natural argument to the 2HDM in order to find the analogous mass hierarchy, and to ascertain the dependence of $\sin\alpha$ on $\tan\beta$. The analysis utilizes the results of (3.3) with all Higgs self couplings set equal to 1. Plotted in Figure 8.1 is the squared mass of h_1 and H (the

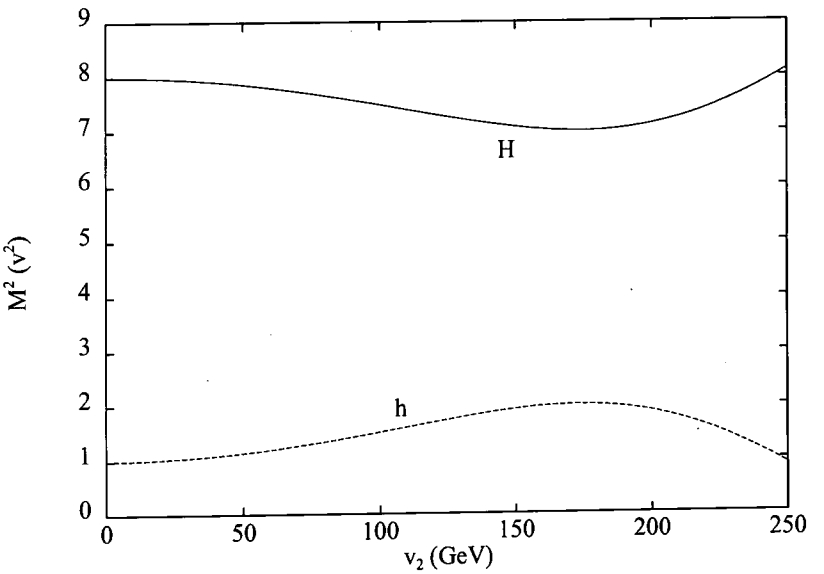

Figure 8.1: The squared masses of H and h_1 as a function of v_2.

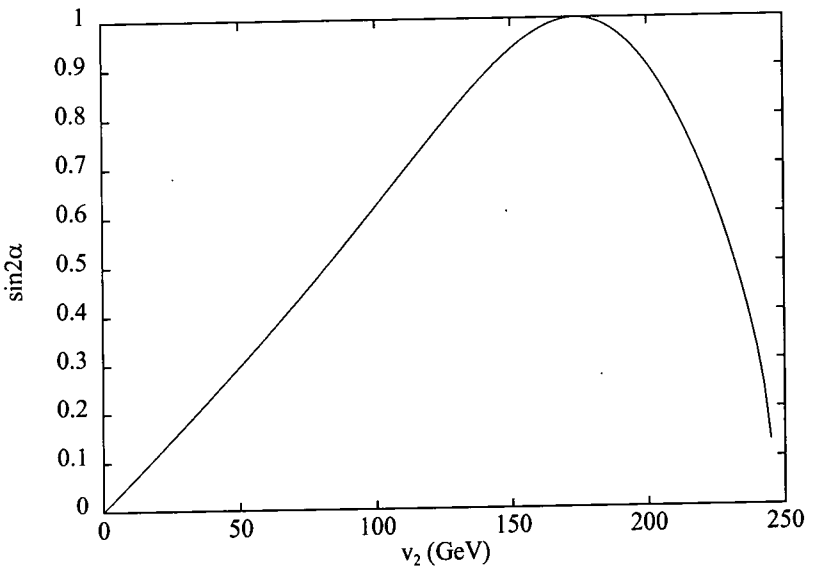

Figure 8.2: $\sin 2\alpha$ as a function of v_2.

two CP–even Higgs bosons) as a function of v_2. From this we see that $7v^2 \leq M_H^2 \leq 8v^2$ and $v^2 \leq M_h^2 \leq 2v^2$. Therefore the mass hierarchy reads as

$$M_H^2 = 7v^2 \rightarrow 8v^2\ ,\quad M_h^2 = v^2 \rightarrow 2v^2\ ,\quad M_{H^\pm}^2 = v^2\ ,\quad M_{A^0}^2 = v^2\ . \tag{8.1}$$

Eq. (8.1) suggests that h_1^F is likely to be of comparable mass to $M_{H^\pm}$ and so justifies the use of the bound $\tan\beta \geq 1.25$ for $M_{H^\pm} \leq 200$ GeV, if one wishes to search for h_1^F at the Tevatron. Plotted in Figure 8.2 is $\sin 2\alpha$ as a function of v_2. We see that maximal mixing ($\sin 2\alpha = 1$, $\alpha = \pi/4$) occurs when $v_2 = v_1 \approx 174$ GeV. For $v_1 \ll 174$ GeV (i.e. $\tan\beta \gg 1$), the two α solutions for $\sin 2\alpha$ approach 0 and $\pi/2$. Hence for fermiophobia ($\pi/2$) this argument would require larger $\tan\beta$, a result consistent with the bound $\tan\beta \geq 1.25$ for $M_{H^\pm} \leq 200$ GeV. It is our aim now study the BRs of H_F.

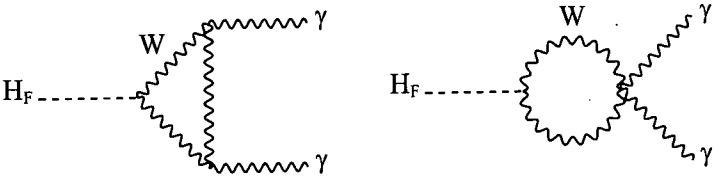

Figure 8.3: Decays of $H_F \rightarrow \gamma\gamma$.

Tree–level decays to fermions are obviously not allowed, and so if $M_F \leq 80$ GeV the only possible tree–level channels are $H_F \rightarrow W^*W^*$, Z^*Z^*, with '*' denoting an off–shell vector boson[1]. Since these latter decays are not very strong (the vector bosons being considerably off–shell) the one–loop mediated decay, $H_F \rightarrow \gamma\gamma$, will certainly have a larger BR than for ϕ^0, and its Feynman diagrams are displayed in Figure 8.3. There are no diagrams with fermion loops, although we recall that these diagrams interfere destructively with the dominating W mediated decays – see (6.5.1). The BRs predicted by Refs.[70] and [75] agree and imply that the channel $H_F \rightarrow \gamma\gamma$ dominates for $M_F \leq 80$ GeV; at $M_F \approx 95$ GeV the tree–level process $H_F \rightarrow WW^*$ is equally likely as $H_F \rightarrow \gamma\gamma$, each having BR=45%; see Figure 8.4 (taken from Ref. [75]).

It is of interest to note that the BRs to W and Z are an order of magnitude higher than those for ϕ^0 in the region $M_F \leq 120$ GeV, and this will be beneficial for detection

[1]Not including decays to other Higgs bosons which will be heavily off–shell.

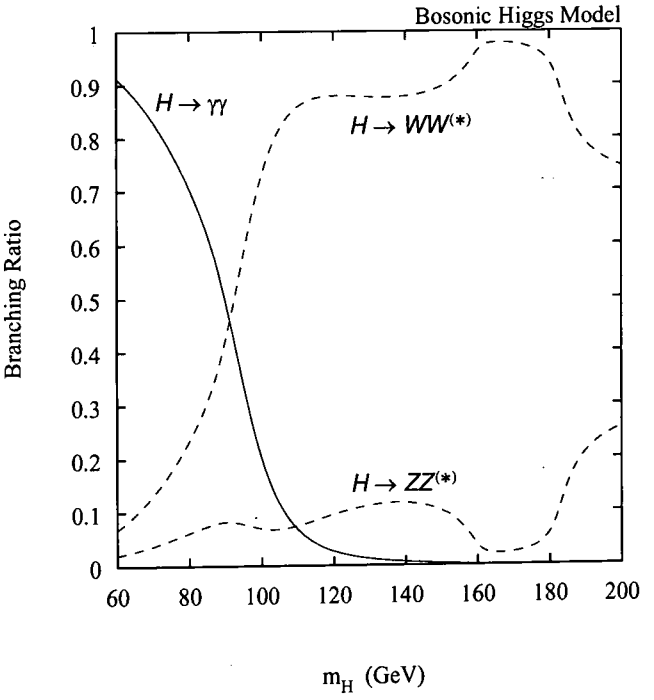

Figure 5

Figure 8.4: The BRs of H_F (from Ref. [75]).

in the $H_F \to ZZ^* \to llll$ channel (see later). In contrast, for ϕ^0 and h^0 of the MSSM the branching ratio to two photons is of the order 0.1%. For higher M_F the vector boson channels dominate along with decays to other Higgs bosons ($H_F \to t\bar{t}$ is not allowed at tree–level). Therefore the distinctive fermiophobic signature of $H_F \to \gamma\gamma$ is disappearing for $M_F \geq 130$ GeV.

The BRs used in Ref. [75] are for a H_F with ϕ^0 strength (i.e. minimal SM strength) couplings to vector bosons. This is not the case for the H_F that we are considering, as can be seen from Eqs. (8.2 → 8.4). The couplings here are expressed relative to those of the minimal SM Higgs boson (with $s_H \equiv \sin\theta_H$) [65]:

$$H_1^{0\prime}W^+W^- : \frac{2\sqrt{2}}{\sqrt{3}}s_H\,, \qquad H_1^{0\prime}ZZ : \frac{2\sqrt{2}}{\sqrt{3}}s_H\,, \tag{8.2}$$

$$H_5^0 W^+W^- : \frac{1}{\sqrt{3}} s_H \,, \qquad H_5^0 ZZ : \frac{-2}{\sqrt{3}} s_H \,, \tag{8.3}$$

$$h_1^F W^+W^- : -\cos\beta \,, \qquad h_1^F ZZ : -\cos\beta \,. \tag{8.4}$$

Eqs. (8.2) and (8.4) show that both the $H_F W^+W^-$ and $H_F ZZ$ couplings for $H_1^{0'}$ and h_1^F are scaled by the same amount, and so the BRs displayed in Fig. 8.4 can be used. This is not true for H_5^0 which has an enhanced $H_5^0 ZZ$ coupling compared to $H_5^0 W^+W^-$. However, in the region of $M_F \leq 80$ GeV (which is of interest at the Tevatron) the channel $H_5^0 \to Z^{(*)}Z^*$ is small and so we may use the BRs in Fig. 8.4 to a very good approximation. Explicitly we can show that BR $(H_5^0 \to \gamma\gamma)$ would be between 0.9 and 0.8 times the values in Figure 8.4 for 60 GeV$\leq M_5 \leq 100$ GeV. For $M_5 \geq 100$ GeV the enhanced BR $(H_5^0 \to Z^*Z)$ (reaching BR $\approx 30\%$ until a sudden dip due to the real WW threshold) relative to BR $(H_5^0 \to W^+W^-)$ would aid detection in the $llll$ channel. Once the real ZZ threshold is reached the ratio of the partial widths of ZZ and WW tends to $2:1$, being vice versa for ϕ^0, $H_1^{0'}$ and h_1^F. These channels saturate the width in the heavy Higgs region unless the decays to other Higgs bosons become strong.

8.3 Phenomenology at the Tevatron

The production cross–sections for ϕ^0 at the Tevatron are shown in Figure 8.5. Gluon–gluon fusion again dominates, although it is relatively less important than at the LHC due to the decreased gluon luminosity at the Tevatron. For H_F the relevant processes are associated production with a vector boson and vector boson fusion, since the other mechanisms require a Higgs–fermion coupling. Vector boson fusion has a smaller cross–section and it was shown in Ref. [75] that the detection prospects for H_F are worse. Therefore we shall focus on the associated production process whose Feynman diagram is displayed in Figure 8.6. As mentioned in the previous section, Ref. [75] assumed minimal SM strength couplings to vector bosons for H_F and so the production cross–sections for $H_1^{0'}$, H_5^0 and h_1^F relative to those for ϕ^0 will scale by the squares of the couplings given in Eqs. (8.2 → 8.4). Thus for the process $q\bar{q} \to W^* \to WH_F$ we find the following

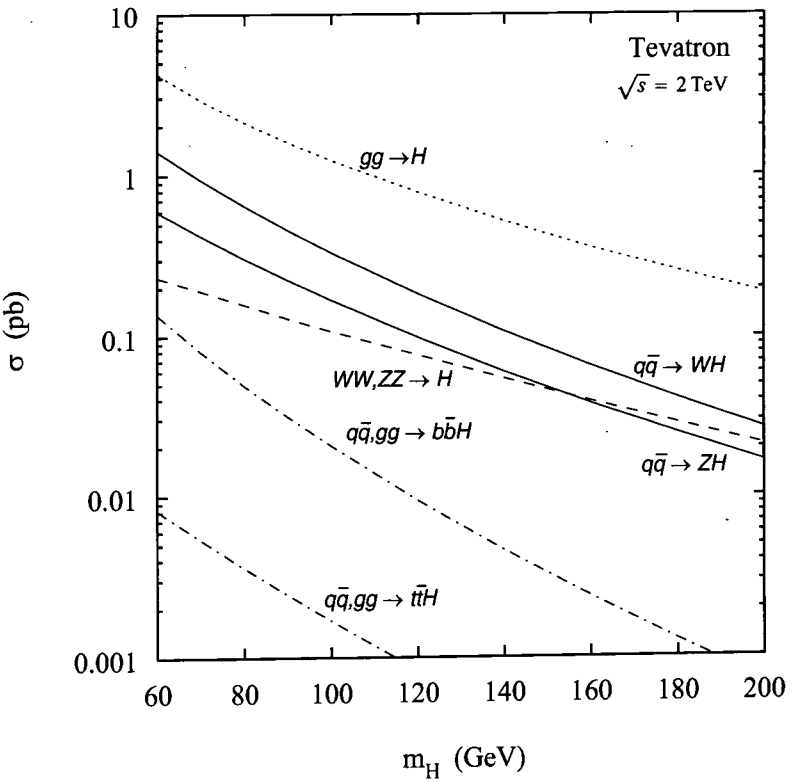

Figure 1

Figure 8.5: The production cross-sections of H_F at the Tevatron (from Ref. [75]).

cross–section ratios:

$$H_5^0 : H_1^{0\prime} : h_1^F : \phi^0 = \frac{1}{3}s_H^2 : \frac{8}{3}s_H^2 : \cos^2\beta : 1 \,, \tag{8.5}$$

and for $q\overline{q} \to Z^* \to ZH_F$

$$H_5^0 : H_1^{0\prime} : h_1^F : \phi^0 = \frac{4}{3}s_H^2 : \frac{8}{3}s_H^2 : \cos^2\beta : 1 \,. \tag{8.6}$$

Due to the bounds $\sin^2\theta_H \leq 0.39$ and $\cos^2\beta \leq 0.39$ we see that $H_1^{0\prime}$ may be produced with ϕ^0 strength in both channels, while h_1^F has at best a cross–section 0.39 that of ϕ^0. H_5^0 has very weak couplings to W^+W^- (at best 0.13 that of $\phi^0 W^+W^-$), but better to

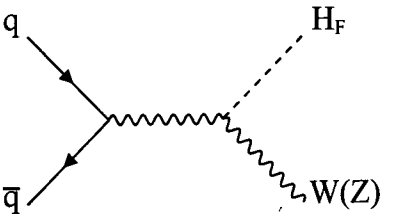

Figure 8.6: The main production mechanism of H_F at the Tevatron.

ZZ. We note that a H_F with ϕ^0 strength couplings to ZZ would have been seen at LEP if $M_F \leq 60$ GeV [76]. Eq. (8.2 → 8.4) show that this lower bound will in general be weaker for $H_1^{0\prime}$, h and H_5^0. The method of searching for H_F at the Tevatron is described in Ref. [75] and we shall briefly review it here. The photons from H_F act as a trigger for the events, and then one may use either the hadronic or leptonic decay of the vector bosons. For the leptonic decay there are two detection channels. One can exploit production in association with a $W^{\pm}$, and demand two photons plus an isolated lepton and missing energy ($W \to l\nu_l$); alternatively one can use the Z channel and demand two photons with two leptons ($Z \to l^+l^-$) or missing energy ($Z \to \nu\overline{\nu}$). The main background ($W\gamma\gamma$ and $Z\gamma\gamma$) is caused by $q\overline{q}$ annihilation with γ emission from any charged line i.e. from the quark line or W line, or one from each. The background is integrated over an invariant mass bin of ≈ 3 GeV centered on M_F, which contains nearly all the signal events; it is found that the background is far below one event (of order 10^{-1}) for $M_F \geq 60$ GeV. Hence the signal is effectively background free and so one only requires a reasonable number of events (≥ 3) in this channel for detection. For the hadronic decays of the vector bosons there is a background ($jj\gamma\gamma$) from the processes[77]:

$$\begin{aligned} q\overline{q} &\to \gamma\gamma gg\,, \\ qg &\to \gamma\gamma qg\,, \\ g\overline{q} &\to \gamma\gamma g\overline{q}\,, \\ gg &\to \gamma\gamma q\overline{q}\,, \end{aligned} \tag{8.7}$$

and from the quark scattering processes

$$qq \to \gamma\gamma qq\,.$$

$$q\overline{q} \rightarrow \gamma\gamma q\overline{q},$$
$$\overline{q}\overline{q} \rightarrow \gamma\gamma\overline{q}\overline{q}. \tag{8.8}$$

For the hadronic channel the WH_F and ZH_F signals are combined due to the invariant mass distribution being unable to separate the W and Z peaks. The invariant mass bin for the signal is taken to be between 65 GeV and 105 GeV, while the photon mass bin is the same as in the leptonic channel. Table 8.1 shows the expected number of signal and background events[2] for 67 pb^{-1} of data, which is the current data sample at the Tevatron. The numbers are for $H_1^{0'}$ with $s_H^2 = 0.39$, its maximum value. From Table 8.1 we see

M_F (GeV)	WH/ZH (leptonic)	WH/ZH (jets)	$jj\gamma\gamma$
60	9.8/7.7	50.9	3.5
80	3.7/3.5	20.2	1.9
100	0.6/0.5	3.1	1.0

Table 8.1: Number of signal (columns 2 and 3) and background events (column 4) for the process $q\overline{q} \rightarrow W^*(Z^*) \rightarrow H_1^{0'}W(Z)$, with $H_1^{0'} \rightarrow \gamma\gamma$ and $W \rightarrow l\nu$, $Z \rightarrow l\overline{l}$, $\nu\overline{\nu}$, or W, $Z \rightarrow jj$.

that the region $M_F \leq 80$ GeV can be covered with ≥ 3 events in the background free leptonic channel, and a $\geq 4.3\sigma$ signal ($S/\sqrt{(S+B)}$) in the hadronic channel. With 140 pb^{-1} available by the end of 1995 the event numbers in Table 8.1 will be increased by a factor of approximately 2.1. This should enable the region $M_F \leq 90$ GeV to be covered, i.e. the mass at which the $\gamma\gamma$ decay starts to fall rapidly. It is very possible that s_H^2 is considerably less than 0.39, and if this is the case then the signal becomes weaker. With 140 pb^{-1} of luminosity and $M_F = 60$ (80) GeV one can obtain ≥ 3 events in the leptonic channel if $s_H^2 \geq 0.06$ ($s_H^2 \geq 0.16$).

For the case of h_1^F the maximum number of signal events is less due to the cross-section being proportional to $\cos^2\beta$. Table 8.2 is the analogy of Table 8.1 for h_1^F with $\cos^2\beta = 0.39$.

We see that $M_F \leq 60$ GeV can be probed (≥ 3 events in the leptonic channel and a $\geq 4\sigma$ signal in the hadronic channel). The coverage increases to $M_F \leq 80$ GeV with 140 pb^{-1}.

[2]The event numbers in all our tables are obtained from Ref. [75] with appropriate scaling for a particular Higgs model.

M_F (GeV)	WH/ZH (leptonic)	WH/ZH (jets)	$jj\gamma\gamma$
60	3.7/2.9	19.1	3.5
80	1.4/1.3	7.6	1.9
100	0.2/0.2	1.2	1.0

Table 8.2: Equivalent of Table 8.1 for the process $q\overline{q} \to W^*(Z^*) \to h_1^F W(Z)$.

Would it be possible to distinguish between $H_0^{1'}$ and h_1^F? If s_H^2 is near its maximum of 0.39 then the cross-section for a given M_F is considerably larger for $H_0^{1'}$ than that for h_1^F (see Eqs. (8.5) and (8.6)). Once the mass of H_F is measured one can estimate the cross-section and thus distinguish between the two models. Of course a sufficient number of $\gamma\gamma$ events will be needed to reconstruct the mass and so one should use the hadronic channel. Sufficient events should be present, certainly up to $M_F \approx 80$ GeV.

The above analysis has assumed that the lighter mass eigenstate ψ_2 is composed dominantly of $H_0^{1'}$ (see Eqs. (7.19, 7.20)). If this is not the case then $\psi_2 \approx H_1^0$ and the heavier eigenstate ψ_1 will be equal to $H_0^{1'}$. Therefore H_5^0 will be the lighter H_F in the HTM. If $M_{H_5^0} \leq 90$ GeV then one may search for the $\gamma\gamma$ decays at the Tevatron, and the mass hierarchy (Eq. (7.18.)) would suggest that H_3^0, $H_3^\pm$, and H_1^0 would also be light. However, Ref. [75] shows that at least 1000 pb^{-1} of luminosity would be needed to search for the SM Higgs (ϕ^0), and so more would be needed for H_1^0 which has ϕ^0 strength couplings only in the limit of $s_H \to 0$. The threeplet bosons (H_3^0 and $H_3^\pm$) would be difficult to detect at the Tevatron. The former decays primarily to quarks, and its $\gamma\gamma$ channel is reduced relative to ϕ^0 due to there being no W loops; $H_3^\pm$ is best searched for at an e^+e^- collider where the backgrounds are less (see Chapter 5). The doubly charged Higgs ($H_5^{\pm\pm}$) is likely to have a similar mass to H_5^0 (the fiveplet members are degenerate at tree-level) and would offer the best signature of the HTM. It can be easily searched for at LEP2 (see Chapter 7). Returning to H_5^0, we find that if $s_H^2 = 0.39$ then ≥ 3 events are predicted in the $Z^* \to ZH_5^0$ leptonic channel for $M_F \leq 60$ (80) GeV with a data sample of 67 pb^{-1} (140 pb^{-1}). Prospects for detection are therefore approximately the same as for h; its ZZH_0^5 coupling is slightly larger than that for h_1^F while its WWH_0^5 coupling is substantially weaker.

It is probable that the Tevatron will be upgraded in luminosity with 2 fb^{-1} being

possible by the year 2000. The increased number of events would allow heavier M_F to be probed. For $H_1^{0'}$ with $s_H^2 = 0.39$ one would expect ≥ 3 events in the leptonic channel if $M_F \leq 110$ GeV. To probe beyond this mass region in the $\gamma\gamma$ channel requires another large increase in luminosity due to the rapid weakening of BR $(H_F \to \gamma\gamma)$. In Chapter 7 we suggested that the theoretical motivation for the HTM would require $s_H \geq 0.1$ $(s_H^2 \geq 0.01)$. For this 'minimum' value the upgraded Tevatron would produce ≥ 3 events in the leptonic channel if $M_F \leq 80$ GeV. Therefore the coverage would be superior to that of LEP2, the latter being likely to probe the region $M_F \leq \sqrt{s} - 100$ GeV at best (if H_F has ϕ^0 strength couplings). For previous searches at LEP see Refs. [76], [78], [79]. Here one searches for the event $e^+e^- \to Z^* H_F$, $H_F \to \gamma\gamma$ and $Z \to jj$. The simulations obtained a good selection efficiency for the signal between 16% and 34%; the background is from initial state radiation, final state radiation and neutral hadrons faking photons. Demanding both photons to possess $E_\gamma \geq 10$ GeV removes most of the background for $M_F > 15$ GeV.

8.4 Phenomenology at the LHC

We now consider prospects at the LHC. From Figure 8.4 we see that the BR $(H_F \to \gamma\gamma)$ BR is falling rapidly for $M_F \geq 90$ GeV, and this channel will become unobservable as one approaches the real WW threshold. We are interested in the region $M_F \geq 110$ GeV, in order to search beyond the mass range of the upgraded Tevatron. If the BR $(H_F \to \gamma\gamma)$ is still reasonable (i.e. $\geq 1\%$) one could again exploit the associated production channel. Here we use the results of Chapter 6. Table 6.5 is for ϕ^0, and so for H_F the enhanced BR $(H_F \to \gamma\gamma)$, with values 20% (7%) for $M_F = 100$ (110) GeV, would provide a very strong signal. For example for $M_F = 110$ GeV and $s_H^2 = 0.39$ one would find $S/\sqrt{B} \geq 100$; this is due to the BR $(H_F \to \gamma\gamma)$ being 40 times larger than that for ϕ^0 for this mass. Hence a very large parameter space of s_H^2 and $\cos^2\beta$ would be covered. When BR $(H_F \to \gamma\gamma) \leq 1\%$ (for $M_F \geq 130$ GeV) there will not be much difference between the signal for ϕ^0 and the signal for H_F.

For $M_F \geq 130$ GeV the vector boson channels dominate and thus one must rely on the 'gold plated' channel, $H_F \to ZZ^{(*)} \to llll$. For $M_F < 2M_Z$ one Z boson must be

off–shell. This detection channel has been described in Chapters 3 and 6. However, due to the lack of gluon–gluon fusion the production cross–section of H_F is markedly diminished compared to that of ϕ^0. In addition, VV fusion will be suppressed by at least a factor of 0.5 for H_5^0 and h_1^F, although $H_1^{0'}$ may be produced with the same rate as ϕ^0. The associated production process contributes to the cross–section for H_F, although for $M_F \geq 150$ GeV this contribution is significantly smaller than the vector boson fusion process. The overall cross–sections, $\sigma(pp \to H_F X)$ for h_1^F, $H_1^{0'}$ and H_5^0 are scaled relative to the cross–section for ϕ^0 by approximately 0.10, 0.27 and 0.05 respectively, in the range 80 GeV$\leq M_F \leq$ 120 GeV; these results are the optimal values with $\cos^2\beta = \sin^2\theta_H = 0.39$. Hence it would seem that a reasonable signal in the $llll$ channel would be very unlikely for this mass range. However, BR $(H_F \to ZZ^*)$ is larger than that for ϕ^0 and this will help save some of the signal. For h_1^F and $H_1^{0'}$ in the region 80 GeV$\leq M_F \leq$ 120 GeV BR $(H_F \to ZZ^*)$ varies from 6% $\to$ 9%, while for H_0^5 the the respective values are 20% $\to$ 29%. This is in contrast to BR $(\phi^0 \to ZZ^*)$ which varies from 0.01% $\to$ 1.3%. Therefore the signal event number may be considerably greater (an order of magnitude) for H_F in the region $M_F \leq 100$ GeV than for ϕ^0; this is due to BR $(H_F \to ZZ^*)$ being up to two orders of magnitude greater than BR $(\phi^0 \to ZZ^*)$. In fact, a signal for ϕ^0 in this channel is unlikely for $M_{\phi^0} \leq 120$ GeV (see Table 6.9), but may be possible for H_F with a few events over a small background. For $M_F \geq 120$ GeV the signal for H_F becomes weaker than that for ϕ^0 since BR $(\phi^0 \to ZZ^*)$ is increasing rapidly, and coupled with the latter's superior cross–section produces more events overall.

For heavier Higgs masses, $M_F \geq 2M_Z$, H_F decays to on–shell vector bosons. Again we can use the analysis of Chapter 6. For h_1^F the cross–section is roughly 10 times less than for ϕ^0 throughout the range $2M_Z \leq M_F \leq 800$ GeV, with BR $(h_1^F \to ZZ) \approx$ BR $(\phi^0 \to ZZ)$, and thus we would find that a 4σ signal is only possible up to $M_F = 400$ GeV, in contrast to a 40σ signal for ϕ^0 of the same mass. Therefore it transpires that there is a very large parameter space for a hidden h_1^F at the LHC i.e. $\sin^2(\beta - \alpha) \ll 0.39$ and/or $M_F \geq 500$ GeV. We stress that the distinctive signature of a fermiophobic Higgs $(H_F \to \gamma\gamma)$ is lost in this heavier mass region, and the suppressed $llll$ signal could be mimicked by another h_1 with suppressed ZZ decays and/or production cross–section. Prospects for $H_1^{0'}$ are better since it possesses exactly the same BRs as h_1^F but a production cross–section improved

by a factor 8/3. Therefore one would obtain a good signal (4σ) with $s_H^2 = 0.39$ up to $M_F \approx 600$ GeV. Of course if $s_H^2 \ll 0.39$ then $H_1^{0'}$ would also be hidden over a large parameter space. For H_5^0 there is the added complication of its couplings to vector bosons being scaled by different amounts relative to ϕ^0. From the couplings in Eq. (8.3) we see that the WW fusion channel will be heavily suppressed. The effect of this is that the overall production cross–section is approximately 20 times less that of ϕ^0 throughout the relevant mass range. However, BR ($H_5^0 \to ZZ$) is twice that of BR ($\phi \to ZZ$) and so the overall $llll$ events number will be very similar to that of h_1^F.

As a final note we wish to mention that in the scenario of fermiophobia ($\cos\alpha \to 0$) the gg fusion cross–section for the heavier CP–even Higgs boson (H) will be of ϕ^0 strength or greater ($t\bar{t}$ coupling proportional to $\sin\alpha/\cos\beta$), and may have a better chance of detection. Since one of the requirements for a hidden H_F is $\sin^2(\beta-\alpha) \to 0$, this would cause $\cos^2(\beta-\alpha) \to 1$ and so the H boson of the 2HDM would have unsuppressed couplings to VV. Therefore we would expect a very good signature in the $llll$ channel for masses up to 800 GeV, with the result that H_F may be mistaken for H. In the MSSM this misidentity would not arise since one expects $M_{h^0} \leq 150$ GeV and a possible signal in the $\gamma\gamma$ channel, and $H^0 \to t\bar{t}$ or hh.

8.5 Conclusions

We have studied the detection prospects of fermiophobic Higgs bosons (H_F) at the Fermilab Tevatron and at the LHC. Such particles do not possess a tree–level coupling to fermions and can arise in various non–minimal Higgs models. Importantly, fermiophobia is not possible in the minimal supersymmetric model (MSSM) and thus searching for H_F is well motivated. We considered the 2HDM (Model I) and the HTM in which can arise the fermiophobic bosons $H_1^{0'}$, h and H_5^0. The dominant decay channel for $M_F \leq 80$ GeV is $H_F \to \gamma\gamma$, and backgrounds are small at the Tevatron. Such a decay has a branching ratio of the order 0.1% for the minimal SM Higgs (ϕ^0) and the lightest CP–even Higgs of the MSSM (h^{SUSY}). If the $H_F VV$ ($V = W$ or Z) coupling is close to its maximum value then with 140 pb^{-1} of data at the Tevatron a strong signal would be present for $H_1^{0'}$ (h, H_5^0) if $M_{H_F} \leq 90$ (80) GeV. It is possible to distinguish $H_1^{0'}$ from h and H_5^0 due to

the possibility of a significantly larger cross section, although we suggested that the mere detection of a H_F would indicate the HTM.

Prospects are improved at an upgraded Tevatron (2 fb^{-1}). For $H_1^{0'}$ with maximum H_FVV coupling detection is possible if $M_{H_F} \leq 110$ GeV. This collider covers more parameter (M_{H_F}, s_H) space than is possible at LEP2. For larger M_F the decay channel $H_F \rightarrow \gamma\gamma$ weakens rapidly and thus the distinctive signature of H_F becomes increasingly difficult to extract.

If the Tevatron is not upgraded then the Large Hadron Collider should cover the range inaccessible at LEP2 (i.e. $M_{H_F} \geq 80$ GeV). The associated production channel with $H_F \rightarrow \gamma\gamma$ will provide a distinct signature for $M_F \leq 130$ GeV. Above this mass BR ($H_F \rightarrow \gamma\gamma$) is of comparable magnitude to BR ($\phi^0 \rightarrow \gamma\gamma$), and does not produce a good signal. The alternative is to use the $H_F \rightarrow ZZ^{(*)} \rightarrow llll$ channel. For the low Higgs mass range, 90 GeV$\leq M_F \leq 120$ GeV, a signal is possible for H_F as long as the cross-section suppression is not too great; this is in contrast to ϕ^0 which can only be detected in this channel for $M_{\phi^0} \geq 120$ GeV. For the heavier Higgs mass region, $M_F \geq 130$ GeV the domination of vector bosons decays means that utilizing the $llll$ channel is the only chance of detection. A strong signal is possible for ϕ^0, but for H_F the lack of gg fusion diminishes the signal markedly. For the most favourable values of s_H and $\tan\beta$ a 4σ signal could be obtained for h_1^F and H_5^0 for $M_F \leq 400$ GeV, while for $H_1^{0'}$ prospects are better with the range $M_F \leq 600$ GeV being covered. The relative smallness of this signal compared to the signal from ϕ^0 would be a good discriminator, but this property could be mimicked by any other non-minimal Higgs sector.

Chapter 9

Conclusions

This thesis has studied the phenomenology of various non–minimal Higgs models at future colliders. Considered were the 2HDM, the MHDM and the HTM in the context of the non–minimal SM, that is, assuming no other new particles apart from Higgs bosons. The recurring aim was to ascertain distinct signatures for each model considered.

It was shown in Chapter 5 that light charged Higgs scalars ($M_{H^\pm} \leq M_W$) are possible in the 2HDM (Models I and I′) and MHDM, since they avoid the mass constraints from $b \to s\gamma$. In contrast, $H^\pm$ of the MSSM is predicted to be out of the LEP2 discovery range. Charged scalars with mass below the W mass would register a statistically significant signal, although the scenario of $M_{H^\pm} \approx M_W$ is problematic. By exploiting the possibility of an enhanced $H^\pm \to cb$, which is exclusive to the MHDM, we showed that detection may be possible in this region. Prospects are good at higher energy colliders with increased luminosity.

Chapter 6 covered the phenomenology of the neutral Higgs sector of the non–minimal SM. Although the Higgs boson of the minimal SM (ϕ^0) is also neutral, its branching ratios and production cross–sections are fixed for a given Higgs mass. The greater freedom in the couplings for the neutral Higgs bosons in the 2HDM and MHDM allow regions of parameter space for a significantly different phenomenology. We showed that distinct signatures included enhanced signals (relative to ϕ^0) of $\gamma\gamma$, $\tau^+\tau^-$, $t\bar{t}$ and $llll$, and suppressed signals are always possible. Indeed, it unlikely that a neutral Higgs boson from these

models would possess the same phenomenology as ϕ^0. The analysis showed that these distinct signatures (if present) may be observed at LEP2 and at the LHC, by comparison to the expected signal for ϕ^0.

Chapter 7 considered a non–minimal model containing Higgs triplets. Using a natural argument and the latest experimental bounds on the Higgs parameters we derived some new results concerning the masses and mixings of the neutral mass eigenstates. Using a natural mass hierarchy obtained from the Higgs potential we then considered in turn the possible combinations of Higgs bosons in range at LEP2. In addition to the strong signature of the doubly charged $H^{\pm\pm}$ (already considered in the literature) we show that an alternative distinctive signature of the model would be the discovery of a 'fermiophobic' Higgs i.e. a Higgs with negligible coupling to fermions. The natural argument shows that this particle has a large chance of being the lightest.

In the final chapter the phenomenon of fermiophobia was explored in more detail, and we presented a full analysis of the detection prospects at the Fermilab Tevatron and at the LHC. At the Tevatron the enhanced $\gamma\gamma$ would provide a good signal for masses below 80 GeV, while the LHC may probe this signature up to masses of 130 GeV. Above 130 GeV one must exploit the $llll$ channel, in which the fermiophobic Higgs would give a much weaker signal compared to ϕ^0.

To conclude, this thesis has shown that the Higgs sector of the non–minimal SM contains a more flexible parameter space than the Higgs sectors of the minimal SM and MSSM; thus significant differences in its phenomenology are possible which may be exploited at future colliders. Throughout we emphasized that one must be aware of the many theoretically sound Higgs models, and if a Higgs boson is detected it is imperative to know from which model it originates. Observing signatures which are exclusive to particular Higgs representations is one way of achieving this.

Bibliography

[1] S. Weinberg, Phys. Rev. Lett. **19** (1967) 1264; S. Glashow, Nucl. Phys. **20**, (1961) 579; A. Salam, in *Elementary Particle Theory*, ed. N. Svartholm, (1968).

[2] A. Blondel, talk given at the 28th International Conference on High Energy Physics, Warsaw, July 1996.

[3] F. Halzen and A.D. Martin, *Quarks and Leptons* (John Wiley and Sons, Inc. New York, 1984).

[4] P.W. Higgs, Phys. Lett. **B12** (1964) 132, Phys. Rev. Lett. **13** (1964) 508.

[5] B.W. Lee, C. Quigg and G.B. Thacker, Phys. Rev. Lett. **38** (1977) 883; Phys. Rev. **D16** (1977) 1519.

[6] M. Chanowitz and M.K. Gaillard, Phys. Lett. **B142** (1984) 85; Nucl. Phys. **B261** (1985) 379.

[7] N. Cabibbo, L. Maiani, G. Parisi and R. Petronzio, Nucl. Phys. **B158** (1979) 295.

[8] M. Lindner, Z. Phys **C31** (1986) 295.

[9] P.Q. Hung and M. Sher, Phys. Lett. **B374** (1996) 138.

[10] Final report of workshop at LEP2, CERN 96-01, edited by G. Altarelli, T. Sjostrand and F. Zwirner (1996).

[11] ATLAS report Phys-0-74, (1996).

[12] ATLAS report Phys-0-48, (1994).

[13] ATLAS report Phys-0-51, (1995).

[14] ATLAS report Phys-0-43, (1994).

[15] L. Resnick, M.K. Sundaresan and P.J.S. Watson, Phys. Rev. **D8** (1973) 172.

[16] E. Braaten and J.P. Leveille, Phys. Rev **D22** (1980) 715; N. Sakai, Phys. Rev **D22** (1980) 2220; T. Inami and T. Kubota, Nucl. Phys. **B179** (1981) 171; M. Drees and K. Hikasa, Phys. Lett **B240** 455; S.G. Gorishny, A.L. Kataev, S.A. Larin, and L.R. Surguladze, Mod. Phys. Lett. **5** (1990) 2703; A.L. Kataev and V.T. Kim, Mod. Phys. Lett. **A9** (1994) 1309; L.R. Surguladze, Phys. Lett. **B341** (1994) 61.

[17] K.G. Chetyrkin, J.H. Kuhn, and A. Kwiatowski, Proceedings *QCD at LEP*, Aachen 1994.

[18] A. Djouadi, M. Spira and P.W Zerwas, Z. Phys **C70** (1996) 427.

[19] S. Moretti (work in preparation).

[20] J. Ellis, M.K. Gaillard, and D.V. Nanopoulos, Nucl. Phys. **B106** (1976) 292; B.L. Ioffe and V.A. Khoze, Sov. Journal of Phys. **9** (1978) 50; B.W. Lee, C. Quigg, and H.B. Thacker, Phys. Rev. **D16** (1977) 1519; J.D. Bjorken, Proc. Summer Institute on Particle Physics, SLAC Report 198 (1976).

[21] D.R.T. Jones and S.T. Petcov, Phys. Lett. **B84** (1979) 440; R.N. Cahn and S. Dawson, Phys. Lett. **B136** (1984) 96; G. Altarelli, B. Mele and F. Pitolli, Nucl. Phys. **B287** (1987) 205.

[22] J. Fleischer and F. Jegerlehner, Nucl. Phys. **B216** (1983) 469; B.A. Kniehl, Z. Phys. **C55** (1992) 605.

[23] F.A. Berends, W.L. van Neerven and G.J.H. Burgers, Nucl. Phys. **B297** (1988) 429; erratum **B304** (1988) 921.

[24] Proceedings of the '*Large Hadron Collider Workshop*', Aachen, 4-9 October 1990, eds. G. Jarlskog and D. Rein, Report CERN 90-10, ECFA 90-133, Geneva, 1990.

[25] H. Georgi, S. Glashow, M. Machacek and D. Nanopoulos, Phys. Rev. Lett. **40** (1978) 692.

[26] R.N. Cahn and S. Dawson, Phys. Lett. **B136** (1984) 196; K. Hikasa, Phys. Lett. **B164** (1985) 341; T. Han, G. Valencia and S. Willenbrock, Phys. Rev. Lett. **69** (1992) 3274.

[27] S.L. Glashow, D.V. Nanopoulos and A. Yildiz, Phys. Rev. **D18** (1978) 1724; Z. Kunszt, Z. Trocsanyi and W.J. Stirling, Phys. Lett. **B271** (1991) 247; T. Han and S. Willenbrock, Phys. Lett. **B273** (1991) 167.

[28] Z. Kunszt, Nucl. Phys. **B247** (1984) 339; J.F. Gunion, Phys. Lett. **B253** (1991) 269; W.J. Marciano and F.E. Paige, Phys. Rev. Lett. **66** (1991) 2433.

[29] L. Fayard and G. Unal, EAGLE Note NO-001 (1991) and Addenda (1992).

[30] J.F. Gunion, H.E. Haber, G.L. Kane and S. Dawson, *The Higgs Hunter's Guide* (Addison-Wesley, Reading, 1990).

[31] M. Veltman, Nucl. Phys. **B123** (1977) 89.

[32] Review of Particle Properties, Phys. Rev. **D50** (1994).

[33] A. Grant, Phys. Rev. **D51** (1995) 207.

[34] S.L. Glashow and S. Weinberg, Phys. Rev. **D15** (1977) 1958.

[35] V. Barger, J.L. Hewett and R.J.N. Phillips, Phys. Rev. **D41** (1990) 3421.

[36] J.F. Gunion, H.E. Haber and J. Wudka, Phys. Rev. **D43** (1991) 904.

[37] M. Veltman, Acta. Phys. Pol. **B8** (1977) 475.

[38] A. Denner, R.J. Guth and J.H. Kuhn, Phys. Lett. **240** (1990) 438.

[39] H.E. Haber and G.L. Kane, Phys. Rep. **117** (1985) 75.

[40] M.A. Diaz and H.E. Haber, Phys. Rev. **D45** (1992) 4246.

[41] S.P. Li and M. Sher, Phys. Lett. **B140** (1984) 339; J. F. Gunion and A. Turski, Phys. Rev. **D39** (1989) 2701; H. Haber and R. Hempfling, Phys. Rev. Lett. **66** (1991) 1815.

[42] H.E. Haber, preprint CERN–TH/95–109, SCIPP 95/15, (1995) and references therein.

[43] J.F. Gunion and H.E. Haber, Nucl. Phys. **B278** (1986) 449.

[44] G.L. Kane, G.D. Kribs, S.P. Martin and J.D. Wells, Phys. Rev. **D53** (1996) 213.

[45] C. Albright, J. Smith and S.H.H. Tye, Phys. Rev. **D21** (1980) 711.

[46] Y. Grossman, Nucl. Phys. **B426** (1994) 355.

[47] J.L. Hewett, preprint SLAC–PUB–6521 (1994).

[48] P. Krawczyk and S. Pokorski, Nucl. Phys. **B364** (1991) 10.

[49] W.S. Hou and R.S. Willey, Phys. Lett. **B202** (1988) 591.

[50] T.G. Rizzo, Phys. Rev. **D38** (1988) 820.

[51] B. Grinstein, R. Springer and M. Wise, Nucl. Phys. **B339** (1990) 269.

[52] CLEO collaboration: M.S. Alam *et al.*, Phys. Rev. Lett. **74** 1995 (2885).

[53] A. Djoudi, G. Giraldi, W. Hollik, F.M. Renard and C. Verzegnassi, Nucl. Phys. **B349** (1991) 48.

[54] S. Komamiya, Phys. Rev. **D38** (1988) 2158.

[55] A. Sopczak, Int. J. Mod. Phys **A9** (1994) 1747.

[56] J. Alcaraz, M. Felcini, M. Pieri and B. Zhou, preprint CERN–PPE/93–28 (1993).

[57] Proceedings of the Munich – Annecy – Hamburg Workshop on 'e^+e^- *collisions at 500 GeV*', December 1993, ed. P.M. Zerwas, DESY 92–123C (1993).

[58] J. Alexander, D.L. Burke, C.K. Jung, S. Komamiya, and P.R. Burchat in *Proceedings of the Summer Study on High Energy Physics in the 1990s*, Snowmass 1988, ed. S. Jensen (World Scientific, Singapore, 1989) p. 135.

[59] G.C. Branco, A.J. Buras and J.M. Gerard, Nucl. Phys. **B259** (1985) 306.

[60] T.V. Duong, E. Keith, E. Ma and H. Kikuchi, Phys. Rev. **D52** (1995) 5045.

[61] J. Kalinowski and M. Krawczyk, Phys. Lett. **B361** (1995) 66.

[62] P. Abreu *et al.*, Delphi Collaboration CERN-PPE/94-218 (1994).

[63] M. Spira, A. Djouadi, D. Graudenz, P.M. Zerwas, Nucl. Phys. **B453** (1995) 17.

[64] H. Georgi and M. Machacek, Nucl. Phys. **B262** (1985) 463.

[65] J.F. Gunion, R. Vega, and J. Wudka, Phys. Rev. **D42** (1990) 1673; Phys. Rev. **D43** (1991) 2322.

[66] P. Bamert and Z. Kunszt, Phys. Lett. **B306** (1993) 335.

[67] M. Swartz *et al.*, Phys. Rev. Lett. **64** (1990) 2877.

[68] OPAL Collaboration, P.D. Acton *et al.*, Phys. Lett. **B295** (1992) 347.

[69] T. Asaka and Ken-ichi Hikasa, Phys. Lett. **B345** (1995) 36.

[70] M.D. Diaz and T. Weiler, preprint VAND-TH-94-1 (1994).

[71] H. Haber, G. Kane and T. Sterling, Nucl. Phys. **B161** (1979) 493.

[72] R. Godbole, B. Mukhopadhyaya and M. Nowakowski, Phys. Lett. **B352** (1995) 388.

[73] K. Cheung, R.J.N. Phillips and A. Pilaftsis, Phys. Rev. **D51** (1995) 4731.

[74] R. Vega and D.A. Dicus, Nucl. Phys. **B329** (1990) 533.

[75] A. Stange, W. Marciano and S. Willenbrock, Phys. Rev. **D49** (1994) 1354.

[76] D. Buskulic *et al.*, Phys. Lett. **B308**, 425 (1993); OPAL Collaboration, P. Acton *et al.*, Phys. Lett. **B311**, 391 (1993).

[77] V. Barger, T. Han, J. Ohnemus and D. Zeppenfeld, Phys. Rev. **D41** (1990) 2782.

[78] V. Barger, N.G. Deshpande, J.L. Hewett, and T.G. Rizzo, preprint MAD-PH-728 (1992) (hep–ph 9211234).

[79] L3 Collaboration: M. Acciarri *et al*, preprint CERN–PPE/96–50 (1996).